NANO · MICRO small
www.small-journal.com

Exploring $CsPbX_3$ (X = Cl, Br, I) Perovskite Nanocrystals in Amorphous Oxide Glasses: Innovations in Fabrication and Applications

Sadaf Samiei, Ehsan Soheyli, Kunnathodi Vighnesh, Gholamreza Nabiyouni, and Andrey L. Rogach**

Metal halide perovskites with excellent optical and electronic properties have become a trending material in the current research. However, their limited stability under ambient conditions degrades quality and threatens their potential commercialization as optoelectronic devices. Various approaches are adopted to improve the stability of perovskite nanocrystals (PeNC) while maintaining their advantageous optical properties, particularly strong luminescence. Among different possible improvement strategies, encapsulation of PeNCs within the amorphous glass matrices of inorganic oxides has drawn widespread attention because it ensures high resistance against chemical corrosion and high temperature, thus enhancing their chemical, thermal, and mechanical stability with improved light-emission characteristics. In this article, two types of materials, namely all-inorganic metal halide PeNCs and amorphous oxide glasses are briefly introduced, and then the methods are reviewed to fabricate and improve the quality of PeNC@glass composites. These methods are classified into three universal categories: compositional modification, structural modification, and dual encapsulation. In the final part of this review paper, examples of applications of PeNCs@glass composites in light-emitting devices and displays, data storage and anti-counterfeiting, lasing, photodetectors and X-ray detectors, photocatalysis, optical filters, solar concentrators, and batteries are provided.

1. Introduction

Perovskite materials with a structure of ABX_3, such as $CaTiO_3$, $BaTiO_3$, $CaSiO_3$, $MgSiO_3$, etc., whose crystal lattice consists of corner-sharing $[BX_6]$ octahedra are abundant materials on Earth with a total 38% of the planet mass and a history dating back to 1839.[1] However, a tremendous level of global attention to these structures began much more recently with reports on the wet-chemical synthesis of metal halide perovskites (MHPs), either in the form of thin films or colloidal nanocrystals (NCs).[2–4] While these compounds were first synthesized in 1893,[5,6] they have been intensively explored since the last decade for a variety of applications such as light-emitting diodes (LEDs), lasers, solar cells, and photodetectors.[7–10] When produced in the form of NCs, lead halide perovskites (LHPs) offer several advantageous properties, such as narrow-band photoluminescence (PL) and high PL quantum efficiency (PLQE) which are tunable over the whole visible spectrum.[3] One of the most often studied compositions of LHPs is so-called all-inorganic perovskites with a composition of $CsPbX_3$ (X = Cl, Br, I, or binary mixture of these anions), whose PL tunability can be achieved both by change of the anion composition and by the NC size. Size-governed emission tunability is a well-documented phenomenon in the conventional II-VI and III-V semiconductors NCs;[11–13] while yet another attractive property leveling up perovskite NCs (PeNCs) is the negligible effect of structural

S. Samiei, G. Nabiyouni
Department of Physics
Faculty of Science
Arak University
Arak 38156-88349, Iran

S. Samiei, G. Nabiyouni
Institute of Nanoscience and Nanotechnology
Arak University
Arak 38156-88349, Iran

E. Soheyli
Department of Physics
Faculty of Science
Ilam University
Ilam 69315-516, Iran
E-mail: e.soheyli@ilam.ac.ir

E. Soheyli
Department of Electrical-Electronics Engineering
Abdullah Gul University
Kayseri 38080, Türkiye

K. Vighnesh, A. L. Rogach
Department of Materials Science and Engineering
and Centre for Functional Photonics (CFP)
City University of Hong Kong
83 Tat Chee Avenue, Hong Kong SAR 999077, P. R. China
E-mail: andrey.rogach@cityu.edu.hk

The ORCID identification number(s) for the author(s) of this article can be found under https://doi.org/10.1002/smll.202307972

DOI: 10.1002/smll.202307972

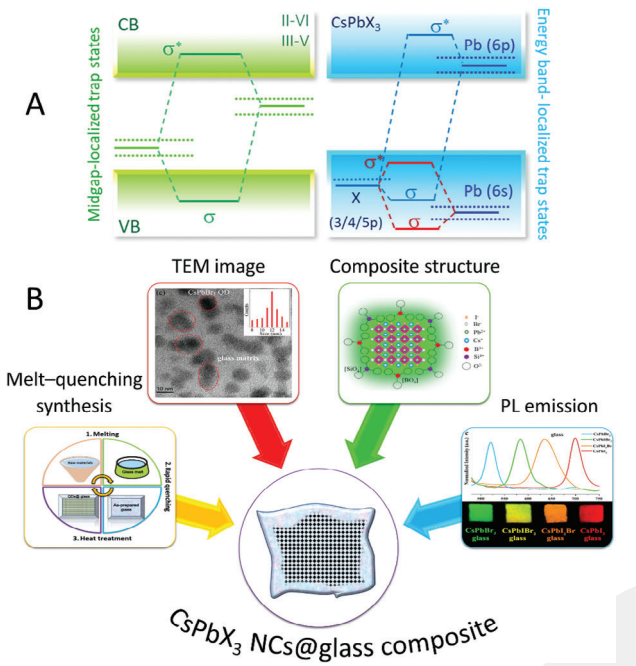

Figure 1. A) Illustration of the "defect tolerance" of LHP NCs whose energy structure is shown on the right, as compared to "defect-intolerant" conventional II-IV and III-V semiconductor NCs shown on the left. B) Illustration of basic features of $CsPbX_3$ PeNCs@glass composite. TEM image of (B) Reproduced with permission.[31] Copyright 2018, Royal Society of Chemistry. Composite structure and PL emission of (B) Reproduced with permission.[32] Copyright 2021, ACS Publications.

defects on the electronic structure of those compounds. This particular property of PeNCs is often referred to as "defect tolerance"[14] and is illustrated in **Figure 1**A, which compares band structures of II-VI (such as CdSe) or III-V (such as InP) NCs with those of PeNCs. For example, in CdSe, the removal or displacement of cadmium cations leads to the occurrence of non-bonded orbitals that are located within the bandgap and play the role of deep trap states. However, the bandgap of LHPs is formed between the two sets of anti-bonding orbitals, and even though these highly ionic materials may easily accept vacancies, the respective defect states will be merged within the valence band and conduction band. Thus, they do not act as trap states for charge carriers.[15] In other words, despite the abundance of surface and volume defects and vacancies in LHP NCs, they still possess high PLQE, because their bandgap remains free of deep energy trap states. Such an advantageous property allows us to produce LHP NCs with a bright emission without the requirement of additional surface passivation (i.e., through deposition of wide-bandgap semiconductor shells), which is otherwise a necessity for most of the conventional NCs such as CdSe,[16] Cu-In-S,[17] and InP (the PLQE of the bare InP NCs is typically 1%).[18] We also refer an interested reader to a recent comprehensive review on PeNCs.[19]

At the same time, both PeNCs and MHPs have some disadvantages, among which the most problematic is the ease of their structural decomposition triggered by external stimuli, such as moisture, light, and heat. This intrinsic property is related to the highly ionic nature of MHPs and the high surface energy of the PeNCs,[20] and makes them unstable against the operational conditions of many devices in real-world applications.[1,5,21] For that very reason, plenty of efforts have been devoted to improving the stability of PeNCs. Among different possible improvement strategies, encapsulation of PeNCs within amorphous glass matrices has drawn widespread attention, because it ensures high resistance against chemical corrosion and high temperature, thus enhancing their chemical, thermal, and mechanical stability while maintaining the optical merits of PeNCs.[22,23] Encapsulation in relatively rigid glasses also prevents nanoparticles from agglomeration and enables us to control the size and distribution of PeNCs embedded in glass (we will denote such composite materials as PeNCs@glass from here on). In fact, encapsulation in glass matrices is a general method that works well for different kinds of luminescent NCs, such as II-VI semiconductors and upconversion rare-earth nanoparticles.[24–27] From the historical perspective, the rise of semiconductor NCs started with the study of quantum size effects in semiconductor microcrystals embedded in a glassy matrix[28] which recently won the Nobel Prize in chemistry. The availability of NCs@glass composites allows us to preserve the outstanding luminescent properties of NCs while providing them with high chemical, mechanical, and thermal stability, which may facilitate wider applications of NCs in nonlinear optical devices, light-emitting devices, and signal amplification in the fiber-optic communication systems.[29] Obviously, with the emergence of PeNCs that suffer from unstable properties, perovskite@glass composites are attracting attention, and this is what we will consider in detail in this review. As schematically illustrated in Figure 1B, $CsPbX_3$ PeNCs@glass composites are generally synthesized by melt-quenching and subsequent heat-treatment processes.[30] The resulting composite nanoparticles typically possess a spherical shape, and the PeNCs are uniformly distributed within the glass matrix, surrounded by structural units of the glass network. They also show bright and tunable emissions depending on the perovskite compositions.[31,32]

Figure 2 outlines some important milestones illustrating the historical progress of fabrication and studies of $CsPbX_3$ PeNCs@glass composites. As can be seen from this timeline, researchers have been able to achieve improved stability while retaining the bright and tunable emission of PeNC@glass composites by applying different techniques, which resulted in their promising anticipated applications in various areas, such as photodetectors and X-ray detectors,[33,34] color conversion white-light-emitting diodes (WLED), monochrome LEDs and displays,[35–38] Li-ion batteries,[39] laser-active media,[40,41] anti-counterfeiting,[42] optical filters (for example, high-transmittance in the long-wavelengths and a superior shielding effect in the short-wavelengths),[43] rewritable data storage,[44] and photocatalysis.[45]

Throughout this review, we divided existing approaches toward the improvement of as-fabricated PeNCs@glass composites into three categories: compositional modification, structural modification, and dual encapsulation (**Figure 3**). Among these approaches, the compositional modification is generally applied before the fabrication of the composites, while the two other strategies are applied after the fabrication of the initial PeNCs@glass composites. The compositional modification can be categorized into four approaches: B-site perovskite doping, glass network doping, glass-former modification, and

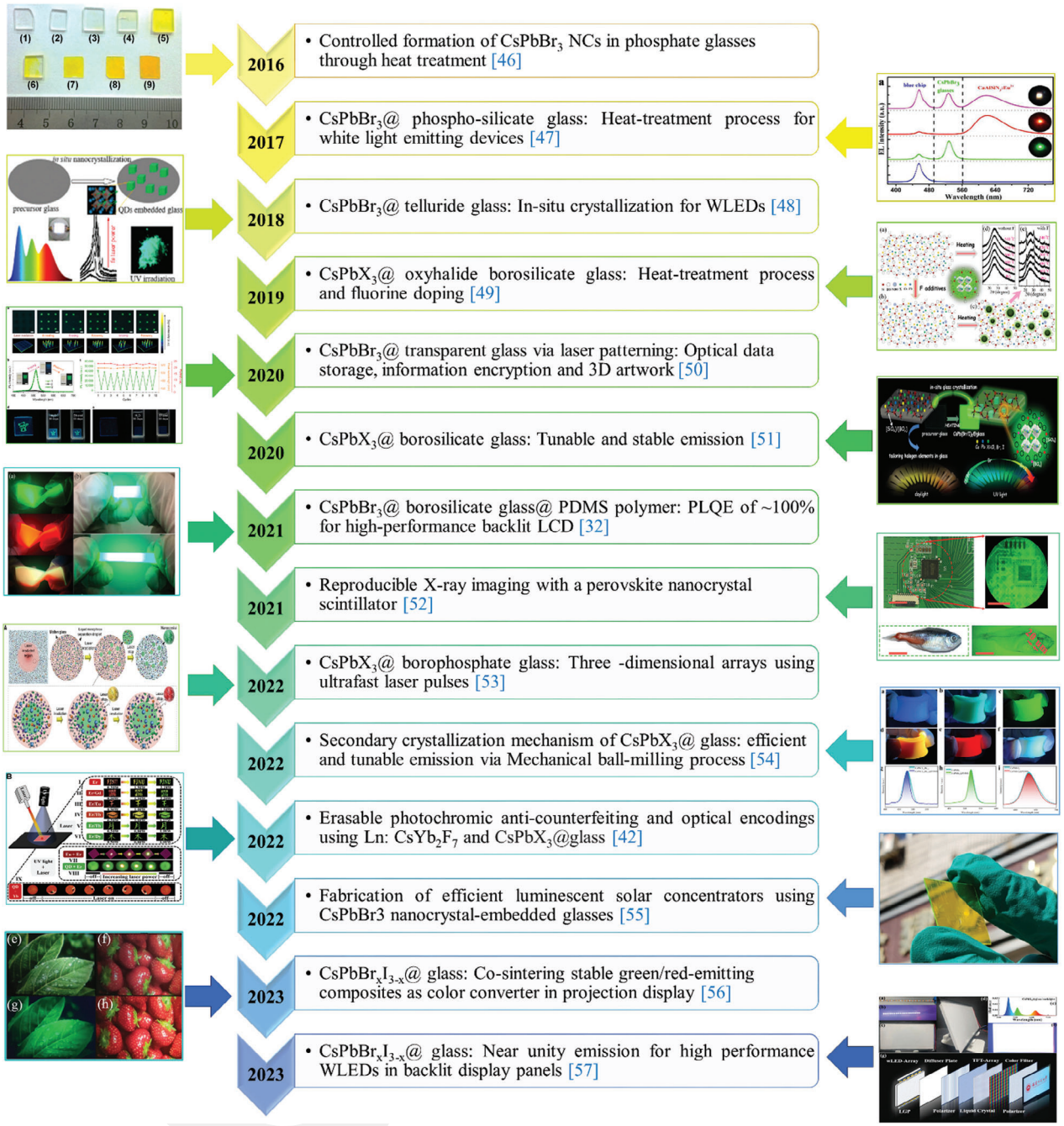

Figure 2. Some important fabrication milestones and studies of $CsPbX_3$@glass composite, Reproduced with permission.[46] Copyright 2016. American Ceramic Society. Reproduced with permission.[47] Copyright 2017, Royal Society of Chemistry. Reproduced with permission.[48] Copyright 2018, ACS Publications. Reproduced with permission.[49] Copyright 2019, Royal Society of Chemistry. Reproduced with permission.[50] Copyright 2020, Nature. Reproduced with permission.[51] Copyright 2020, Elsevier. Reproduced with permission.[32] Copyright 2021, ACS Publications. Reproduced with permission.[52] Copyright 2021, Wiley-VCH. Reproduced with the term of CC BY 4.0 license.[53] Copyright 2022, Science. Reproduced with permission.[54] Copyright 2022, ACS Publications. Reproduced with permission.[42] Copyright 2022, Physical Science. Reproduced with permission.[55] Copyright 2022, Elsevier. Reproduced with permission.[56] Copyright 2022, Wiley-VCH. Reproduced with permission.[57] Copyright 2023, Wiley-VCH.

molar-ratio modification. Structural modification can be divided into two methods: heat-treatment modification and mechanical/hydration crystallization, while dual encapsulation can be carried out in two ways: by using polymer or secondary glass matrices. All these methods can be applied on demand depending on anticipated applications (Figure 3). While in this review we have summarized the recent progress in fabrication and properties of $CsPbX_3$ PeNC@glass composites, it should be noted that glass matrices can also embrace other fully inorganic compositions of PeNCs, such as Pb-free perovskite structures.[25,58–62] One

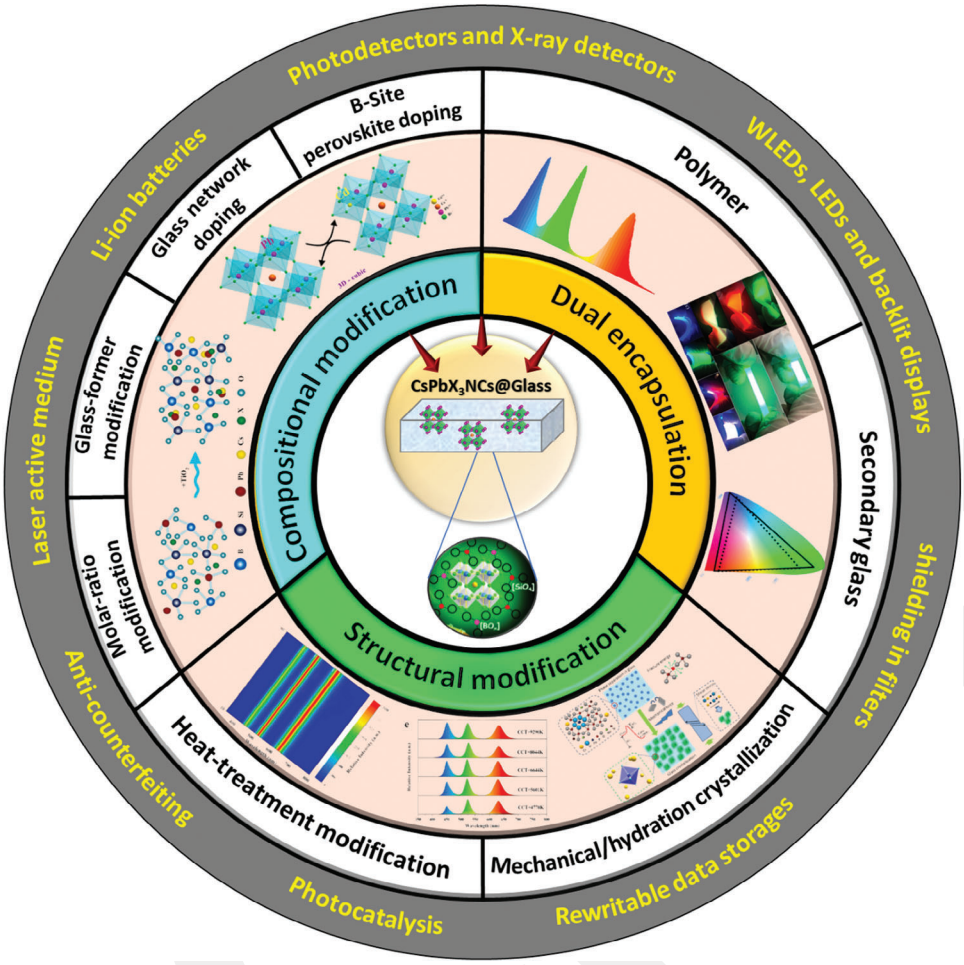

Figure 3. Schematics of the different modification approaches and related potential applications of PeNCs@glass composites. Reproduced with permission.[32] Copyright 2021, ACS Publications. Reproduced with permission.[63] Copyright 2021, ACS Publications. Reproduced with permission.[64] Copyright 2020, Elsevier. Reproduced with permission.[65] Copyright 2022, Elsevier. Reproduced with permission.[66] Copyright 2019, Springer Nature. Reproduced with permission.[67] Copyright 2022, Elsevier.

of those is related to the manganese halide PeNCs embedded inside borate glasses,[61] which provided red-emissive composites with PLQE of 41.8% and negligible reabsorption for stable X-ray scintillation performance and high-resolution X-ray imaging. In another study, Zhang's group fabricated lead-free double perovskites of $Cs_2AgIn_{1-x}Er_xCl_6$ in amorphous fluoride glass, which showed strong and stable mid-infrared luminescent located ≈2750 nm, suitable for monitoring of carbon dioxide in hydrogen gas.[62]

2. All-Inorganic Lead Halide Perovskites (LHPs)

2.1. Basic Characteristics

All-inorganic LHPs with a structure of $CsPbX_3$ (X = Cl^-, Br^-, and I^-) consist of corner-sharing [PbX_6] octahedrals. Their two common structures of cubic and orthorhombic phases are presented in **Figure** 4A,B, respectively. As an example, the cubic phase of the $CsPbI_3$ structure forms at temperatures above 300 °C; with a decrease in temperature, a phase transition to the orthorhombic phase occurs at ≈25 °C which means that this perovskite would crystallize in the orthorhombic phase during the room temperature synthesis.[68–70] Excellent monodispersity and high crystallinity of $CsPbBr_3$ PeNCs are exemplified in Figure 4C,D, where transmission electron microscopy (TEM) and high-resolution TEM (HRTEM) images demonstrate their uniform size of ≈8.4 nm (the cube edge) along with lattice fringes and recognizable interplanar distances [0.563 nm for (100), and 0.397 nm for (110)] related to cubic phase. The inset in Figure 4D shows the selected area electron diffraction (SAED) pattern which confirms the cubic phase structure of $CsPbBr_3$ PeNCs. Figure 4E presents X-ray diffraction (XRD) patterns of a series of $CsPbX_3$ (X = Cl^-, Br^-, and I^-, and a mixture of Br/Cl, I/Br anions) NCs, which again demonstrate the cubic phase of the PeNCs synthesized at a high temperature. As mentioned earlier, an attractive feature of LHP NCs is the bright and narrow-band PL, which is easily adjustable from ultraviolet to near-infrared wavelengths by changing the anion composition or NCs size. Figure 4F shows photographs of light-emitting colloidal solutions of LHP NCs with different halide anions, while Figure 4G

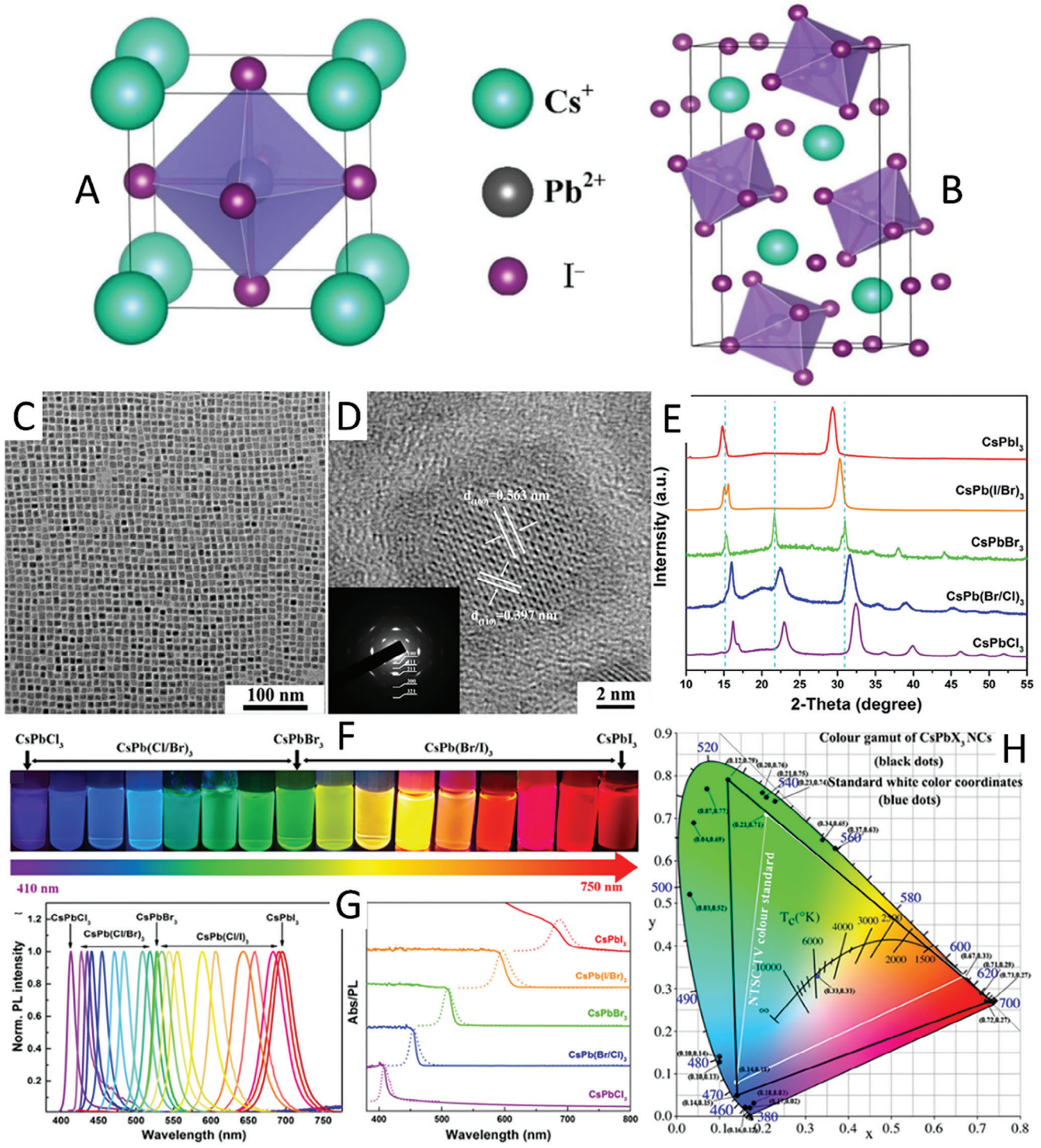

Figure 4. Crystal structure of $CsPbI_3$ perovskites for A) cubic phase and B) orthorhombic phase. Reproduced under the term of CC BY-NC 3.0.[68] Copyright 2021, MDPI. C) TEM and D) HRTEM images of $CsPbBr_3$ NCs; the inset in (D) shows their SAED pattern. E) XRD patterns of $CsPbX_3$ (X = Cl, Br, I, and mixed-halide Br/Cl and I/Br compositions) NCs. F) Photographs of light-emitting colloidal solutions of $CsPbX_3$ NCs with different halide anions taken under a UV lamp (λ_{exc} = 365 nm), and G) PL spectra of these PeNCs (λ_{exc} = 400 nm for all but 350 nm for $CsPbCl_3$ samples. Reproduced with permission.[71] Copyright 2019, Engineered Science Publisher. H) The CIE chromaticity diagram for the $CsPbX_3$ NC emission (black dots), as compared to NTSC TV color standard (solid white triangle). Reproduced under the term of CC BY-NC 4.0.[3] Copyright 2015, ACS Publications.

demonstrates that their emission peaks are indeed narrow and symmetric and they shift to longer wavelengths depending on the halide contents.[71] The same redshift occurs in the UV–vis absorption spectra, which show a sharp excitonic absorption edge and a relatively small Stokes shift similar to the PL maximum. Figure 4H further emphasizes the adjustable emission color of $CsPbX_3$ NCs covering a wide region of the Commission Internationale de L'Eclairage (CIE) chromaticity diagram and encompassing 140% of the National Television Standard Committee (NTSC) TV color standard.[3]

2.2. Stability Issues

Despite the outstanding optical features of LHPs, their stability is one of the main obstacles in advancing these materials toward real-world applications. The instability originates from the low crystal lattice energy of LHPs, which also causes their low melting points (T_m).[72] A decrease in the lattice energy was observed for LHPs with larger anions [for example, $T_m \approx 460$ °C for $CsPbI_3$, while T_m is 570 °C for $CsPbBr_3$].[73] The crystal structure of perovskite compounds with respect to their stability is often judged by the so-called Goldschmidt tolerance factor (τ), which is also an experimental index widely used to predict the formation of various ABX_3 crystal structures.[74] The value of τ varies with the ionic radii of A, B, and X constituents in the ABX_3 structure; if the difference of ionic radii among A, B, and X is large, it can cause deviation from the ideal perovskite lattice structure and even a phase separation.

The ionic bonding in LHP NCs allows them to form within just a few seconds, even for the synthesis at room temperature. However, the ionic bonding also causes LHPs to easily dissolve in polar solvents, which is one of the challenges in their handling and processing. Apart from that, there are several other intrinsic and extrinsic factors causing the easy decomposition of LHPs, namely environmental conditions, and post-synthetic purification procedures. Among the detrimental environmental factors, there are light, moisture, heat, or oxygen, and mechanisms involved in perovskite degradation may include hydration, decomposition, and oxidation.[75] Moreover, the binding of organic ligands to the surface of PeNCs is rather dynamic, so they can be easily removed during several washing cycles of purification.[76] Solvent polarity is yet another important factor that determines the stability of PeNCs. Low-polarity solvents such as toluene, tetrahydrofuran,[77] methyl acetate, or ethyl acetate ensure the stability of their colloidal suspensions.[78–80] It was shown that the solvent polarity also affects the morphology and crystalline structure of the LHP NCs and subsequently the optical quality of the samples.[81]

2.3. Approaches Toward Improving the Long-Term Stability of LHPs

The high sensitivity of LHPs to external conditions like moisture, oxygen, heat, and light is a matter of concern when considering them for real-world applications. As listed in **Figure 5**, several strategies for improving perovskite stability can be applied to mitigate various instability factors. These strategies can be divided into two categories: encapsulation and post-synthesis modification.

Encapsulation of PeNCs is one of the potential strategies to solve the issue of stability. The use of suitable physically and chemically inert and/or stable materials such as oxides, metal–organic frameworks (MOFs), polymers, or other stable semiconductor NCs as shells can protect the perovskite NCs against oxygen- and moisture-induced degradation. PeNCs embedded in titanium oxide (TiO_2), zirconium oxide (ZrO_2), or silicon oxide (SiO_2) exhibited improved resistance against oxidation and moisture, with reduced ion diffusion rates and improved dispersibility in water.[82–84] Due to the chemically inert nature and thermal stability of SiO_2, several studies have also reported SiO_2-coated PeNCs with improved stability in water.[85,86] Besides, growing PeNCs in porous materials enhances their stability and prevents ion diffusion and ion exchange in mixed halide PeNCs.[87] Synthesis of PeNCs in mesoporous silica templates demonstrated optical features due to the quantum confinement effect.[88,89] MOFs are yet another kind of porous materials that have been used as hosts for the synthesis of PeNCs. Chen et al.[90] fabricated PeNCs inside MOF HKUST-1 ($Cu_3(BTC)_2$, BTC = 1,3,5-benzene tricarboxylate thin film) acting as the template,[90] which remained stable even under 70% relative humidity conditions. Additionally, encapsulating the PeNCs with polymer materials has also improved their stability.[91,92] Pan et al.[93] demonstrated a UV-induced polymerization over the functionalized PeNCs surface, resulting in water-stable $CsPbX_3$ NC-polymer composites.[93] In addition, inorganic salts that are more thermally resistant than most organic compounds can efficiently shield the PeNCs from the harmful environment. It has been demonstrated that nanocomposites of $CH_3NH_3PbX_3$ NCs embedded in porous inorganic salts such as magnesium silicate hollow spheres exhibited better thermal and photostability.[94] Eychmuller's group[95] showed that the incorporation of $CsPbX_3$ NCs into ionic matrices of potassium halide salts (KCl, KBr, and KI) via solid-state anion exchange reactions did not affect their initial PLQE, improving the stability of iodide-containing NCs.[95] Core/shell heterostructures between PeNCs and metal chalcogenide NCs is another exciting area of research, where more stable, covalently bound NCs such as II-VI metal chalcogenides act as shells to enhance the stability of the bare PeNCs. Ravi et al.[96] reported that $CsPbBr_3$/ZnS core/shell NCs had enhanced stability in water. Blue-emitting $CsPbCl_xBr_{1-x}$ NCs coated with ZnS shells were also found to exhibit better structural stability in water, minimizing the ion migration and providing structural integrity to the core NCs.[97] The epitaxial growth of double perovskite Cs_2GeF_6 over $CsPbBr_3$ NCs with similar crystal structures was shown to enhance the stability of the hybrid structure as it prevents the agglomeration between the NCs.[98] In another report, the core-shell $Cs_4PbBr_6/CsPbBr_3$ NCs with fluorinated surface ligand passivation were found to enhance the water stability of the NCs, preserving their PLQE for ≈1 month.[99]

Surface chemistry plays a crucial role in determining the stability of luminescent PeNCs. Therefore, post-synthesis surface modification of the PeNCs aimed to improve the interactions between the NC surface and the surface ligands can have a significant effect on their overall stability. Huang et al.[100] showed that the post-synthesis surface treatment of $CsPbBr_3$ NCs using potassium oleate increased the PLQE up to 83%, and their

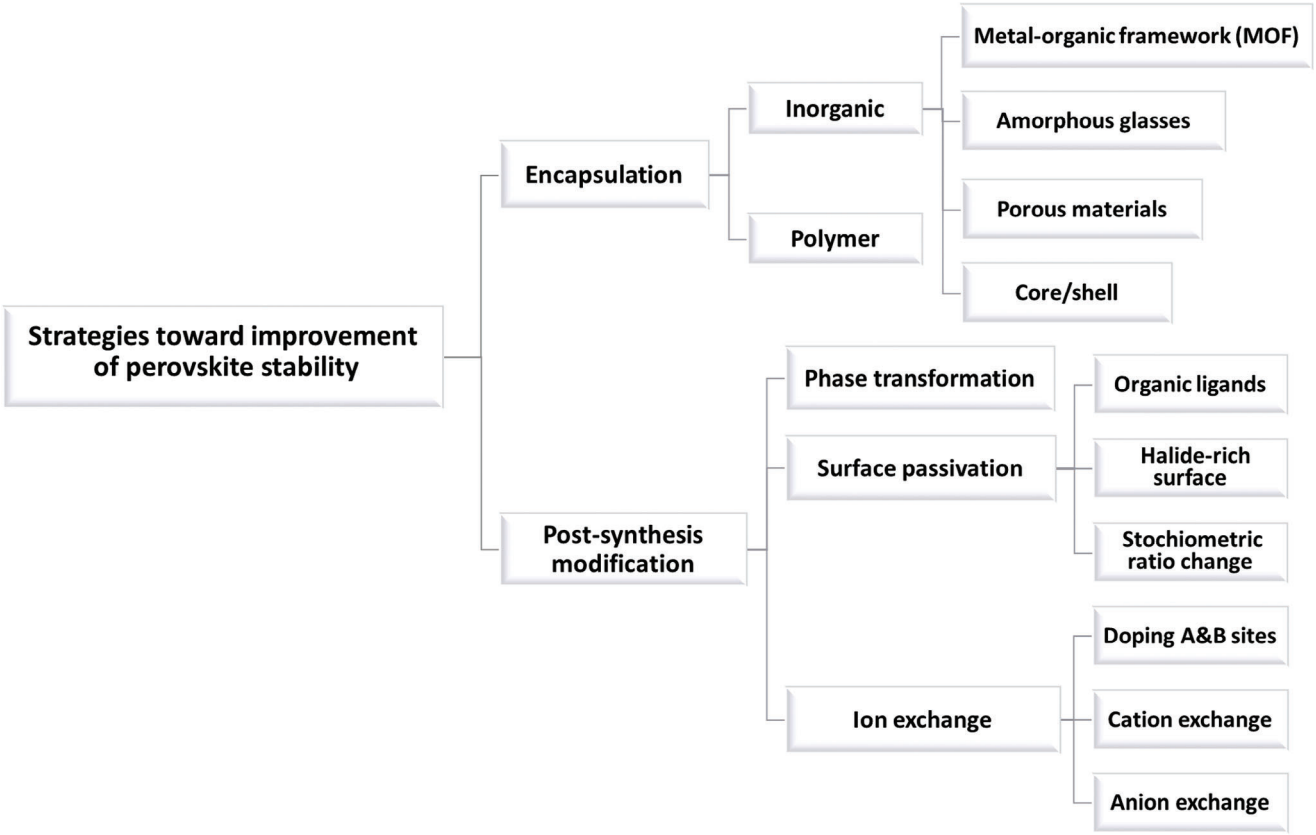

Figure 5. Different strategies toward the improvement of perovskite stability by encapsulation and post-synthesis modification.

films could maintain 100% of the PL intensity for over 153 h.[100] Didodecyl dimethyl ammonium bromide (DDAB) a relatively short-chain ligand was used for replacing oleylamine and oleic acid ligands in $CsPbX_3$ NCs via the ligand-exchange strategy to yield PeNCs films with better stability and enhanced LED performance.[101] In another work, Manna's group[102] demonstrated a simultaneous cationic and anionic ligand displacement on the surface of $CsPbBr_3$ NCs with quaternary ammonium bromides (R_4NBr) exhibiting enhanced colloidal and thermal stability and higher PLQE than untreated $CsPbBr_3$ NCs. Moreover, doping or alloying of PeNCs increases their formation energy, resulting in enhanced colloidal stability and optical features. Over the years, several reports have been focused on improving the stability of the PeNCs via A- and B- -site doping or alloying with metal cations like Mn^{2+}, Sn^{2+}, Zn^{2+}, Sr^{2+}, and Ni^{2+}.[103–105] Zou et al.[106] showed that the partial substitution of Pb^{2+} by Mn^{2+} in $CsPbX_3$ NCs improved the thermal stability of the perovskite lattice, being stable up to 200 °C under ambient conditions. **Table 1** provides some selected examples of the stability improvements achieved for $CsPbX_3$ NCs modified with different materials, in terms of the degree of perseverance of their PLQE, resistance to UV light, thermal and water treatments, and overall stability

Table 1. Selected examples of reported stability improvements toward several factors achieved by modification of $CsPbX_3$ NCs by different materials.

PeNCs	Modification material	Best PLQE [%]	UV light resistance [h]	Thermal resistance [°C]	Water resistance [h]	Stability under ambient conditions [days]	Reference
$CsPbBr_3$	Amorphous glasses	70	>20	80	>1080	>45	[48]
$CsPbX_3$	MOF	62	80	>80	_	>60	[107]
$CsPbBr_3$	Mesoporous silica	46.2	>120	95	>120	>30	[108]
$CsPbBr_3$	Polymer matrix (PMMA)	54.6	_	>80	>48	>30	[109]
$CsPbX_3$	Silica gel matrix	60	360	>50	>24	_	[110]
$CsPbBr_3$	Core/shell (TiO_2)	_	>24	_	>2160	_	[82]
$CsPbCl_3$	B-site doping (Mn^{2+})	40	_	>110	_	_	[111]
$CsPbBr_3$	Surface passivation (halide-rich surface)	75	_	_	_	_	[111]

under ambient conditions. One can recognize that in situ encapsulation with inorganic amorphous glasses offers significant protection, among other methods.

3. $CsPbX_3$ NCs@Glass Composites

3.1. Amorphous Glasses: Exploring the Evolution of Glass Structures

Glasses have been used by mankind since ancient times; however, a new research avenue appeared in the 1950s when amorphous semiconductor glasses were introduced.[112,113] Their main categories are chalcogenide glasses and oxide glasses, both of which are regularly prepared via melt-quenching technique. However, the former ones require an evacuation system, as their precursors are highly reactive with oxygen at high temperatures. Therefore, the fabrication process must be performed in an evacuated silica tube which needs more complicated fabrication instruments, and it takes at least 10 h of melting process at high temperatures (regularly more than 900 °C). In comparison, the fabrication process of the oxide glasses can be performed under air, and it typically takes less than 20 min of heating at melting temperature. For these reasons, oxide glasses are better choices to encapsulate PeNCs. As a compact amorphous structure, oxide glasses are based on a main component (denoted as a glass-former), typically GeO, P_2O_5, B_2O_3, SiO_2, or TeO_2. Additionally, to improve the characteristics of these glasses, other oxides, termed glass-modifiers, are often included; among those are transition metal, alkali, or alkaline earth oxides.[114,115] These additives improve the structural stability of the matrix and may change the optical and electrical features of the whole system. By utilizing molecular dynamics simulations, Achraf et al. showed that the mixed alkali (Na_2O substitution with Li_2O or K_2O) does not influence the connectivity of the glass matrix but determines its elastic moduli and ionic mobility.[116] A second glass-former can also be employed to fine-tune the composition of glasses, for example, decreasing the melting temperature or enhancing the ionic conductivity.[117] These structures also have a unique polaronic site-assisted electron conductivity that is explained by hoping the electron between these sites.[115]

3.2. Unlocking the Existing Properties of PeNCs@Glass Composites

Structural and morphological properties: The most widely used inorganic glass is silicate glass, with continuous Si-O tetrahedrons possessing a short-range order amorphous network. As mentioned earlier, the simultaneous use of two glass formers for the preparation of glass matrices can promote the advantages of the resulting composite, such as a decrease in melting temperature and subsequent improvement in the distribution of PeNCs inside the matrix. In a recent study on borosilicate glasses,[51] luminescent $CsPbX_3$ PeNCs were embedded in the interstitials of the glass network via in situ glass crystallization method, where they were surrounded by [SiO_4], [BO_4], and [BO_3] structural units (**Figure** 6A), without any evidence of the phase separation.

TEM images of the $CsPb(Br/I)_3$ NCs@glass composite provided in Figure 6B show that PeNCs were indeed homogeneously distributed within the host matrix, comparable with other methods used for improving the stability of PeNCs like MOFs,[118] SiO_2,[119] polymers,[120] etc. Due to the homogeneity of the amorphous glass matrix, there was no preferential direction for the growth of these crystallites, so the PeNCs had a spherical shape, which is also exemplified by the HRTEM micrograph in the inset of Figure 6B with distinct crystal lattice fringes (0.293 nm for (200) crystal planes). The PeNCs possessed small sizes in the range of 5–10 nm and thus experienced a quantum confinement effect. Therefore, the in situ glass encapsulation results in the formation of tiny PeNCs with sizes identical to the other encapsulation methods. Perovskite-related reflexes appeared in the broad XRD pattern of the precursor glass (PG-melt quenched and annealed glass, before the heat-treatment process) as shown in Figure 6C, which were superimposed on the amorphous background after employing the heat-treatment processing. Those distinct diffraction peaks appeared after the crystallization of perovskites and shifted toward smaller diffraction angles when the composition changed from $CsPbBr_3$ to $CsPb(Br/I)_3$ with the increase of the I-to-Br ratio. The PL intensity of PeNCs protected by glass has been monitored for up to one month when the composite was in direct contact with water, and only a ≈10% reduction in PL intensity has been observed. This was a remarkable improvement compared to the colloidal PeNCs experiencing a complete PL quenching after 4 h in contact with water.

Tuning the bandgap: Importantly, by growing PeNCs in glasses, one can still ensure the tuning of their bandgap, pretty much like the case for colloidal PeNCs synthesized in solution, which could be conveniently achieved by changing the molar ratio of I/Br anions in the $CsPbI_xBr_{3-x}$ NCs.[121] As shown in **Figure** 7A, the bandgap of the $CsPbI_xBr_{3-x}$ NCs@glass composites determined from the Tauc plots was significantly smaller for iodide-only based PeNCs (1.87 eV) than for bromide-only based PeNCs (2.42 eV), while bandgaps for mixed-halide compositions located in between those extremes. Figure 7B provides estimated bandgaps along with absolute positions for conduction band minima (CBM)/ valence band maxima (VBM) for the studied cases.

Emission properties: Similarly, ensuring tunable PL emission characteristics of the PeNCs@glass composites while preserving high PLQE and narrow PL bandwidth (full width at half maximum, FWHM) is critical. This again could be provided by varying the halogen composition of PeNCs, as was demonstrated by Yang et al.[51] The PL emission of the reported $CsPbX_3$ NCs@glass composites could be tuned over the wide range of the visible spectrum from 499 to 627 nm by changing the anion composition from Cl/Br to Br and finally to Br/I with different anion ratios (**Figure** 8A). Figure 8B provides the dependence of the FWHM value on the emission wavelength: a red shift in the PL position resulted in some broadening of the emission, with FWHM increased from 21 nm for the green-emitting composites to 36 nm for the red-emitting ones. Importantly, PLQE for the $CsPbBr_3$ NCs@glass (emitting at 517 nm) was as high as 63%, and 46% for $CsPbBr_{1.5}I_{1.5}$ NCs@glass (emitting at 627 nm), as shown in Figure 8C. PL decay times of those composites with varying mixed-halide compositions, summarized in Figure 8D, indicate that those values were rather long, in the range of 100–440 ns.

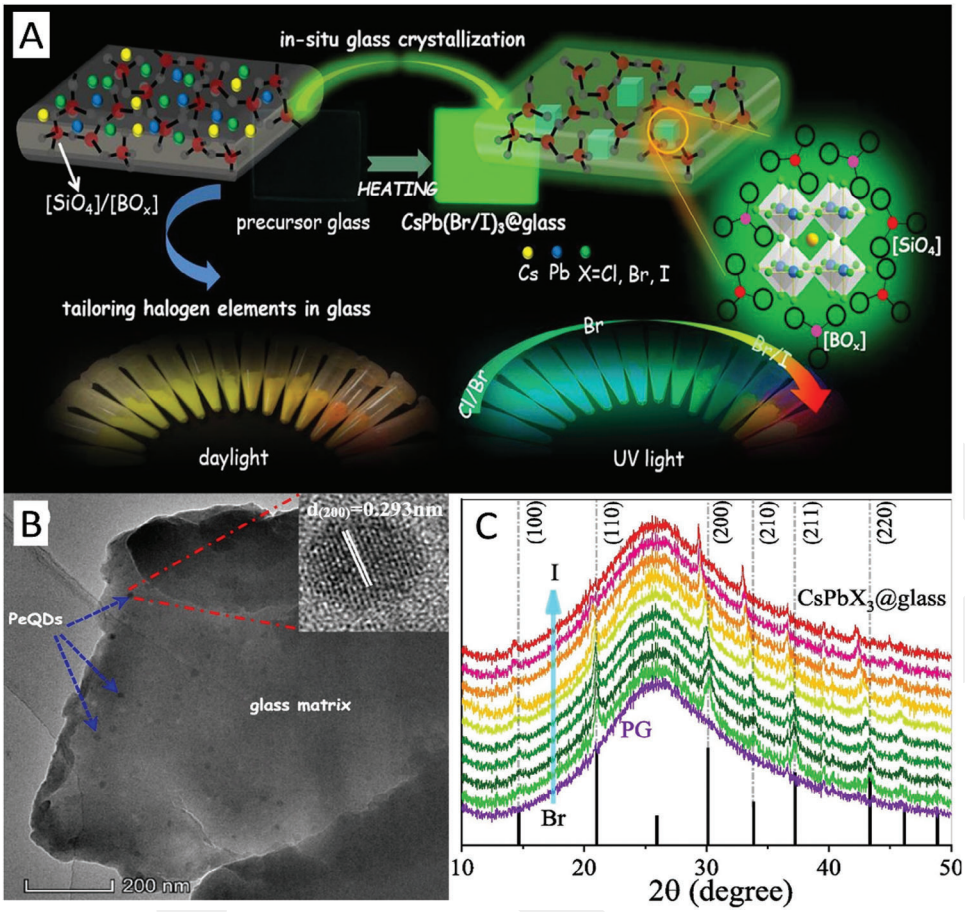

Figure 6. A) Schematics of the fabrication process of $CsPbX_3$ NCs@borosilicate glass composites via in situ glass crystallization method, together with photographs demonstrating their emission color under UV excitation. B) TEM image of $CsPbBr_{2.52}I_{0.48}$ NCs@glass; inset is the HRTEM micrograph of an individual PeNC. C) XRD patterns of the precursor glass (PG- melt quenched and annealed glass, before heat-treatment process) and the prepared $CsPb(Br/I)_3$ NCs@glass composites. Reproduced with permission.[51] Copyright 2020, Elsevier.

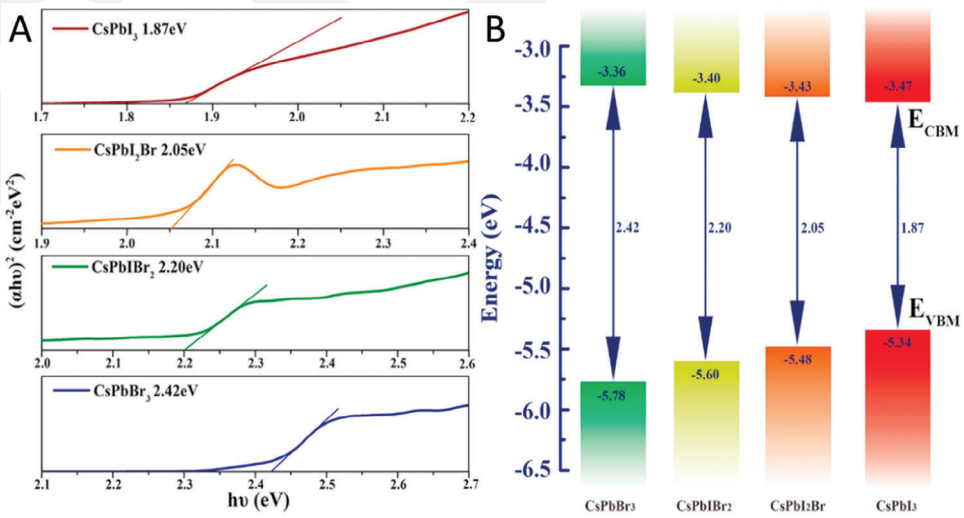

Figure 7. A) Tauc plots for $CsPbI_xBr_{3-x}$ NCs fabricated in glass matrix; straight lines point out the values of the optical bandgaps. B) Energy level diagram of these $CsPbI_xBr_{3-x}$ NCs. Reproduced with permission.[121] Copyright 2018, Elsevier.

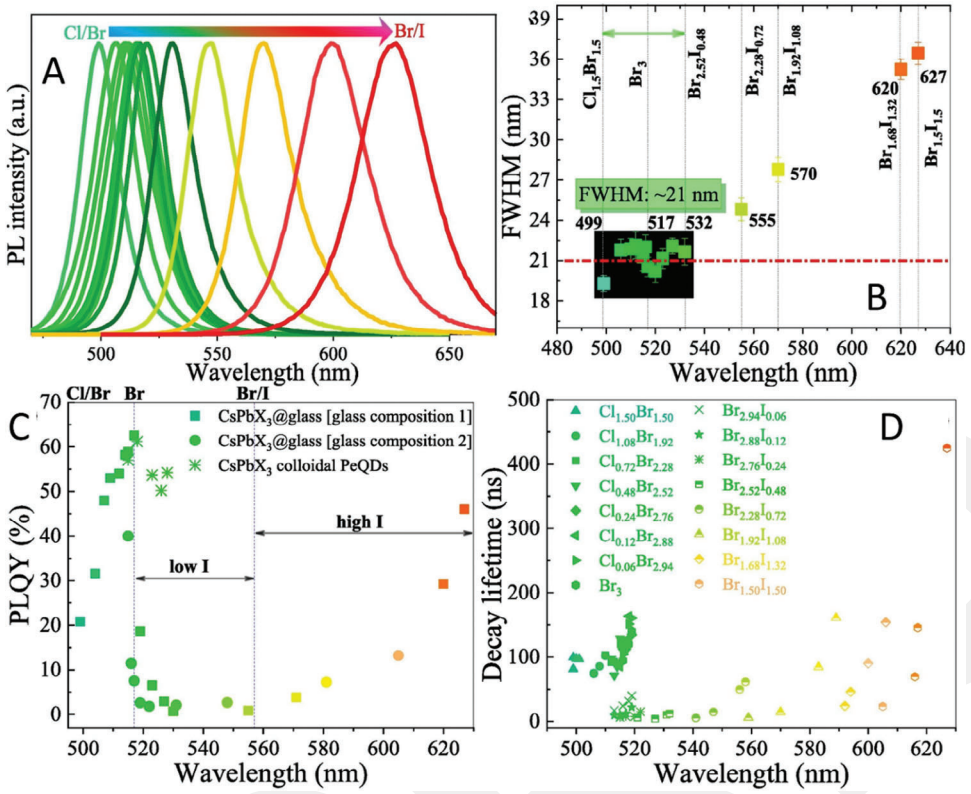

Figure 8. A) PL spectra of the $CsPbX_3$ NCs@glass composites with varying halide anions. B) FWHM of PL spectra, and C) PLQEs of the $CsPbX_3$ NCs@glass composites of two different kinds. D) PL decay times of the $CsPbX_3$ NCs@glass samples with varying mixed-halide compositions. Reproduced with permission.[51] Copyright 2020. Elsevier.

Tunability and stability of emission: The beneficial stability of $CsPbBr_xI_{(3-x)}$ NCs@glass composites produced within the multi-component B_2O_3-SiO_2-ZnO-Cs_2CO_3-$PbBr_2$/I_2-NaBr/NaI glass matrix was evaluated in Ref.[[67]]. First of all, the variation of the Br/I halogen content resulted in PeNCs with broadly tunable absorption/emission colors (**Figure** 9A,B), including a pure green emission at 522 nm with FWHM of 26 nm and a purely red emission at 629 nm with FWHM of 35 nm. The protective role of the glass matrix against external conditions is demonstrated by photographs and respective PL intensity provided in Figure 9C–F, which exemplify the long-time stability (preservation of more than 90% of the initial PL intensity) for both green- and red-emissive composites after 360 h immersion in water (Figure 9C,D) and under continuous light irradiation with 365 nm UV LED (Figure 9E,F).

3.3. Fabrication of PeNCs@Glass Composites: Innovative Techniques for Advanced Composites

There are many methods for the fabrication of NC-embedded glass ceramics, such as melt-quenching, sol-gel, ion-implantation, ion exchange, ball milling, and laser ablation methods.[26,122,123] Among them, melt-quenching (also known as co-melting) is much more common for the preparation of PeNCs@glass composites, because it is a simple method without the necessity of using ligands or an inert reaction atmosphere, which offers the possibility of fabrication of composites on a large-scale. Schematic diagrams of the melt-quenching route and heat-treatment are given in **Figure** 10A. In this method, the raw materials, including perovskite components and glass components are mixed and ground into fine powders. Then, the glass melt is obtained by heating the raw materials to the melting temperature, during which the constituents of PeNCs become uniformly distributed in the glass melt. Herein, the glass matrix can be considered a "solid solution" and the PeNCs can be considered a "solute". The required melting temperature is typically between 700–1350°C, making it impossible to fabricate organic-inorganic PeNCs such as $FAPbX_3$ with organic cations (FA stands for formamidinium) inside glassy matrices. This temperature depends on the type and molar ratios of the glass formers used. From this point of view, the glass melting temperature of various glass-formers conforms to the sequence of phosphate (650–800 °C) < tellurite (750–950 °C) < borophosphate (800–1000 °C) < borate (≈1000 °C) < phosphosilicate (≈1100 °C) < borogermanate (1000–1200 °C) < boro-germanosilicate (1100–1300 °C) < borosilicate (1200–1350 °C) < silicate (<1300 °C). Since the halide components of PeNCs used in the synthesis of these composites are volatile at high temperatures, glasses with a low enough melting point are more desired, and fabrication of PeNCs@glass compositions using multiple glass-formers could be a rational way to fulfill this requirement. Besides the presence of glass-formers, other glass-modifiers, including transition metal oxides or alkaline oxides have been widely considered to

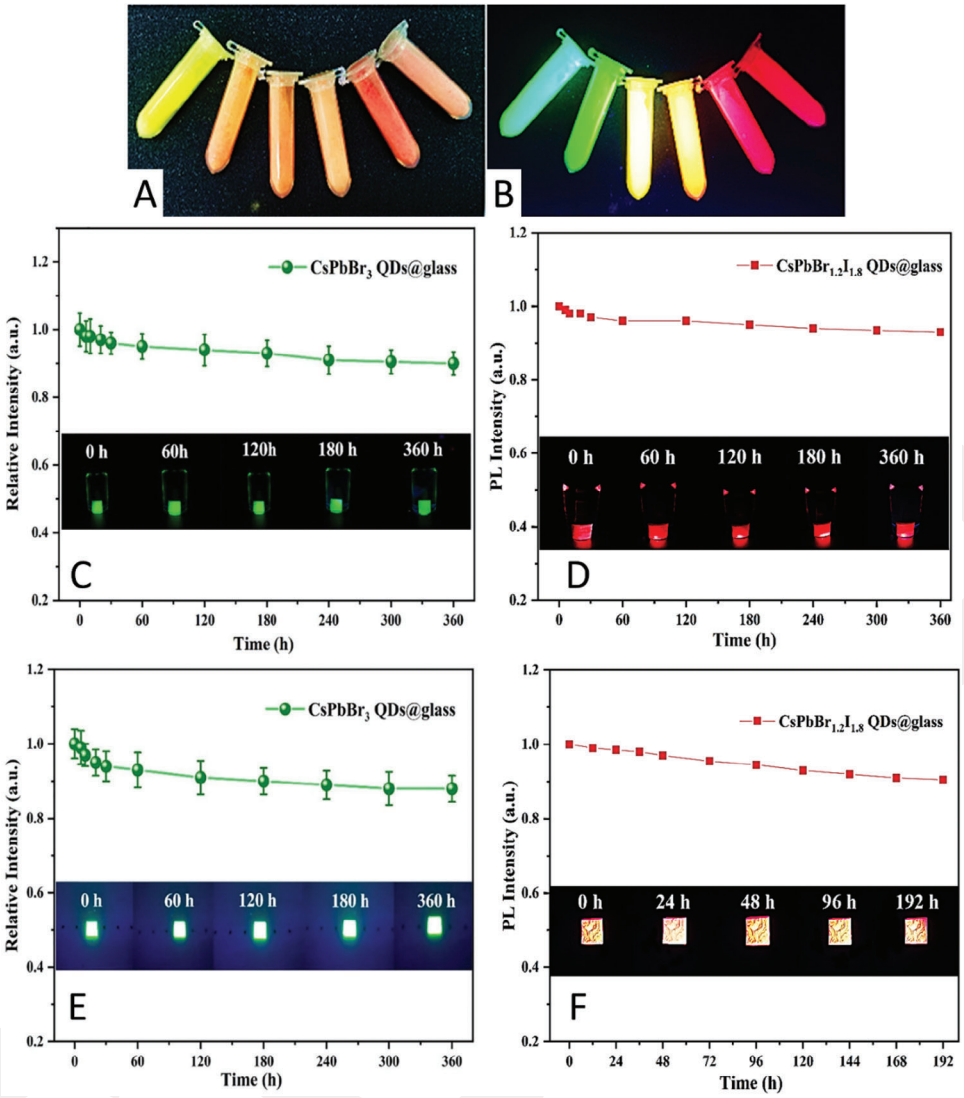

Figure 9. A,B) Photographs of $CsPbBr_xI_{(3-x)}$ PeNCs@glass composition taken under daylight and 365 nm UV light irradiation, respectively. The water stability of C) green-emitting $CsPbBr_3$@glass and D) red-emitting $CsPbBr_3$@glass (under continuous illumination with 365 nm UV LED). The optical stability of E) green-emitting $CsPbBr_3$@glass and F) red-emitting $CsPbBr_3$@glass (under continuous illumination with 365 nm UV LED). Insets show corresponding photographs of the samples. Reproduced with permission.[67] Copyright 2022, Elsevier.

modify the physicochemical properties of the glassy network. As exemplified in **Table 2**, such glass modifiers help to achieve durable glasses with lower melting/quenching temperatures or changes in different properties of the glasses.

In the next step, the melted compounds (including the solid solution and solute) are rapidly quenched in a mold pre-heated at a lower temperature to form the glass matrix, and the PeNCs@glass system remains at this temperature to reduce the whole energy of the composite by releasing the stress of the lattice.[22,29] Such a rapid quenching process causes the perovskite precursors not to have enough time to combine and agglomerate, and hence they can be uniformly distributed in the glass matrix. Afterward, the glassy structure is formed; nonetheless, the rigidity of the glass matrix itself can be a barrier limiting the growth of PeNCs. Therefore, a further heating process known as heat treatment is usually required to facilitate the growth (precipitation) of PeNCs (Figure 10A). This process should be performed at a temperature higher than the glass transition temperature (T_g) of the selected PeNCs@glass composite. Below T_g, the glass network is still quite rigid, so the driving force of the diffusion process for the formation of PeNCs is not enough. But at temperatures above T_g, the matrix is not that rigid, facilitating the movement of perovskite precursors, and thus more PeNCs can be formed. In this case, the average size of an ensemble of NCs will depend directly on the temperature and duration of the heat-treatment process. In general, higher heat-treatment temperature leads to the easier formation of PeNCs and bigger average sizes. As a result, higher concentrations of PeNCs in a glass matrix may reduce the transparency and efficiency of the emitted light.[131] Therefore, this step needs precise and well-arranged processing. Ion exchange also has a great potential to control the spatial distribution of NCs in glasses. Depending on the exchanged ions in glasses, various

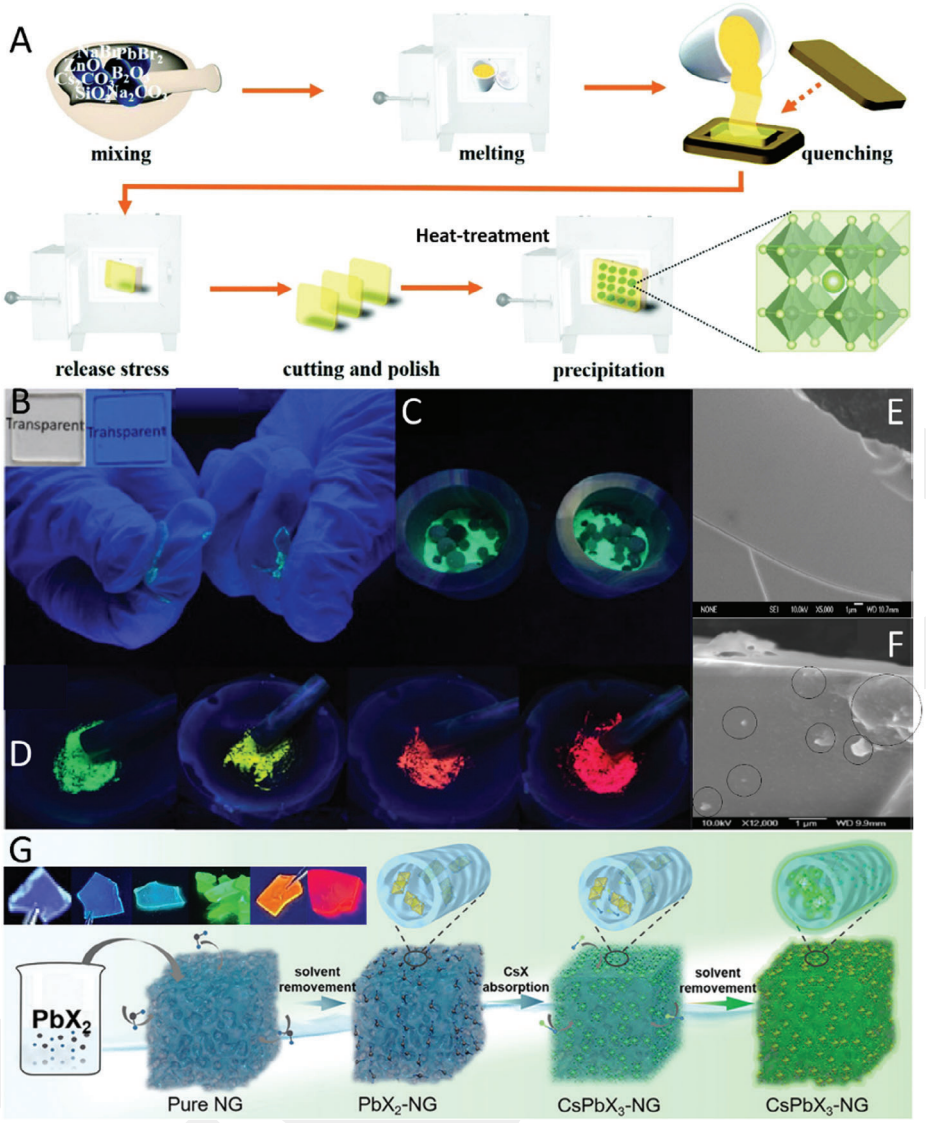

Figure 10. A) The fabrication process of PeNCs@glass through melt-quenching technique and controllable heat treatment. Reproduced with permission.[22] Copyright 2021, Royal Society of Chemistry. B) Photographs of PG under daylight and 365 nm UV light show a transparent sample with no emission. C) Large-scale production of luminescent glass composite powders through ball milling, which shows fracture-induced luminescence. D) Multi-color emission was obtained in the grounded PeNC@glass samples with various ratios of Br/I. E,F) The SEM images of the PG and ground glass powder. Reproduced with permission.[66] Copyright 2019, Springer Nature. G) Schematic diagram of the preparation of $CsPbX_3$ NCs within nanoporous glass (inset shows $CsPbX_3$ NCs@nanoporous glass with different ratios of halogens under UV light covering emission wavelengths of 420–630 nm). Reproduced with permission.[133] Copyright 2022, Wiley-VCH.

Table 2. Effects of some glass modifiers on amorphous oxide glass matrices.

Glass-modifier	Function	Reference
Na_2CO_3	Lowering the glass transition temperature (T_g).	[124]
CaO	Modifying the network to obtain stable glasses with lower melting temperature and facile nucleation/growth.	[125]
Al_2O_3	Increasing the thermal resistance, and creating high durability of the glass.	[126]
MgO	Increasing stability of the glass.	[127]
PbO	Reducing the melting temperature and melt viscosity of silicate glass.	[128]
ZnO	Increasing thermal, mechanical, and chemical resistance.	[44]
SrF_2	Adjusting the properties of the glass matrix, including the melting temperature, the halide solubility, and the hydroxyl content.	[129]
CaF_2	Promoting the NCs' precipitation and growth.	[130]

types of NCs can be precipitated in the ion-exchanged layer. Noble metal ions introduced into glasses through ion exchange are promising choices to control the spatial precipitation of semiconductor NCs in the surface layer of glasses. It also changes the refractive index of the ion-exchanged glasses, making it possible to realize linear and plate waveguides using the glass medium. In Ref.[132], borosilicate glasses containing alkali, lead, and halogen elements were prepared, and $CsPbX_3$ PeNCs were precipitated in the surface layer of the glasses simultaneously during the cesium-potassium ion exchange. $CsPbX_3$ PeNCs were successfully precipitated on the glass surface through ion exchange in molten cesium nitrate salt. By adjusting the amount of halide components in the glass, $CsPbCl_{3-x}Br_x$ and $CsPbBr_{3-x}I_x$ PeNCs with tunable composition and emission (from blue to red) were obtained, as well.

There have also been other approaches to assist the crystallization of PeNCs in the glass. Wang's group prepared transparent phosphate-based $CsPbBr_{3-x}/I_3$@glass nanocomposites via stress-induced crystallization of glasses and formation of $CsPbBr_3$ NCs at the surface of the glass, where the bond breakage was responsible for crystallization.[66] The authors indicated that while the PG is quite transparent with no PL (Figure 10B), after breaking or grinding the as-fabricated samples (using an external mechanical force), PL emission becomes observable in the fractured cross-section of the broken specimen or all parts, respectively (Figure 10C). Interestingly, this method was extended to different molar ratios (*x* value), resulting in powdered composites with tunable emission from 510 nm (green) to 690 nm (deep red) (Figure 10D). They also prepared materials on a large scale (60 g per batch), which emitted over the visible spectrum region, from green to red, with a proven ability for use in pressure-sensitive pens. The SEM images of the PG (Figure 10E) and ground glass (Figure 10F) powder also confirmed the assertion of stress-induced precipitation of PeNCs, because tiny particles were observable in Figure 10F, whereas nothing was detected in the SEM of the PG.

Besides the melt-quenching technique, oxide glasses can be fabricated via the sol-gel method. Hu et al. used this approach to grow confined $CsPbX_3$ (X = Br, Cl, I) PeNCs within an optically transparent, robust, and monolithic matrix of nanoporous glass via a wet chemistry approach (Figure 10G).[133] They initially prepared a nanoporous glass (Al_2O_3-SiO_2) using aluminum lactate and tetraethyl orthosilicate with pore sizes of ≈2.9 to ≈7.8 nm. Then, it was immersed into a PbX_2 solution to absorb perovskite precursor into the nanoporous channels. After removing the extra solvent, the composite was immersed inside the CsBr solution, where the immediate formation of $CsPbX_3$ PeNCs was realized (the Inset of Figure 10G shows the wide-tunability of emission color for the final composite). After one more round of vacuum drying to remove the solvent, the luminescent composites with bright green emission (in the case of $CsPbBr_3$) were used to fabricate LEDs with a recoverable sensing ability of CH_3I. This synthetic protocol also provided fine control over the size of precipitated PeNCs by tailoring the pore sizes.

In another method recently proposed by Li et al., $CsPbX_3$ (X = Cl, Br, I) PeNCs were obtained within a mesoporous SiO_2 layer using the template-assisted method.[134] However, since the pores might still be the source of instability, the authors used low-melting temperature phosphate glass to fully encapsulate the PeNCs. The encapsulation process was performed via solution-combustion in such a way that metal nitrate precursors of glass (KNO_3, $Al(NO_3)_3.9H_2O$, $Zn(NO_3)_2.6H_2O$) were used as oxidizers while $CO(NH_2)_2$ worked as the fuel. Then, a desired amount of $CsPbX_3$@SiO_2 composite was added to the aqueous solution of the mentioned chemicals, followed by heating at 520 °C for 30 min under air. The produced samples showed strong and stable PL at 470, 518, and 658 nm alongside with FWHM of 18 nm for green-emissive and 32 nm for red-emissive composite.

Xiang et al.[135] reported a facile self-crystallization for a well-designed PeNC@glass composite during the melt-quenching step and evaluated the effect of various crystallization techniques on the preparation of the $CsPbBr_3$ NCs@silicophosphate glasses (**Figure 11**). They considered three different routes: route 1: without heat-treatment ("self-crystallization"), route 2: controlled glass crystallization through heat-treatment ("heat treatment"), and route 3: mechanical-driven glass crystallization ("grinding"). In route 1, the lack of heat-treatment caused uncontrolled growth of PeNCs in the melt, which ended in the large $CsPbBr_3$ crystals and correspondingly opaque appearance of the final composites. In route 2, the crystallization was controlled by applying further heat-treatment, which drove the diffusion and rearrangement of atoms in a controlled manner; therefore, it led to the relatively narrow size distribution of PeNCs and good transparency of composites. In route 3, glass crystallization occurred in the stress-concentrated area; by applying mechanical force, the glass network bonds were broken and provided the required activation energy for crystallization. In this route, rapid ionic exchange of Br^-, Pb^{2+}, and Cs^+ during the grinding process could produce a large number of $CsPbBr_3$ nuclei and result in limited crystal growth because of quick consumption of Br, Pb, and Cs sources in the glass matrix. XRD patterns of $CsPbBr_3$ NCs@silicophosphate glass composites originating from these three routes (Figure 11A) illustrate the differences. Samples prepared via route 2 and route 3 showed weaker diffraction peaks of $CsPbBr_3$, whereas the one made via route 1 (self-crystallization) possessed much stronger diffraction peaks due to the successful crystallization of the $CsPbBr_3$ NCs. This result was achieved by the higher ionic mobility of the perovskite constituents during glass melting than in cases of thermal-annealing or mechanically affecting the "frozen" glass, and at the same time, employing a proper glass composition. The outcome was a higher density of PeNCs precipitated in glass and an increase in the intensity of peaks in the XRD pattern in the case of route 1. Therefore, the uncontrolled nucleation and growth in the glass melt led to the formation of larger $CsPbBr_3$ crystallites with a rather broad size distribution. That is why the samples obtained via route 1 (self-crystallization) appeared opaque; at the same time, they showed strong PL under 360 nm UV light excitation (Figure 11B) with the peak wavelength located at 523 nm (Figure 11C). Also, there was no PL signal for PG samples, which confirmed the main role of precipitated PeNCs in the emission characteristic of the composites. $CsPbBr_3$ NCs prepared via route 1 had a narrower PL FWHM of ≈30 nm, the highest PLQE of 48%, and showed better environmental stability as compared to composites fabricated via the other two routes. The SEM images of the surface of the composites prepared via the three mentioned routes are provided in Figure 11D–F and indeed demonstrate the formation of $CsPbBr_3$ crystals with bigger sizes in the case of self-crystallization route

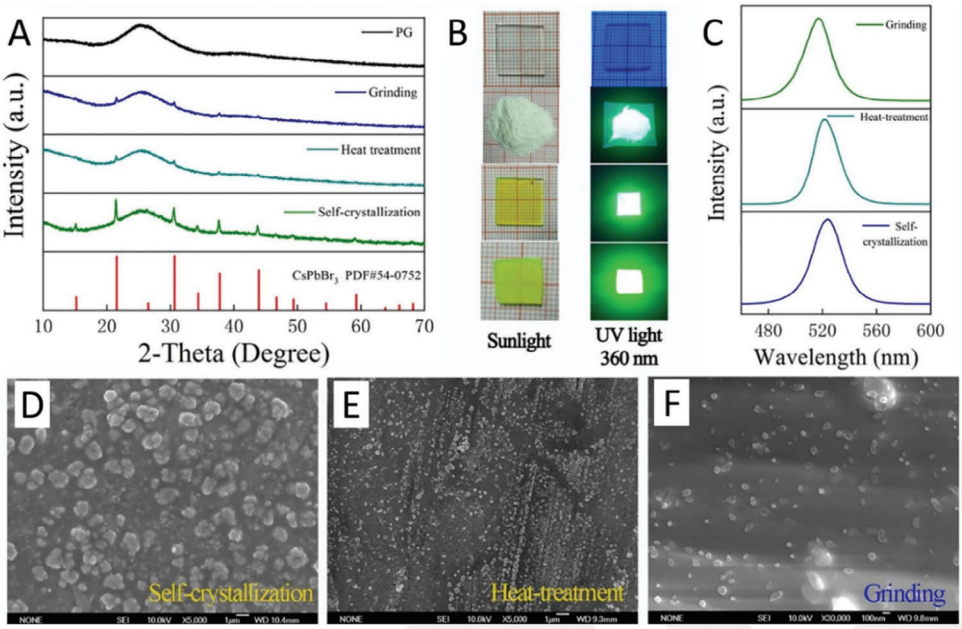

Figure 11. A) Comparison of XRD patterns of PG and $CsPbBr_3$ NCs@ silico-phosphate glass composites obtained via three different routes: self-crystallization, heat-treatment, and grinding. B) Photographs of these samples under sunlight and UV excitation at 360 nm UV light. C) PL spectra of three composites. D–F) SEM images of the surface of three composites were prepared via different routes. Reproduced with permission.[135] Copyright 2019, Elsevier.

(63–1450 nm) (Figure 11D) rather than other routes (90–120 and 16–160 nm for route 2 and 3, respectively) (Figure 11E,F). These observations support the idea of facile growth of $CsPbBr_3$ NCs in the glass matrix in the case of employing self-crystallization. While reaching an improved emission is always demanding, however, in this case, SEM images imply uncontrollable growth of PeNCs for self-crystallization. This is an undesired property because it decreases the composite's reproducibility and the ability to manage/control the properties of the composite (as evidence, the self-crystallized composite is opaque under daylight in Figure 11B). Therefore, applying heat-treatment is useful to achieve control over the physicochemical properties of a composite.

4. Approaches Used to Improve the Properties of $CsPbX_3$ NCs@Glass Composites

The melt-quenching technique is considered a relatively straightforward method that allows precipitation and encapsulation of NCs within the glass matrix. However, the intrinsic features of the glass networks sometimes create destructive effects, making it mandatory to apply proper modifications to ensure the precipitation and encapsulation of PeNCs. One of the challenges is the necessity of employing very high temperatures for melting powders, which can go as high as 1300 °C, depending on the volatility of halides at high temperatures.[31] Another limitation is related to the difficulty of precipitation of PeNCs in the glass matrix with a tight binding, which inhibits the release and diffusion of perovskite's precursors.[49] It is also significant for many applications to ensure high PLQE of resulting PeNCs@glass composites, and to prevent undesired reabsorption.[32] To deal with these challenges, various approaches have been proposed, which are summarized in **Table 3** and will be further discussed in this review. We divided them into three categories: compositional modifications, structural modifications, and dual encapsulation. The approaches related to the variation of the precursors to manipulate the properties of the PeNCs@glass composites fall under the category of compositional modifications, which are applied before the fabrication of the composite. Structural modifications are applied to the glass matrix to facilitate the growth of PeNCs after the fabrication of the initial composite, while dual-encapsulation refers to the use of a proper secondary component to incorporate PeNCs in a matrix and to improve their stability and functionality.

4.1. Compositional Modification

4.1.1. Glass Network Doping

One of the limitations of silicate glasses is their compact, dense structure which reduces the chemical activity of perovskite precursors. Indeed, strong Si—O bonds prevent the release of cations and anions inside the glass.[147] There are two approaches to address this issue: using non-silicate glass, and doping the glass network. Non-silicate glasses are characterized by weak bonding and low melting temperature, which may have advantages and disadvantages, such as a more effortless fabrication process and lower stability of the PeNCs@glass composites.[148] Therefore, the strategy that still offers the benefits of silicate glass's compact structure while simultaneously achieving more optimal PeNC precipitation is doping the glass network using suitable additives. Popular additives in oxide glasses are metal oxides, such as TiO_2 and Ag_2O used for doping into silicate glass matrices,[65,137] which play the role of oxidizing agent in the formation of the

Table 3. Summary of reported approaches and materials used to improve the properties of $CsPbX_3$ NCs@glass composites, including the course of action and their specific advantages.

	Approach	Specific examples	The course of action and specific advantages	Reference
Compositional modification	Glass network doping	F^- doping Li^+ doping Ag_2O doping TiO_2 doping	F^- ions enter the glass network by breaking the Si—O bonds to generate the non-bridging oxygen, which provides sufficient space for the diffusion of perovskite ions. Some other ions like Li^+ promote phase separation in the glass matrix, creating sufficient sites for the nucleation of PeNCs. Metal oxides used as an oxidizing agent during the formation of the crystal phase modify the heat-treatment conditions and subsequent annealing at high temperatures, and enhance the stability of perovskite nanocomposites against water and heat.	[49] [136] [137] [65]
	B-site perovskite doping	Mn^{2+} doping Zn^{2+} doping Sn^{2+} doping Cd^{2+} doping Ni^{2+} doping Lanthanide doping	Doping with metal ions on a B-site using (mostly divalent) cations with a smaller radius than Pb^{2+} can improve the electronic structure of PeNCs by creating additional energy levels within the host energy gap. Doping not only plays a significant role in adjusting PL but can also help to improve structural and chemical stability and reduce the amount of toxic lead.	[131,138] [139] [140] [64] [141] [142,143]
	Glass-former modification	Using non-silicate glass (borate-phosphate-telluride) or modified one (borosilicate)	Non-silicate glasses offer lower melting temperatures and a weaker glass backbone, resulting in improved PeNCs precipitation.	[48]
	Molar-ratio modification	Modification in glass-related components	Changing the molar ratio of glass components helps to make the glass structure with lower melting temperature, promoting precipitation of PeNCs with higher PLQE.	[31,44,130]
		Modification in perovskite-related components	Changing the molar ratio of perovskite components can affect the stability and the PL properties of the PeNCs@glass composite.	[67,135]
Structural modification	Heat-treatment modification	Applying post-synthesis heat-treatment	Applying appropriate heat-treatment in terms of temperature and duration helps to regulate the growth and crystallization of PeNCs inside the glass matrix. This may also help to achieve composites with higher PLQE and improved stability.	[55,144]
	Mechanical/ hydration crystallization	Applying post-synthesis mechanical forces	Leads to the precipitation of PeNCs inside the glass matrix due to easier transfer of the perovskite precursor ions.	[66,145]
Dual encapsulation	Using polymers Using a secondary glass matrix	Polymer (SEBS)/(PDMS) Second low-temperature inorganic glass (phosphate)	Multiphase composite materials offer improved tolerance to water, heat, and ultraviolet (UV) irradiation.	[32,63,146]

crystalline phase in the glass. Besides, these metal oxides are easily soluble in the molten glass and precipitate as microscopic particles during subsequent thermal processes, which can assist in the formation of the main crystalline phase or even glassy substrate. Also, the presence of metal oxides reduces the crystallization temperature and hence eliminates the necessity of high-temperature heat treatment, which is a beneficial factor for facile precipitation of PeNCs in the host glassy matrix.

Tong et al.[61] reported positive effects of TiO_2 on the crystallization of $CsPbX_3$ (X = Br, Cl, I) NCs within borosilicate glasses (SiO_2-B_2O_3-ZnO-Al_2O_3-MgO-Cs_2CO_3-$PbBr_2$-NaBr-(0–3 mol%)TiO_2). They showed that without employing subsequent annealing and heat treatment for this composition, PeNCs were self-crystallized upon adding a proper amount of TiO_2. As judged by the structural analyses, the TiO_2 additive significantly changed the structure of glass, accelerating the migration of perovskite precursor ions (Cs^+, Pb^{2+}, and X^-), which promotes controlled nucleation of PeNCs without the need for heat treatment. In the reported case, PeNCs with average sizes below 4 nm showed intense and stable emission at ≈485, 520, and 631 nm, depending on the type of anions used.[65]

As studied by Si et al., different alkaline-earth metal oxides worked differently in borosilicate-based perovskite@glasses with composition of H_3BO_3-SiO_2-Al_2O_3-ZnO-MgO-$SrCO_3$-$CaCO_3$-$BaCO_3$-Cs_2CO_3-$PbBr_2$-NaBr.[149] They found out that the addition of CaO or SrO into the PeNCs@glass composite facilitated the formation process of PeNCs, while the addition of MgO or BaO inhibited it. As shown in **Figure 12**A,B, composites formed in the presence of Ca^{2+} or Sr^{2+} are yellow due to the formation of PeNCs, and show bright green emission under UV light. The authors suggested that initial phase separation played an important role and was different for the case of different divalent cations, as depicted in Figure 12C. While Mg^{2+} and Ba^{2+} cations decreased ion mobility by strengthening the glass network, Ca^{2+}, and Sr^{2+} cations assisted the breaking of Si—O—Si bonds and reduced its tightness, thus enabling more efficient nucleation and growth of PeNCs inside the glass matrix. Therefore, a proper glass network modifier should be

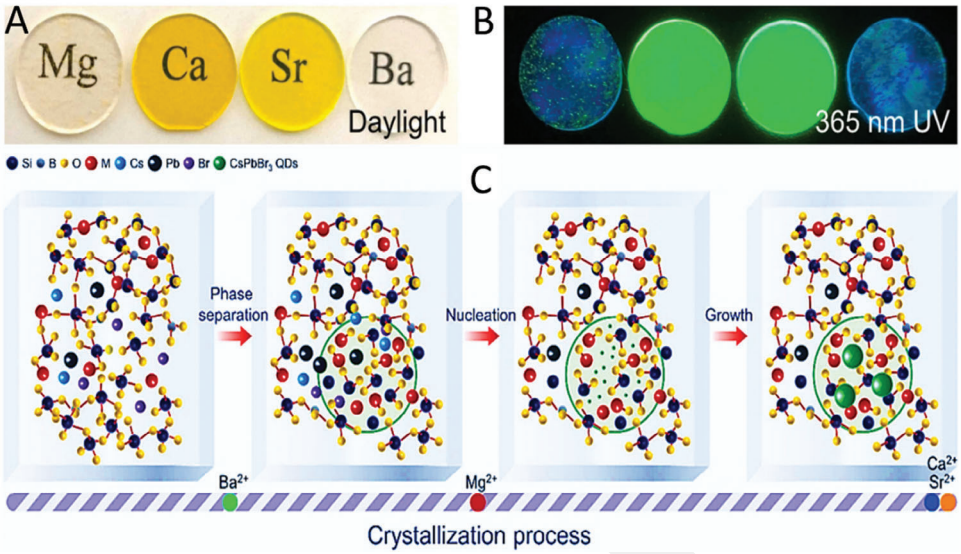

Figure 12. Photographs of the PeNCs@glass composites with MgO, CaO, SrO, and BaO additives, taken under A) daylight, and B) a 365 nm UV lamp. C) Schematics of the in situ crystallization of $CsPbBr_3$ NCs inside the glass networks in the presence of different divalent cations Ba^{2+}, Mg^{2+}, Ca^{2+}, and Sr^{2+}. Reproduced with permission.[149] Copyright 2022, Elsevier.

considered, because some dopants have no effect or even have negative effects on the crystallization of PeNCs. Unlike this, a recent investigation on PeNCs@glass composites made in SiO_2-B_2O_3-ZnO-Al_2O_3-Cs_2CO_3-$PbBr_2$-NaBr-MO (MgO, CaO, SrO, BaO) glass demonstrated the positive effects of all alkaline-earth metal oxides on promoting the crystallization of PeNCs, when they were separately added to the borosilicate glasses.[150] The authors showed that the results obtained for MgO were better than other additives. Mg^{2+} ions have the smallest volume and lowest coordination number compared to the other ions, and thus they created higher fractional free volume and looser glass network, promoting the diffusion of perovskite precursor ions and the formation of PeNCs. Interestingly, the fabricated MgO-modified composites also showed improved stability after six rounds of washing-heating processes.

Apart from the metal oxide precursors, which are compounds of the same kind as the commonly used glass precursors, other additives can also be used to promote nucleation and growth of PeNCs within the glass matrix. As an example, F^- dopant ions from NH_4F precursor have been introduced into oxyhalide borosilicate glass to modify the network structure, facilitating the controllable growth of $CsPbX_3$ (X = Cl, Cl/Br, Br, Br/I, and I) PeNCs.[49] In a typical SiO_2 glass host, [SiO_4] tetrahedrons are firmly connected by bridging oxygen ions (**Figure 13A**). F^- ions entering the lattice structure break some of the Si—O bonds to produce the non-bridging oxygen (Figure 13B), thus providing sufficient space for ionic diffusion of perovskite precursors. However, it still needs an extra activating agent to promote the precipitation of $CsPbX_3$ PeNCs in glass. Applying subsequent heat-treatment triggers the effect of F^- ions resulting in PeNCs (Figure 13C). From the XRD patterns, one can see that no signals were detected for perovskite crystalline structure in F^- ions-free samples even after applying heat-treatment at different temperatures (Figure 13D). At the same time, the diffraction peaks of $CsPbBr_3$ appeared and intensified in the presence of F^- F-dopant ions certifying the formation and growth of crystalline perovskite phases (Figure 13E). The resulting $CsPb(Br_x/I_{1-x})_3$ NCs@glass composites showed bright emission of different colors (Figure 13F), with the highest PLQE reaching 80% for green emission. Another important aspect of this study was the establishment of the dominant role of subsequent heat-treatment on activating the effect of the dopant, demonstrated by increased PLQEs for different perovskite compositions as summarized in Figure 13G. The resulting PeNCs@glass composites showed no significant changes in the PL emission even after 30 days of immersing in water, confirming the durability of the fabricated composites.[49]

To demonstrate the impact of F^- dopant ions in promoting the precipitation and growth of $CsPbBr_3$ NCs within a glassy matrix, another precursor (CaF_2) was added into borosilicate glass SiO_2–B_2O_3–ZnO–BaO–SrO–Cs_2O–$PbBr_2$–NaBr.[130] It was shown that in comparison with the pristine PeNC@glass composites and also the CaO-modified ones, the presence of CaF_2 promoted the formation of PeNCs as confirmed by the appearance of diffraction signals of crystalline $CsPbBr_3$ NCs at all heat-treatment temperatures (490–570 °C). Ca^{2+} ions induced nucleation and growth of PeNCs, while F^- ions increased the interstitial space by breaking the tight glass network due to the conversion of bridging oxygen to non-bridging oxygen bonds. Indeed, the presence of two dopant ions of Ca^{2+} and F^- facilitated the formation of $CsPbBr_3$ NCs in glass due to the reduced activation energy of crystallization. The size of PeNCs increased from 5.6 nm in the case of pristine composite to 17.7 nm in CaF_2-doped composite with narrow green emission (FWHM of 26 nm) and PLQE of ≈40%.

The facilitating role of dopants for the crystallization of PeNCs inside glass structure was demonstrated elsewhere by Li et al., at which the addition of NaF led to the rapid formation of self-crystallized $CsPbX_3$ (X = Cl, Br, I) PeNCs within the borosilicate glass matrix.[151] In this case, both Na^+ and F^- ions concurrently improved the microstructure conditions to assist with the

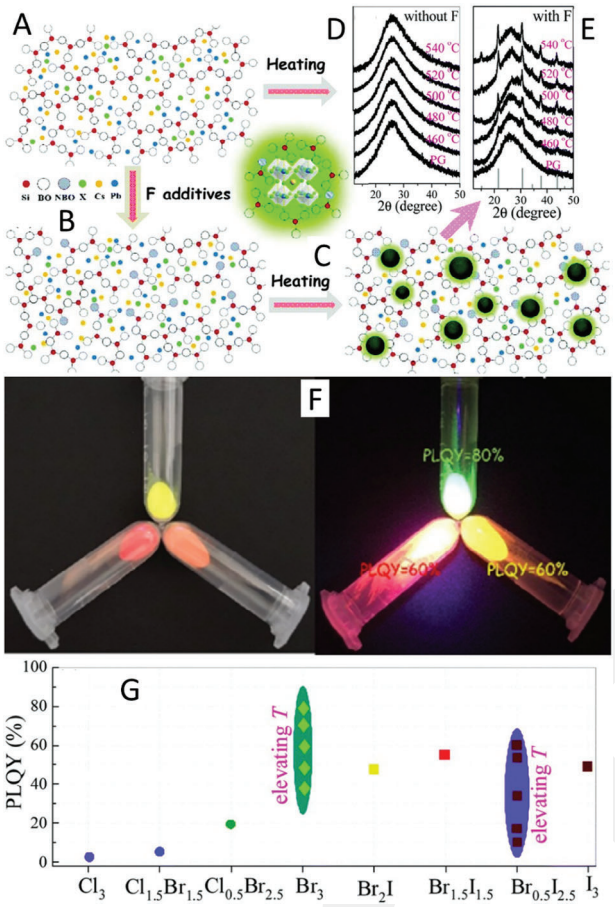

Figure 13. A,B) Schematics of the SiO_2 glass host network without and with F^- ion additives, and C) of the $CsPbX_3$ NC formation in a F-modified glass matrix after heat-treatment. XRD patterns of the samples without F^- (D) and with F^- ions (E) heated at different temperatures. F) Photographs of $CsPbX_3$ (X = Br, I) @glass composites taken under daylight (left) and UV light (right). G) PLQE values for the $CsPbX_3$ (X = Cl, Br, I) NCs@glass composites obtained under increased crystallization temperature. Reproduced with permission.[49] Copyright 2019, Royal Society of Chemistry.

formation of PeNCs during the conventional melt-quenching method without the need for further heat-treatment process. Authors suggested that Na^+ cations enabled the depolymerization of the glass network by disconnecting the Si—O and B—O bonds, which resulted in an extended 3D glassy matrix with more available interior empty spaces to accept perovskite precursor ions. At the same time, F^- anions with strong electronegativity attracted Pb^{2+} and Cs^+ cations, promoting the nucleation and growth of PeNCs in the interstitials of the glass network. By varying the concentration of NaF from 0 to 20 mol%, the undoped composite showed 6% PLQE while it reached 49% for NaF (8 mol%)-doped $CsPbBr_3$ NCs.

Wang et al. reported that the addition of a proper amount of LiBr into borosilicate glass had a dual positive effect on the formation of $CsPbBr_3$ NCs through the simultaneous improvement of the glass network and an increase in the degree of phase separation.[136] Interestingly, their results demonstrated that doping with LiBr could induce self-crystalization of PeNCs without the necessity of heat-treatment. Li^+ doping can increase the degree of the phase separation in the glass network so that the separation of borate and silicate units from each other reduces interfacial energy and activation energy of nucleation for the formation of PeNCs. Even the stability of the resulting composites obtained in the presence of LiBr became better against environmental conditions as compared to the regular heat-treated compositions without this additive.

4.1.2. B-Site Perovskite Doping

Metal ions doping on the B-site in PeNCs not only can partially replace toxic lead but is also a feasible method to increase the thermal and phase stability of these materials. Various divalent metal cations, such as Sn^{2+}, Cd^{2+}, Zn^{2+}, etc., which can partially replace Pb^{2+} cations have been used as dopants (**Figure 14A**).[152] Generally, divalent cations with a slightly smaller ion radius than that of Pb^{2+} (1.19 Å) are suitable alternatives to replace Pb and to improve phase stability by B-site doping. Such substitutional doping results in a slight contraction of the perovskite lattice, which is beneficial for their stability. Among divalent metal cations, Sn^{2+} has been considered a candidate to replace Pb^{2+} (which can be considered as an alloy rather than doping) due to its very similar ionic radius (1.18 Å). However, Sn^{2+}-based PeNCs are highly sensitive to air because Sn^{2+} can easily be oxidized to Sn^{4+}. Liu et al. produced Sn^{2+}-doped $CsPbBr_3$ PeNCs@borosilicate glasses by melt-quenching method and subsequent heat-treatment at different temperatures.[140] As shown in Figure 14B, when the molar amount (x) of Sn increased, the positions of both the absorption edge and PL peaks shifted slightly from 518 nm ($x = 0$) to 506 nm ($x = 0.7$) while maintaining the narrow PL FWHM of 52 meV. At the same time, a significant increase in Sn content ($x = 0.5$ or 0.7) caused the PLQE to decrease. The produced composition also showed outstanding stability in the environment for over 100 days, far better than the bare PeNCs (Figure 14C). Doping the PeNC@glass composite with Zn^{2+} ions, whose ionic radii (0.83 Å) are much smaller than Pb^{2+}, resulted in a slight blue shift of the PL spectrum. Liang's team[139] incorporated Zn^{2+} dopant ions into the $CsPbBr_3$ NCs@glass composites and reported the shift of the PL maximum from 529 to 517 nm (Figure 14D). Figure 14E shows photographs and PL spectra of bare and Zn-doped PeNC@glass composites (PLQE 32–36%). They retained more than 80% of their initial PL intensity after immersion in water for 28 days (Figure 14F).

Another divalent cation that has been used to dope the B-site in perovskites is Ni^{2+}. Ni cations have the same valence as Pb, and almost the same ionic radius as Pb ions, and thus they can easily replace Pb^{2+} ions in the perovskite lattice. Moreover, upon doping with Ni^{2+} ions, the toxicity of the perovskites decreased.[141] Liu et al. produced $CsPbBr_3$ NCs@glasses doped with Ni^{2+} ions via a melt-quenching method.[153] The doping increased the formation energy of PeNCs and improved the short-range order of the perovskite crystal lattice so that the PeNCs@glass composites showed a higher PLQE. Referring to Figure 14G–I, the TEM and HRTEM images of the samples revealed the formation of crystalline perovskites with different lattice fringes, depending on the Ni dopant level. As the concentration of Ni^{2+} increased (from Figure 14G–I), the interplanar distance of the precipitated NCs decreased from 2.89 to 2.41 A°, and the size distribution of NCs

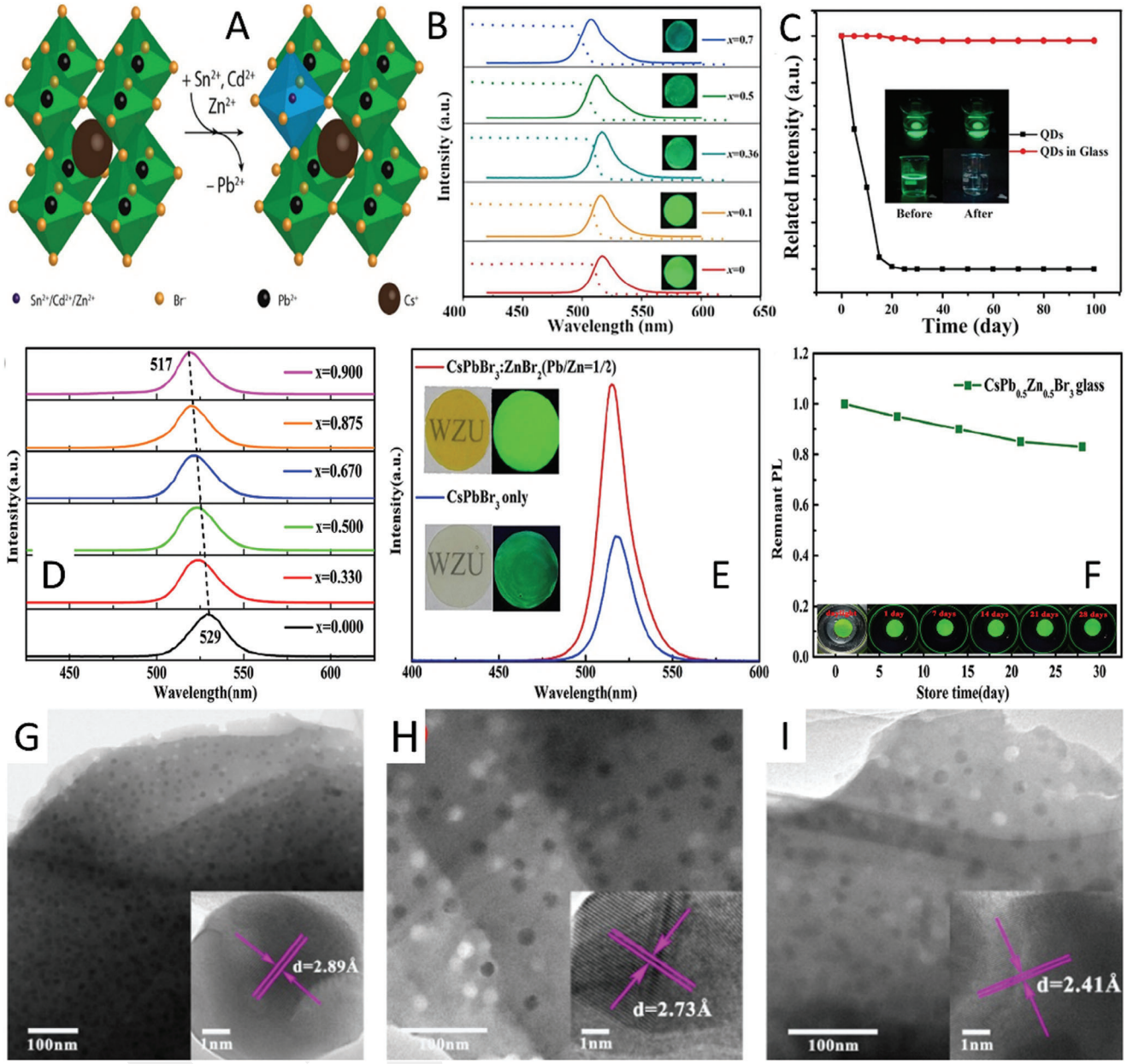

Figure 14. A) Illustration of the B-site doping of $CsPbBr_3$ perovskite lattice with divalent Sn^{2+}, Cd^{2+}, and Zn^{2+} cations having slightly smaller ionic radius than partially substituted Pb^{2+} cations. Reproduced under the term of CC BY-NC-ND.[152] Copyright 2017, ACS Publications. B) PL spectra of $CsPb_{1-x}Sn_xBr_3$ ($x = 0$, 0.1, 0.36, 0.5, 0.7 at 550 °C, respectively) NCs@glass, and C) Photographs of PL intensity trends for $CsPb_{0.64}Sn_{0.36}Br_3$ NCs and $CsPb_{0.64}Sn_{0.3}6Br_3$ NCs@glass kept in air for over 100 days. Reproduced with permission.[140] Copyright 2019, Elsevier. D) PL spectra of $CsPb_{1-x}Zn_xBr_3$ NCs@glass composites with different molar ratios of Pb: Zn. E) Photographs and PL spectra of $CsPbBr_3$ only and $CsPbBr_3$:$ZnBr_2$ NCs@ glasses at 500 °C for 5 h. F) Water resistance test performed by soaking $CsPb_{1-x}Zn_xBr_3$ ($x = 0.5$) NCs@glass in water, and its remaining PL signal over 28 days. Reproduced with permission.[139] Copyright 2019. Elsevier. TEM images of G) undoped, H) 5% Ni^{2+}-doped $CsPbBr_3$ NCs@glass, and I) 10% Ni^{2+}-doped $CsPbBr_3$ NCs@glass, with respective HRTEM images in the insets. Reproduced with permission.[153] Copyright 2020, Elsevier.

became more uniform. A theoretical study performed by density functional theory (DFT) confirmed that the introduction of Ni^{2+} ions into the network should remove the structural defects of PeNCs and improve the order of the perovskite network. Indeed, the formation energy of Pb vacancies (V_{Pb}) is much larger than that of Cs vacancies (V_{Cs}) and Br vacancies (V_{Br}), pointing out that the V_{Cs} and V_{Br} are the main sources of defects in $CsPbBr_3$. Ni^{2+} doping increases the formation energy of V_{Cs}, V_{Br}, and V_{Pb}, and thus is effective in preventing the formation of $CsPbBr_3$ structural defects. The PLQE of PeNC@glass composite enhanced remarkably after Ni^{2+} doping, from 37.6% for undoped PeNCs to 84.3% in the case of 5% Ni^{2+}.

Cadmium, although toxic, is a widely used element in optical materials[154] with an ionic radius of 0.95 Å, which was

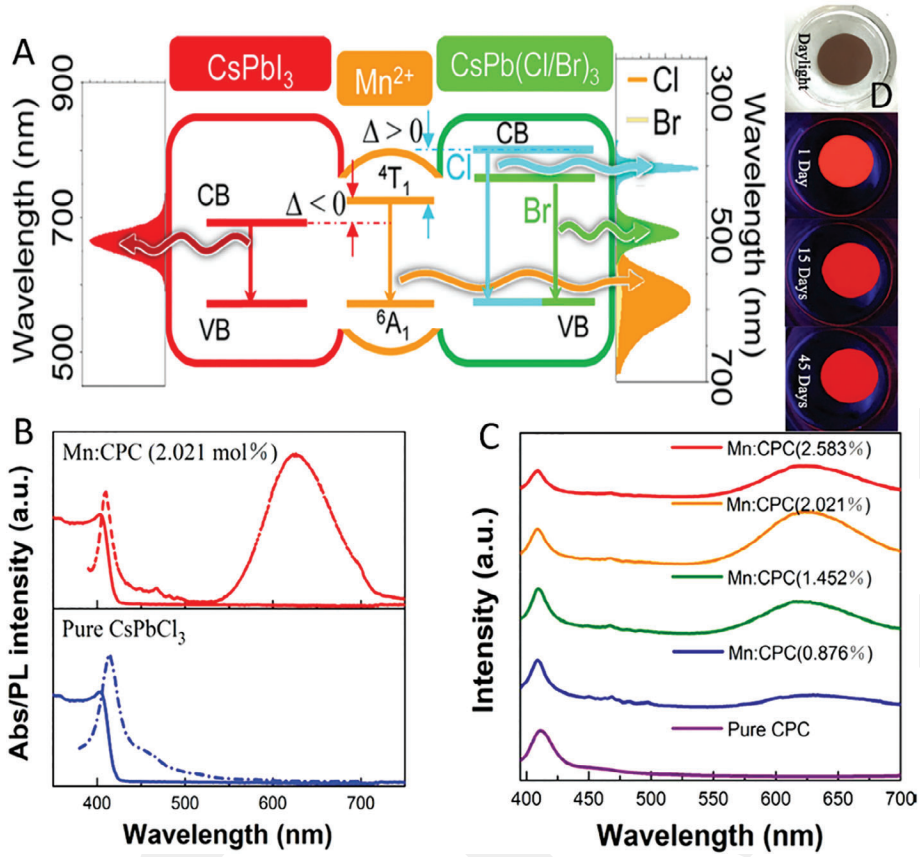

Figure 15. A) Illustration of energy levels and related radiative recombinations of Mn-doped $CsPbX_3$. Reproduced with permission.[155] Copyright 2016, ACS Publications. B) Absorption and PL spectra of $CsPb_xMn_{1-x}Cl_3$ NCs@glass, and C) PL spectra of undoped and Mn-doped compositions with varying Mn^{2+} content. D) Water resistance test and PL intensity after 45 days for the Mn^{2+}-related emission in $CsPb_xMn_{1-x}Cl_3$ NCs@glass. Reproduced with permission.[138] Copyright 2020, American Ceramic Society.

also considered for the B-site perovskite doping. As reported for $CsPbBr_3$@borosilicate glasses, the substitution of Pb^{2+} with Cd^{2+} ions increased the electron density in the $CsPbBr_3$ conduction band.[64] With the increase in Cd^{2+} content, the PL maximum of $CsPb_xCd_{1-x}Br_3$ NCs@glass composites experienced a blueshift from 518 to 473 nm, which was assigned to the contraction of perovskite unit cells and enhanced interaction between Pb and Br orbitals. The obtained PeNCs@glass composites showed a stable green luminescence under UV light with a high PLQE of 69%.

Doping with divalent Mn^{2+} ions represents a somewhat special case, because when they were doped into $CsPbCl_3$ or $CsPb(Cl/Br)_3$ NCs with larger energy gaps, d-d orbital Mn^{2+} transfer caused an intense orange-red emission at ≈600 nm, as illustrated in **Figure 15**A.[155] This was also observed for many other types of perovskite and classical II-VI NCs and their thin films.[156–158] Due to the rather large difference between the ionic radii of Mn^{2+} (0.8 Å) and Pb^{2+} (1.19 Å) cations, the possibility of phase separation is large, and therefore, only a small amount of Mn^{2+} can be doped into the $CsPbBr_3$ perovskite crystal structure. However, Chen et al., showed that Mn^{2+} ions successfully replaced Pb^{2+} ions in $CsPbCl_3$ NCs@glass composite.[138] As shown in Figure 15B, the presence of the Mn^{2+} dopant did not change the absorption spectrum but led to the appearance of a PL signal at ≈620 nm, the PL intensity of which gradually increased, reaching a maximum at 2.012 mol% of the Mn^{2+} precursor (Figure 15C). In the meantime, the intensity of excitonic emission at ≈410 nm decreased, showing the dominating role of Mn-related energy levels in the radiative recombination of excited carriers in the Mn-doped PeNCs. To prove the stability of Mn-doped PeNCs@glass, samples were immersed in water for 45 days, and the red emission intensity related to the Mn^{2+} dopant remained nearly unchanged (Figure 15D).[138] He et al. also showed that the Mn-doped $CsPbBr_xI_{3-x}$ NCs@glass composites possess a strong red fluorescence with improved air and water-resistant properties.[159] They reported that due to the smaller ionic radius of Mn^{2+} (97 pm) as compared to Pb^{2+} (127 pm), doping led to the shift of XRD peaks toward higher 2θ values. Besides, the appearance of the fabricated glassy sample under UV light and ambient light became more transparent after doping with Mn^{2+}. The authors compared the energy levels and showed that the exciton transition energy of the host ($CsPbI_3$ = 1.99 eV) is lower than that of the dopant state (Mn^{2+} = 2.10 eV), which resulted in very little energy transfer between them.

Yet another popular doping source in perovskites are rare-earth ions (lanthanides), which not only can change the emission, but may also have a positive impact in terms of improved structural

and chemical stability, narrow-band emission, longer PL lifetime, and reduced toxicity. In several studies, the doping effects of different lanthanide ions (Gd^{3+}, Dy^{3+}, Tb^{3+}, Eu^{3+},...) on the $CsPbBr_3$ PeNCs were studied, showing that structures with high PLQE and adjustable light emission can be produced in a wide range of wavelengths.[160–163]

4.1.3. Glass-Former Modification

As mentioned earlier, the high melting temperature in the glass-formation process may be a detrimental factor for the PL emission of PeNCs formed in glass. This issue can be resolved by the two following strategies: using a non-silicate glass former with a lower melting temperature, as will be shortly considered in this section, or a change in the molar ratio of perovskites- and/or glass-related components (discussed in the next section). Zhang's group[44] reported an in situ crystallization strategy, which was developed to directly grow $CsPbBr_3$ NCs in a specially designed TeO_2-based glass matrix with a melting temperature of ≈550–950 °C for 30 min. The obtained PeNCs@glass composites showed bright green emission assigned to the exciton recombination with PLQE of ≈70%, FWHM of ≈25 nm, and decay lifetime of 5.5 ns, which were favorable for the wide-color gamut liquid crystal display (LCD) application. However, the higher cost of these TeO_2-based glass matrices as compared to silicate glass may hinder their applications. The beneficial aspect of using low-melting glass has been also demonstrated by Li et al.,[164] who prepared $CsPbCl_3$, $CsPbBr_3$, and $CsPbI_3$ NCs@phosphate glass composites at a low melting temperature of 650°C, followed by multiple annealing processes at 180 °C and 300–340 °C. Their PL emission was tunable across the entire visible spectrum from 405 to 690 nm with FWHM varying from 16 to 43 nm, confirming a superior ability to realize a wide color gamut.

By regulating the glass-former ingredients, one can also modify the rigidity of the glass network, resulting in facile precipitation of $CsPbX_3$ NCs and optimization of their PL characteristics. Pang et al. showed that in borogermano-silicate glass, the rigidity of the glass network increased with an increase in SiO_2 amount leading to smaller PeNCs.[165] At the same time, while it improved the stability of the perovskite@glass composite, a higher heat-treatment temperature was required leading to a considerable decrease in PLQE from 43.5% to 17.5%. Another report on $CsPbI_3$ NCs embedded in a borosilicate glass network also supported the crucial effect of the glass-network rigidity on the formation of PeNCs and their PL and stability performance.[137] The authors optimized the rigidity of borosilicate glass by modifying the molar ratio of B_2O_3/SiO_2 in the glass, allowing them to control the growth and precipitation of PeNCs within the glass network. They reached a PLQE of 17% for red-emissive compositions with high water stability after 60 days of immersion in water.[166]

4.1.4. Modification of the Molar Ratio of Components

This approach can be applied to both perovskite- and glass-related components of a composite to achieve an improved structure, as illustrated in **Table 4**.

Xiang et al. reported the fabrication of $CsPb(Br, I)_3$ NCs@phosphosilicate glasses with tunable emission and improved stability via changing the perovskite-related components and self-crystallization method.[135] The introduction of iodide ions into a glass composition, namely the $40P_2O_5$-$10SiO_2$-$10Cs_2CO_3$-$10SrCO_3$-$5Al_2O_3$-10NaBr-(15-x)$PbBr_2$-xPbI_2 ($x = 0$, 3, 6, 9, 12, and 15), resulted in a multicolor PL emission from green to red color. As the Br/I ratio decreased, XRD patterns of the composites gradually shifted toward smaller diffraction angles because of the lattice expansion of the perovskites through substitution with larger I^- ions (**Figure 16A**). In addition, significant redshifts were observed for the absorption edge and PL emission wavelengths upon an increase in iodine content (Figure 16B). As illustrated in Figure 16C, with the increase of iodine content (from 0 to 15), the average PL lifetime remarkably increased from 9.64 to 32.85 ns, and the latter was longer than those of regular colloidal counterparts.[3] On the other hand, the luminescent intensity of $CsPb(Br, I)_3$ NCs@glass composites were recorded at different temperatures to investigate the thermal quenching behavior (Figure 16D), and it was observed that an increase in the iodine content decreased the thermal stability.[135]

Liu's group used a proper set of glass fabrication parameters (melting temperature and time, as well as heat-treatment temperature and time) for borosilicate glass (SiO_2-B_2O_3-CaO-ZnO-PbO-Cs_2O-NaBr), to realize an excellent PLQE of ≈91% with a change in the molar ratio between bromine and lead.[167] They showed that the increase in the ratio of Br to Pb (without changing anything else) enhanced the PLQE from 15% to 60% due to the passivation of bromine-related vacancy sites, while PLQE was further improved to 91% upon optimization of the reaction temperature and the reaction time. Another report demonstrated the key role of composition in terms of the glass structure and perovskite precursor concentration on the fabrication of luminescent PeNCs@glass composites.[57] The author showed that the proper amounts of B_2O_3 were used to partially replace silicate units forming a well-extended 2D glass network, Zn^{2+} cations from ZnO were used to compensate for the charge imbalance in the network, and F^- ions from CaF_2 used to assist with the formation of non-bridging oxygen all help to provide most suitable glass medium for nucleation and growth of PeNCs. As a result, the optimized $CsPbBr_3$ PeNCs@glass composite showed extremely bright green emission at 516 nm, with PLQE of 94% and FWHM of 26.5 nm, while $CsPbBr_{1.5}I_{1.5}$@glass composite showed PL emission at 640 nm, with PLQE of 78% and FWHM of 36.1 nm.

4.2. Structural Modification

4.2.1. Heat-Treatment

In the PeNCs@glass composites, the heat-treatment procedure influences the NC separation and, as a result, the insulating effect of the glass medium. Several studies have addressed the thermal-induced crystallization of PeNCs in the glass matrix to examine the effects of the thermal treatment temperature and time. Zheng et al. evaluated the growth of PeNCs in an amorphous oxide matrix using a heating-cooling process (**Figure 17**)[129] using structural and optical analyses to confirm the presence of the PeNCs in a multiphase microstructure. As shown in Figure 17A, at the first step, all the perovskite precursor components were uniformly

Table 4. Effect of variations of the molar ratio of perovskite- and glass-related components on the appearance and optical properties of the PeNCs@glass composites.

Perovskite-related components	Glass-related components	Melting conditions	Characteristics of resulting composites		Reference
			mol%	Appearance / Luminescence & PLQE	
$20Cs_2CO_3$-10$PbBr_2$-20KBr	**(70–110)** $NH_4H_2PO_4$-10SiO_2-6$SrCO_3$-3Al_2O_3	700 °C/20 min	110	Transparent / non-luminescent	[31]
			100	Transparent / non-luminescent	
			90	Light yellow/ translucent green emission	
			80	Light yellow/ translucent green emission 15.6%	
			70	Yellow/ opaque/ green emission	
$7Cs_2O$-7$PbBr_2$-14NaBr	27B_2O_3-20SiO_2-3MgO-2Al_2O_3-**(4,7,10,13,20)** ZnO	1250 °C/5 min	20	Yellow/ opaque/ green emission 15%	[44]
			13	Yellow/ opaque/ green emission 19%	
			10	Yellow/transparent/ green emissions 45%	
			7	Colorless/transparent/ green emission ≈28%	
			4	Colorless/opaque/ blue emission	
5Cs_2CO_3 -10$PbBr_2$ -10KBr	(**55–85**) TeO_2 -2Al_2O_3 14H_3BO_3 -16ZnO-13Na_2CO_3	750 °C/30 min	85	Semi-transparent/ green emission (crystallization condition: 300 °C/10h)	[48]
			75	Yellow/ opaque/ green emission 10% (crystallization conditions: 300 °C/12h)	
			65	Opaque/ non-luminescent (crystallization conditions: 300 °C/12h)	
			55	Bright yellow/opaque/ green emission 60% (crystallization conditions: PG)	
39SiO2-39B2O3-5CaO-5ZnO	2PbO-5Cs2O-**(5-10-25)**NaBr	1250 °C 40 min	5	Dark yellow/opaque/ green emission 15.4% (crystallization condition: 490 °C/10h)	[167]
			10	Yellow/opaque/ green emission ≈45% (crystallization conditions: 500 °C /10 h)	
			25	Yellow/translucent/ green emission 61% (crystallization conditions: 530 °C/10h)	
		1350 °C 20 min	25	Yellow/transparent/ green emissions 91% (crystallization condition: 520 °C/10h)	

distributed in the glass. In the second step, heating above the softening temperature (T_s) led to a phase transformation of what they called "halide nanoglass" from the solid to the liquid state (Figure 17B). By increasing the temperature higher than 718 K, precursor ions of the halide NCs (Cs^+, Pb^{2+}, Cl^-, Br^-, and I^-) migrated more easily, and the size of the nanoglass increased (Figure 17C). Upon increase of the heat treatment time, the composition and size of the nanoglass changed continuously, and the high mobility rate of Cs^+ ions increased Cs content. Therefore, the nanoglass could be described as a Cs-rich halide at a high temperature during the heat-treatment process (Figure 17D,E). After this heating, the cooling process was applied to stop the size and composition changes of the halide nanoglass (Figure 17F). At this stage, the migrating ions froze, leading to a core-shell structure with a non-uniform distribution, but the nanoglass remained in a liquid phase. Finally, a rapid phase transition happened (Figure 17G) at which nanoglass transformed into halide crystals by exceeding the Cs content, which resulted in a multiphase coexistence state (Figure 17H,I). The HRTEM analyses supported these processes and the formation of various structural phases.[99]

Su's group regulated the composition of the glass matrix and the heat-treatment temperature to fabricate $CsPbBr_3$ PeNCs with an average smallest NCs size of 1.96 nm in borosilicate glass (SiO_2-B_2O_3-CaO-ZnO-BaO-K_2O-TiO_2).[144] After melting the powders at 1050–1250 °C for 12 min, $CsPbBr_3$ NCs@glasses were obtained through a controlled crystallization at 490–550°C (near the glass-transition temperature) for 12 h. The increase in the heat-treatment temperature applied to the $CsPbBr_3$ NCs@glass led to a slight red shift of the absorption and emission spectra from 507 to 519 nm (**Figure 18A**). The temperature-dependent PL measurements showed that a decrease in the measurement's temperature increased the PL intensity with narrower FWHM (≈29 nm) because of the reduced contribution of lattice states in non-radiative recombination (Figure 18B,C). They also found that an increase in heat-treatment temperature increased PLQE values from 11% to 26% due to the increase in the number of precipitated $CsPbBr_3$ NCs (Figure 18D).

Optimization of both temperature and time of the heat-treatment process should be considered in any studies regarding PeNC@glass compositions to realize the highest possible PLQE. Lin et al. evaluated the evolution of PLQE and FWHM of $CsPbBr_3$@glass composites upon the duration of heat treatment at various temperatures.[168] They showed that upon temperature increase, the required time of the heat-treatment process to reach the highest PLQE has shifted from 6 h at 460 °C to less than

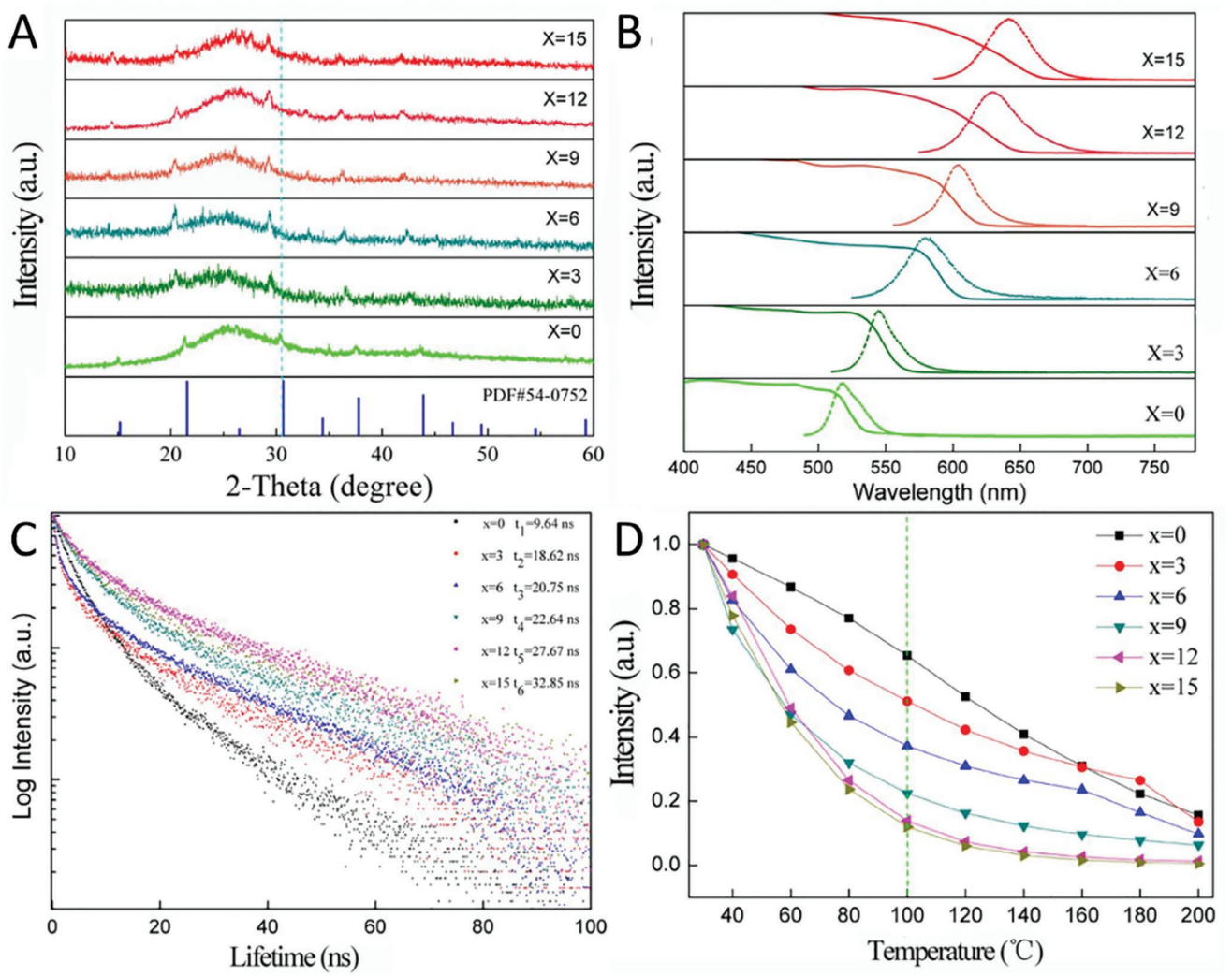

Figure 16. A) XRD patterns, B) absorption and emission spectra, C) PL decay curves, and D) normalized temperature-dependent emission intensities of $CsPb(Br, I)_3$ NCs@glasses formed by using the glass compositions of $40P_2O_5$-$10SiO_2$-$10Cs_2CO_3$-$10SrCO_3$-$5Al_2O_3$-10NaBr-(15-x)$PbBr_2$-xPbI_2 with a varying iodine content ($x = 0$, 3, 6, 9, 12, and 15 mol%). Reproduced with permission.[135] Copyright 2019. Elsevier.

1 h at 600 °C (**Figure 19**A). The authors observed non-linear variation of PLQE with the duration of the heat-treatment process at any temperature, which means that the optimal time should be determined for any selected composition. On the other hand, not related to the temperature used, continuing the thermal treatment for a long time resulted in the narrowing of the PL profiles (from 33 to 25 nm) due to the more uniform size distribution of the resulting PeNCs (Figure 19B). Based on this observation, the authors suggested a two-step heat-treatment for performing nucleation and growth steps at different temperatures (600 and 460 °C) and times (15 to 240 min, respectively) to simultaneously optimize PLQE and FWHM (Figure 19C,D). Following this approach, a narrow emission with FWHM of 22 nm and PLQE of ≈35% was obtained, as emphasized in Figure 19C,D using gray circles.

In another related study, the author showed that employing a proper temperature and time for the heat-treatment process significantly improved the quality of $CsPbBr_3$ NCs embedded in borosilicate inorganic glasses (λ_{em} = 525 nm, FWHM = 25 nm, τ_{avg} = 113 ns, and PLQE = 86%).[169] With an initial increase in temperature (during a cycle of heating and cooling processes), there was a continuous decrease in PL intensity, which was recoverable upon cooling down after two thermal cycles (heating-cooling) between 298 and 418 K (**Figure 20**A,B). For evaluation of stability against water, the obtained $CsPbBr_3$ PeNC@glass composites were immersed in water for 74 days, and only a ≈20% decrease in the PL intensity was detected (Figure 20C). The optical stability tests also confirmed the excellent protecting role of amorphous glass over PeNCs, so that after 7.5 days of continuous irradiation by 365 nm (UV light) and 450 nm (blue light) 6 W lamps, there was only ≈30% decrease in the initial PL intensity (Figure 20D,E). Moreover, the samples remained stable with no change in XRD patterns and were still luminescent after being stored for one year (Figure 20F).

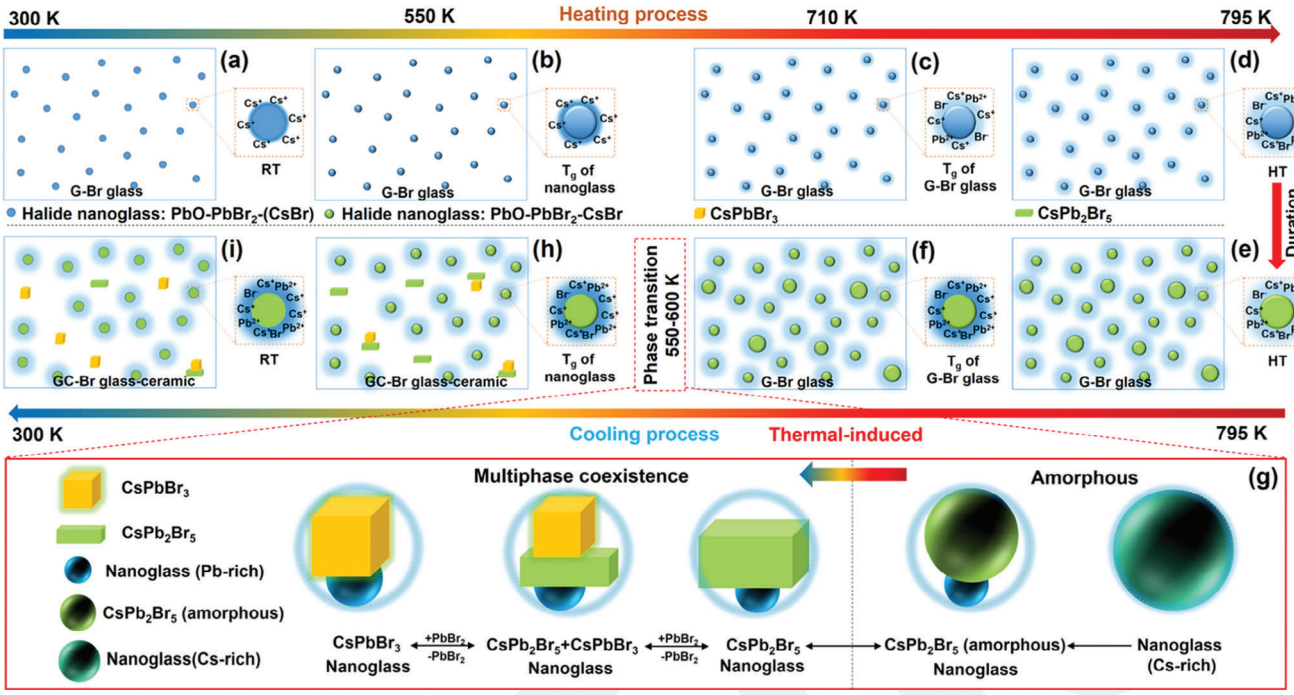

Figure 17. Schematic illustration of multiphase transitions occurring in halide nanoglass during the heat-treatment at different temperatures. Reproduced with permission.[129] Copyright 2022, ACS Publications.

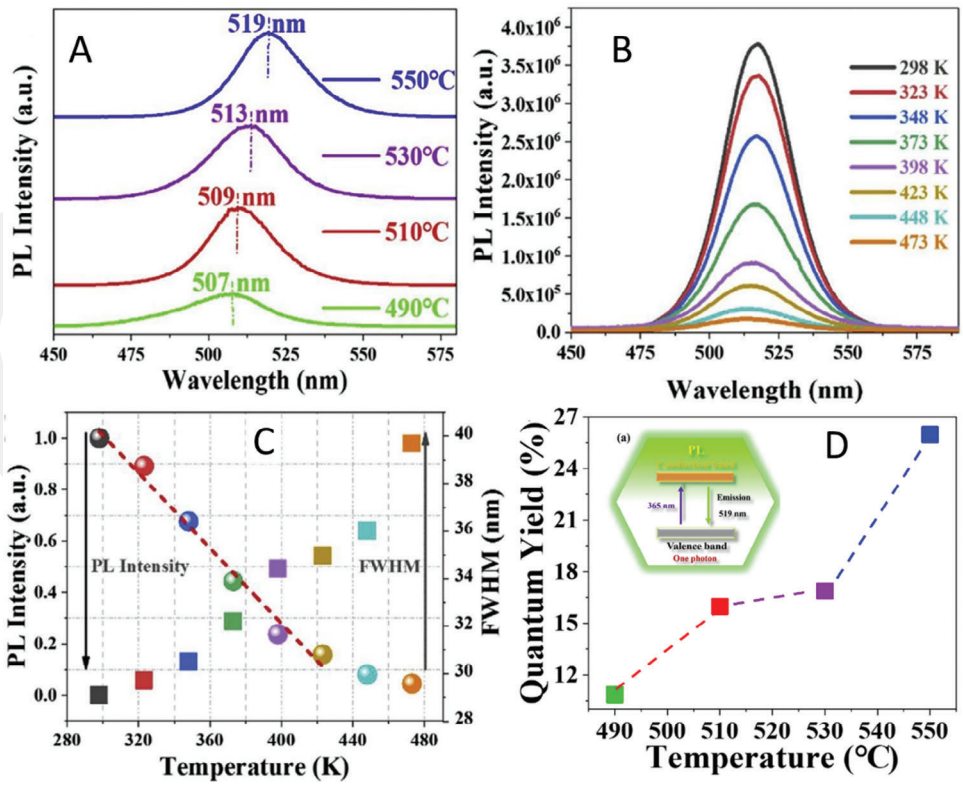

Figure 18. A) PL emission spectra of $CsPbBr_3$ NCs@glasses prepared at different heat-treatment temperatures. B) Temperature-dependent PL spectra, and C) PL intensity and FWHM as a function of the temperature of the sample produced at 550 °C. D) Variation of PLQE for $CsPbBr_3$ NCs@glasses prepared at different heat-treatment temperatures. Reproduced with permission.[144] Copyright 2020, Elsevier.

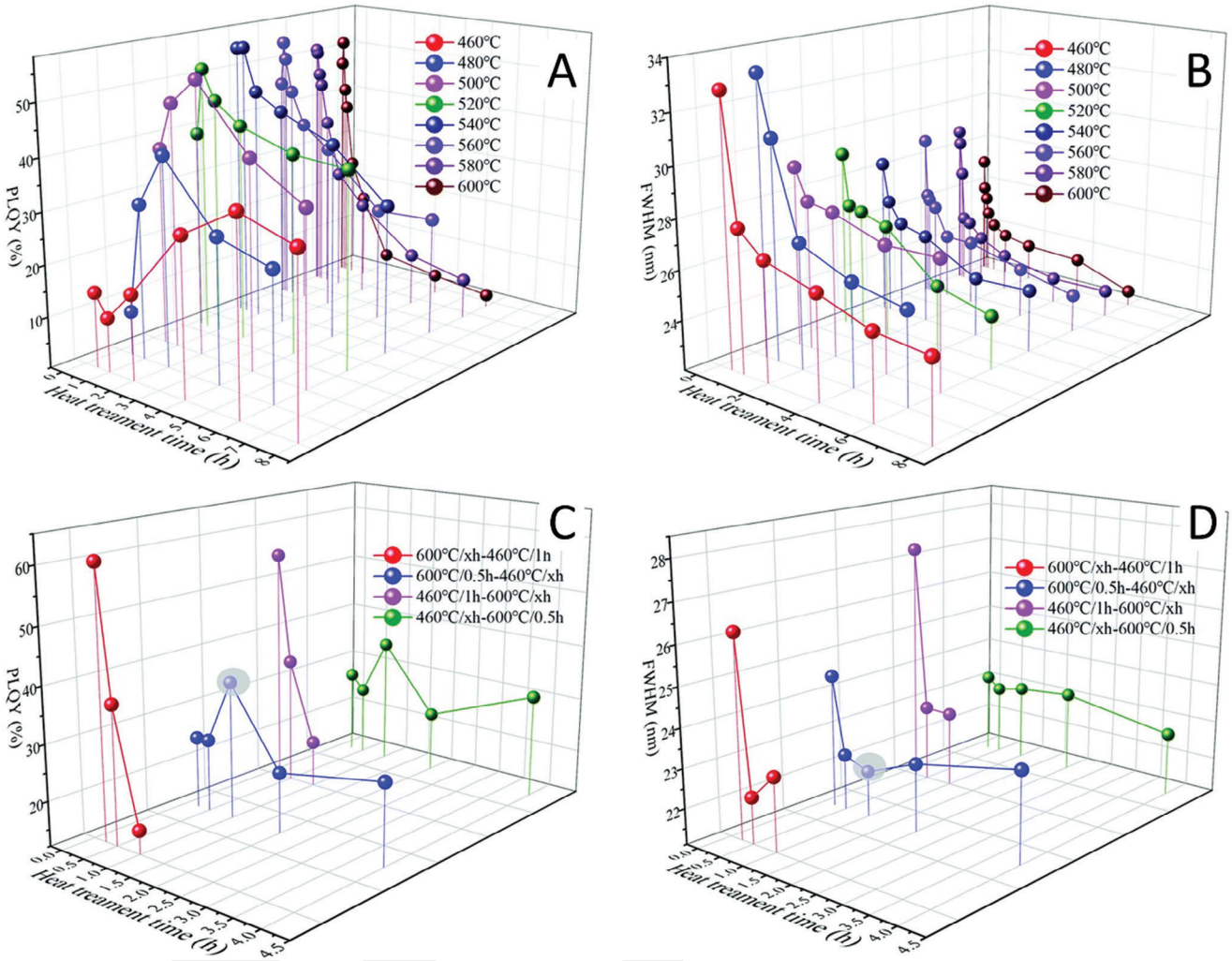

Figure 19. Changes of A) PLQE and B) FWHM of $CsPbBr_3$@glass in the process of one-step heat-treatment upon changing temperature and time. C) Changes of PLQEs and D) FWHMs of $CsPbBr_3$@glass samples obtained by various two-step heat-treatment temperatures and times. Reproduced with permission.[168] Copyright 2022, Royal Society of Chemistry.

4.2.2. Mechanical/Hydration Crystallization

The phase transfer processes in amorphous glasses require a certain amount of energy which is conventionally supplied via heat-treatment, precipitation, or crystallization of PeNCs inside a glass matrix and can also be promoted by applying mechanical stress or force.[54,66,145] In this case, while as-fabricated composites are often not luminescent, PL emerged after they were mechanically broken or ground, indicating the occurrence of stress-assisted crystallization. Zhang's group used a secondary crystallization approach (6 h of ball-milling plus 60 days of keeping under an air environment), resulting in significant improvement of PLQE in green-emitting (from 0.7% to 88.9%) and red-emitting (from 0.39% to 28.9%) PeNC@glass composites.[54] Upon ball-milling, numerous shear bands can be formed due to the impact and shear forces leading to a "free volume zone" metastable phase. The creation of shearing-driven cracks can enhance the local potential energy followed by the atomic displacements or rearrangement of structural units, resulting in a secondary crystallization of PeNCs. In this case, without applying any heat-treatment process, composites were fabricated. On the other hand, it has been reported via Raman spectroscopy that such mechanical crystallization can take place within a particular glass composition range, representing the importance of proper glass composition.[66] It has been also demonstrated that in addition to the mechanical forces, hydration can result in the crystallization of PeNCs.[170] Authors have used glass composition of $NH_4H_2PO_4$–Pb_2O_3–(Cs_2CO_3–$PbBr_2$–NaBr) to obtain green-emitting PeNCs with intense and stable emission at 523 nm after mechanical/hydration treatment. In this method, the relaxation of the glass lattice structure by chemical reaction was the main factor leading to the hydration-based crystallization. The PL intensity increased with the increase in the water immersion time, and the resulting PeNCs showed better stability in terms of thermal and water resistance compared to those produced through the traditional crystallization method.[141] A similar post-treatment water-induced approach was used for the formation of $CsPbBr_3$ NCs in a borophosphate glass.[171] After a short time

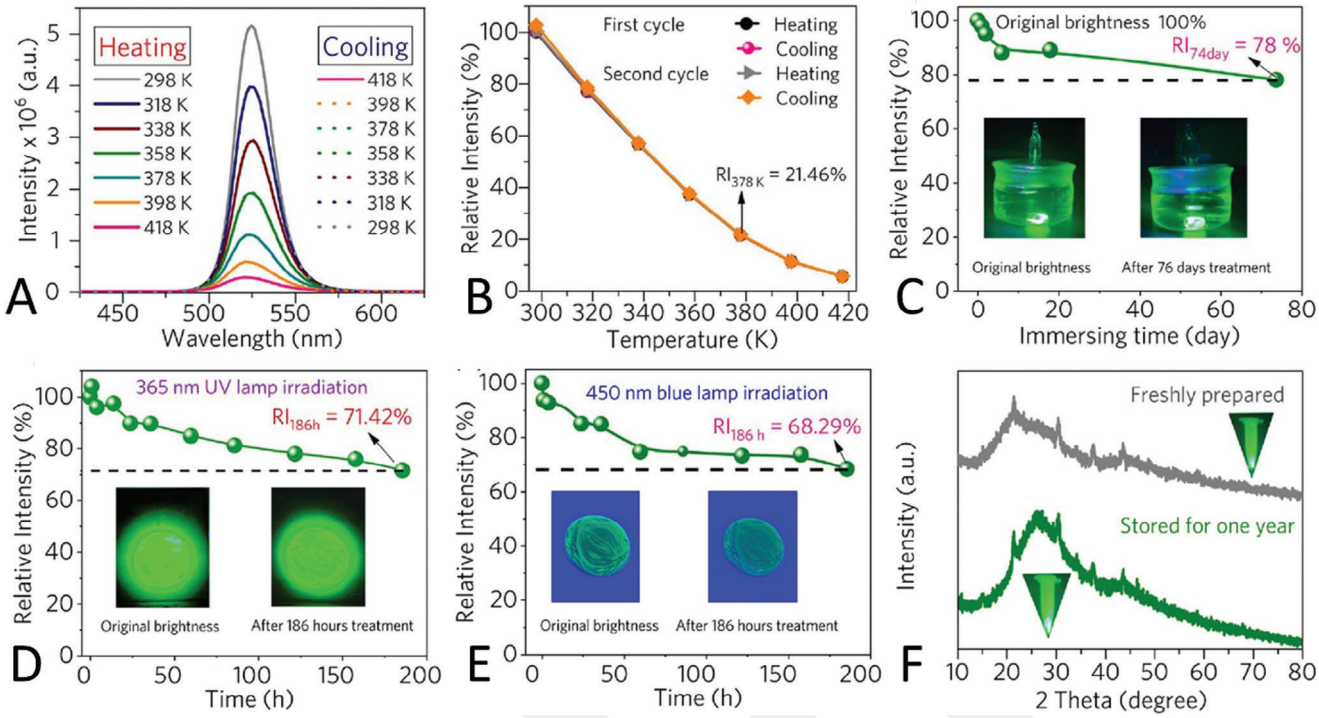

Figure 20. A) Effect of a cycle of heating and cooling on PL spectrum (λ_{ex} = 365 nm) and B) changes of the PL intensity of $CsPbBr_3$ NCs@glass composite during two heating/cooling cycles in the temperature range of 298–418 K. Relative PL intensities of the $CsPbBr_3$ NCs@glass during exposure to C) water, D) UV light, E) blue light, and F) air. Insets provide related photographs of the $CsPbBr_3$ NCs@glass samples. Reproduced with permission.[169] Copyright 2022, ACS Publications.

of applying a certain level of humidity (80%) to the as-fabricated glass network, CsBr transformed to $CsPbBr_3$, showing a PL shift from 478 to 525 nm.

4.3. Dual Encapsulation Using Polymer or Secondary Glasses

As discussed above, glass matrix can effectively prevent PeNCs from interacting with the external environment, but on the other hand, the rigidity of PeNCs@glass composites may somewhat limit their application areas. Therefore, a secondary robust and eventually flexible encapsulation can sometimes be considered. One of the strategies here is to use a second protective layer of a polymer, which may bring together simultaneous enhancement of PLQE, better environmental stability, and applications' demanded flexibility. Chen's group fabricated $CsPbX_3$(X = Br, Br/I) PeNCs@glass nanocomposites with superior optical performance and stability.[32] They used a physical dilution approach via non-luminescent inert Al_2O_3 oxide or polydimethylsiloxane (PDMS) polymer to eliminate the internal filtration effect (i.e., reabsorption effect) and achieve near unity PLQE for $CsPbBr_3$@glass-Al_2O_3 mixtures and $CsPbBr_3$@glass@PDMS films. These composite films showed bright emission after twisting and stretching, demonstrating the flexibility of $CsPbX_3$@glass@PDMS films (**Figure 21**A). The Br-based composite showed intense green emission at ≈520 nm with narrow FWHM (Figure 21B). The PLQE and FWHM of the films were further modified by adjusting the weight ratio of $CsPbX_3$@glass to PDMS, which led to even higher PLQE of up to 95% and FWHM of 21 nm by increasing the PDMS content (Figure 21C,D). The double-protected PeNCs also showed great stabilities against moisture (exposed to air for 90 days, Figure 21E) and light (irradiated by a 6 W UV lamp for 7 days, Figure 21F) with almost no reduction in the PLQE. The authors emphasized that the glass matrix was mainly responsible for stability, while the polymer had a complementary effect.

Positive effects of dual encapsulation with PDMS have been also reported by Lin et al.,[168] where an increase in the amount of PDMS in the green-emitting $CsPbBr_3$@glass composite improved FWHM (from 22 to 17 nm), PLQE (from 40% to 80%), and resistance of the films (those directly immersed into water at 85 °C maintained their emission for more than 250 h). Another study on the dual encapsulation was carried out by Wang et al.,[146] who fabricated mixed PeNC@glass@SEBS (SEBS stays for styrene-ethylene-butylene-styrene polymer) composite in three simple steps. **Figure 22**A illustrates the fabrication process of this so-called MGS nanocomposite, where PeNCs@glass was ground into micron-size powder, and mixed with a SEBS-toluene solution. The mixture was poured into a Petri dish, and placed in a fume hood for 12 h to solidify the film. Benefiting from the dual protection by both the glass matrix and SEBS, the resulting films showed bright emission (PLQE of 50%) and significant improvement in water/thermal resistance. The authors used different molar ratios of their mixtures and found out that the combination of $CsPb(Cl/Br)_3$/ $CsPbBr_3$ with the molar ratio of 0.2015/0.4023 (the sample they called M1) showed the best

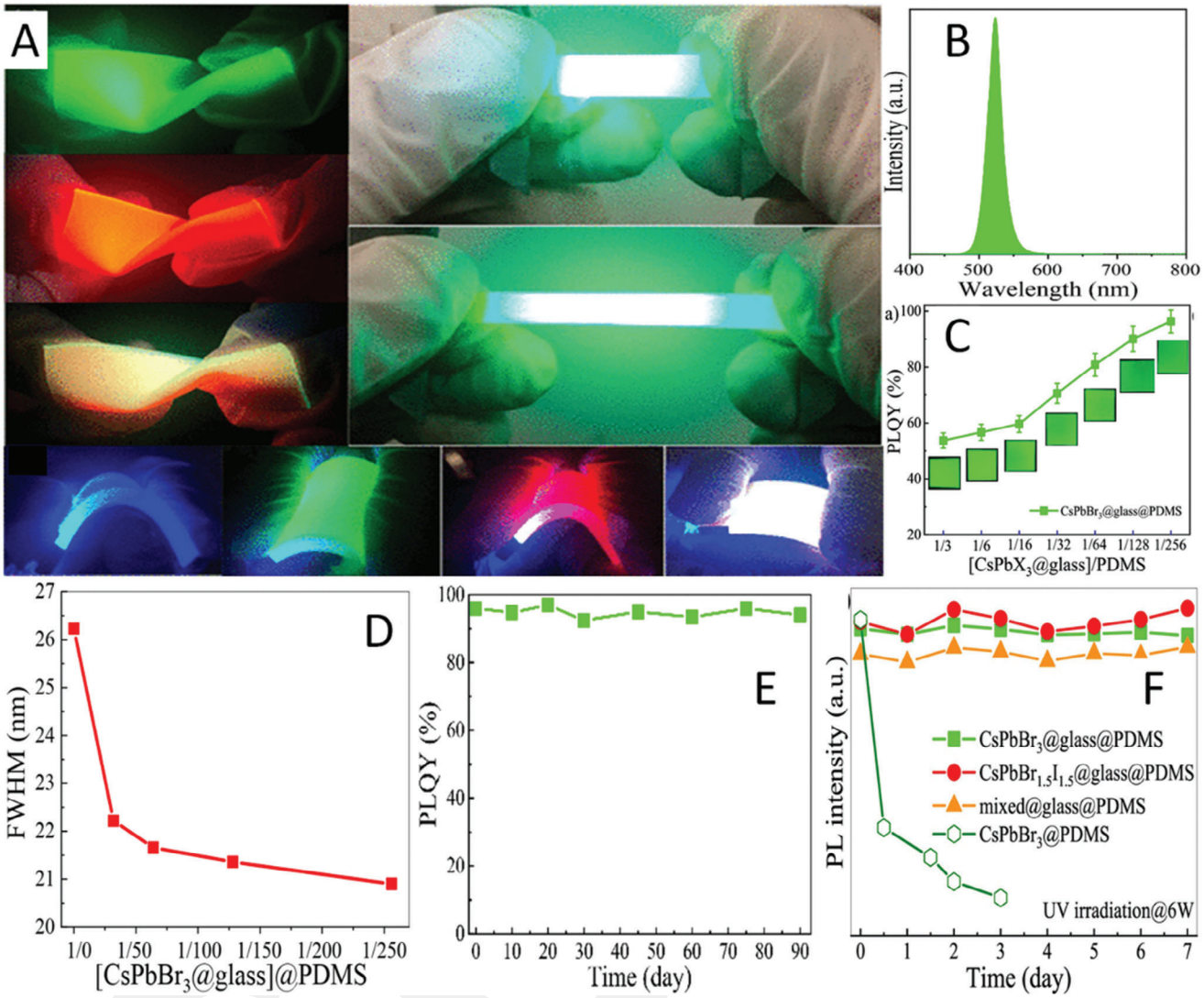

Figure 21. A) Photographs of luminescent stretched and twisted $CsPbX_3$@glass@PDMS films. B) PL spectrum of $CsPbBr_3$@glass@PDMS composite. C) Dependence of PLQE on the weight ratio of [$CsPbBr_3$@glass]/PDMS for the green-emitting film. D) Dependence of PL FWHM on dilution ratio for $CsPbBr_3$@glass@PDMS films. E) Stability test for $CsPbBr_3$@glass@PDMS films in terms of PLQE variation during their exposure to air for up to 90 days, and F) photostability tests of samples with different compositions (indicated) under illumination with UV light (6 W lamp) for up to 7 days. Reproduced with permission.[32] Copyright 2021, ACS Publications.

results in terms of the improved water resistance (Figure 22B). As a main advantage of using dual polymer encapsulation, the obtained MGS films remained green-emissive and flexible after being immersed in water for 60 days, as illustrated by photographs presented in Figure 22C.

Using an appropriate inorganic glass as a secondary glass to achieve additional protection of the PeNCs@glass composites has been recently explored, as well. Nam et al. used a germanate glass with embedded $CsPbBr_3$ NCs as a green phosphor and combined it with transparent silicate glass to fabricate phosphor-in-glass plates.[63] In this case, the presence of two glasses with different refractive indices caused the scattering of exciting light at the interface between the two glasses. Therefore, PeNCs would experience less direct absorption of the incident light, making them eventually more stable. The authors combined a green-emitting layer with two red-emitting phosphors ($CaAlSiN_3:Eu^{2+}$, $K_2SiF_6:Mn^{4+}$) to fabricate white LEDs with a color gamut of up to 116% and 131% of the NTSC. Thus, using a secondary glass (or polymer) provides a possibility when two different PeNCs@glass composites with different emission colors can be embedded inside the second glass (polymer) matrix. Zheng et al. separately fabricated $CsPbBr_3$ PeNCs@borosilicate glasses (with green emission) and $CsPb(BrI)_3$ PeNCs@ borosilicate glasses (with red emission) using the melt-quenching technique.[172] Then, they mixed and milled them to apply in the melting process of another, tellurite glass, which resulted in a layer of the tellurite glass including green and red emitting PeNCs@glass phosphors. In combination with a commercial blue LED chip, these dual encapsulated samples were used to fabricate robust and efficient white LEDs with a wide color gamut of 128% of NTSC 1953.

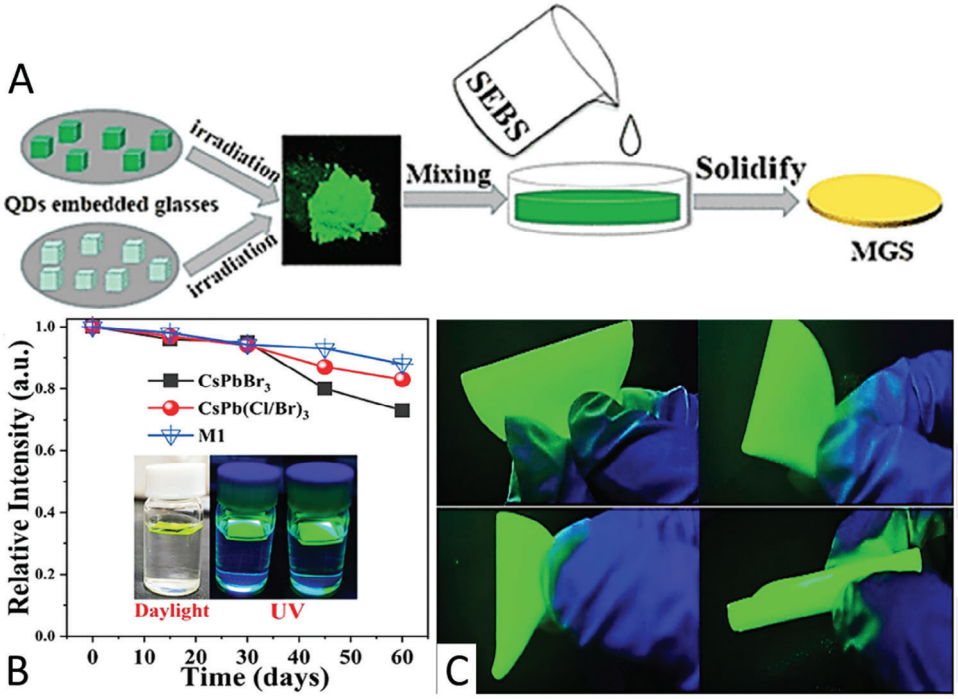

Figure 22. A) Schematic illustration of the fabrication of dual-encapsulated PeNC@glass@SEBS (MGS) composite. B) PL intensities of $CsPbBr_3$@glass, $CsPb(Cl/Br)_3$@glass, and the M1 (see text) dual-protected composite after water immersion for up to 60 days, with photographs of the samples shown in the inset. C) photographs of twisted green MGS films emitting bright green light under UV irradiation. Reproduced with permission.[146] Copyright 2021, ACS Publications.

Table 5 provides an overview of the various fabrication methods for the preparation of different compositions of PeNCs@glass and their corresponding optical properties.

5. Applications of $CsPbX_3$ NCs@Glass Composites

PeNCs@glass composites hold potential for further exploration as active materials in different optoelectronic and energy devices. As outlined in the above sections, the embedding of PeNCs into various glass matrices has resulted in composites with remarkable resistance to thermal, moisture, and illumination stress, while preserving their optical characteristics. This section is dedicated to recent studies on employment of PeNCs@glass composites in a range of applications such as LEDs and displays, data storage and anti-counterfeiting, lasing, photodetectors and X-ray detectors, photocatalysis, optical filters, solar concentrators, and batteries.

5.1. LEDs and Displays

PeNCs have emerged as a potential material to replace traditional phosphors in display technology, due to the wide color gamut and purity of their emission. Studies into PeNCs@glass composites further supported this trend, as they offered improved stability against both moisture and heat. Several reports appeared recently that have explored the use of PeNCs@glass composites in display technology as LEDs, backlight devices, or color converters.

The first demonstration of high-performance LEDs based on PeNCs@glasses was reported by Ye et al.[20] They fabricated boro-germanate glass with embedded green-emitting $CsPbBr_3$ NCs with a PLQE of ≈80% and red-emitting $CsPbBr_{3-x}I_x$ NCs with a PLQE of 20%. Green LEDs based on the former composite (denoted as BrG) showed high luminous efficiency (LE) of 119 lm W^{-1} and an external quantum yield (EQE) of 29%, whereas red LEDs (denoted as BrIG) exhibited lower LE and EQE due to their low PLQE (**Figure 23A**). The authors also followed two different device structures for fabrication of the white LEDs: Scheme 1 – red light emitting slice sandwiched between blue and green layers and Scheme 2 – with green light emitting layer in the middle (Figure 23B), whose recorded LE and EQE were in the range of 50–60 lm W^{-1} and 20–25% at ≈20 mA, respectively. Photographs of operating green, red, and white LEDs are provided in Figure 23C.[20] The same research group also reported how to achieve higher PLQE (above 90%) for the $CsPbBr_3$ NCs@glass composites by varying the Br/Pb precursor molar ratio.[167] Thin slabs of these composites with thicknesses varying from 0.1 to 5.0 mm were mounted on a commercial blue InGaN LED chip to obtain green LEDs, whose maximum LE reached 166 lm W^{-1}, and a maximum EQE of 33%. White LEDs based on these composites demonstrated a maximum LE and EQE of 106 lm W^{-1} and 46.5%, respectively, covering 132.5% of NTSC and 99.2% Rec. 2020 color space. Niu et al.[174] carried out structural modifications on tellurite glass by doping it with Ag^+ ions, and used it as the host matrix for $CsPbBr_3$ NCs, with the resulting composite showing enhanced PLQE of 34%. This composite was used for the fabrication of white LED with an EQE of 20%

Table 5. Summary of demonstrated $CsPbX_3$ NCs@glass composites.

Fabrication approach (Publication Year)	Perovskite and glass components [mol%]	Melting conditions	PL peak wavelength [nm]	PL FWHM [nm]	PL lifetime [ns]	PLQE [%]	Reference
In situ crystallization in a TeO_2 glass host (2018)	$5Cs_2CO_3$-$10PbBr_2$-10KBr (x = 55-85) TeO_2-$2Al_2O_3$-$14H_3BO_3$-16ZnO-$13Na_2CO_3$	950 °C for 30 min	(x = 55) 530	25	5.5	70	[48]
Glass network doping by fluorine (2019)	Cs_2CO_3 -PbX_2 -NaX (X = Cl, Br, I) SiO_2-B_2O_3- ZnO- NH_4F	1200°C for 8 min	(X = Cl) 407 (X = Br) 520 (X = I) 688	15-52	9 25.9 70.1	3 80 50	[49]
B-Site perovskite network doping by Zn^{2+} (2019)	Cs_2CO_3-$PbBr_2$-NaBr-$ZnBr_2$ SiO_2 – B_2O_3 – ZnO	1200°C for 10 min	(Zn = 50%) 517–529	–	96	36	[139]
Modification of perovskite components (2019)	$10Cs_2CO_3$-10NaBr-(15-x) $PbBr_2$-xPbI_2 (X = 0,3, 6, 9, 12,15) $40P_2O_5$-$10SiO_2$-$10SrCO_3$-$5Al_2O_3$-10NaB	900 °C for 30 min	(x = 0) 517 (x = 15) 640	30	9.64 32.85	48 –	[135]
Heat-treatment modification (2020)	$5Cs_2CO$- $5PbBr_2$- 5NaBr $40SiO_2$ -$20B_2O_3$ -10CaO – 5ZnO- 2K2O- 2BaO- $1TiO_2$	1150 °C for 12 min	(490 °C) 507 (510 °C) 509 (530 °C) 513 (550 °C) 519	40 – – 29	49.87 74.52 281.94 294.47	– – – 26	[144]
In situ glass crystallization alongside changing Br-to-I ratio (2020)	$12Cs_2O$- 4.9$PbBr_2$- 0.1PbI_2-14.7NaBr-0.3NaI ($Br_{2.94}I_{0.06}$) $85SiO_2$-$85B_2O_3$-55ZnO-$5CaF_2$	1200 °C for 10 min	(500 °C) 516 (520 °C) 517 (540 °C) 518 (560 °C) 519	21	94.68 116.44 119.57 140.58	63	[51]
Glass modification by modulating ZnO component(2021)	$7Cs_2O$- $7PbBr_2$ -14NaBr $27B_2O_3$ -$20SiO_2$ -3MgO-$2Al_2O_3$ (x = 4,7,10,13,20) ZnO	1250 °C for 5 min	(x = 10) 526–529	–	–	45	[44]
Modification of borate glass – (2021)	$1Cs_2CO_3$- $2PbBr_2$-2NaBr $6Li_2O$-$4Na_2O$-$2K_2O$-10ZnO-15BaO-7SrO-$0.3Sb_2O_3$-$55.7B_2O_3$	1100 °C for 10 min	516	15–17	72.2	82	[173]
Glass network doping by TiO_2 (2021)	$8Cs_2CO_3$ -$4.5PbBr_2$ -8NaBr $27B_2O_3$ -$34SiO_2$ -3MgO – $2.5Al_2O_3$ – 13ZnO – (x = 0-0.5-1-1.5-2-2.5-3) TiO_2	10 °C per min to 1250 °C	(x = 2) 517	–	49.34	41.2	[65]
Modification of perovskite and glass components (2021)	$9Cs_2CO_3$-x$PbBr_2$-6NaBr (X = 11–19) $35B_2O_3$- (35-X) SiO_2-15ZnO	1200 °C for 15 min	(x = 17) 522	24	367.7	47	[67]
Dual encapsulation by SEBS polymer (2021)	6NaBr-$4PbBr_2$-$6Cs_2CO_3$ $20SiO_2$- $14B_2O_3$-10ZnO	1200 °C for 10 min	523	23	45.75	41.5	[146]
Dual encapsulation by PDMS/Al_2O_3 – (2021)	$10Cs_2O$-$5PbX_2$-5NaX (X = Br, I) $30SiO_2$-$30B_2O_3$-20ZnO	1200 °C for 8 min	(X = Br) 518 (X = $Br_{1.5}I_{1.5}$) 630	–	67 85	100 80	[32]
Heat-treatment modification (2022)	$3.57Cs_2O$- 7.15KBr- 4.76PbBr $250B_2O_3$ -27.38ZnO – $4.76Al_2O_3$ – 2.38CaO	1100 °C for 20 min	(3 h) 518 (6 h) 521 (9 h) 525	28 20 18	29 72 241	81 73 53	[55]
Mechanical ball milling of PeNC@glass (2022)	B_2O_3- SiO_2- ZnO- Na_2O-Cs_2CO_3- $PbBr_2$- NaBr	1100 °C for 20 min	520	20	85	88.8	[54]
Introducing $CsPbX_3$ PeNCs inside zinc borosilicate glass by host-secondary heat-treatment (2022)	Cs_2CO_3- PbX_2- NaX (X = Cl, Br, I) $70H_3BO_3$- $35SiO_2$- $5Na_2CO_3$- $4Al_2O_3$- $5BaCO_3$- 12ZnO	1100–1200 °C for 5–15 min	(X = Cl) 411 (X = Br) 520 (X = I) 710	11 31 43	– 	7 47 26	[36]
Optimizing glass structure, perovskite precursor concentration, and in situ crystallization of $CsPbX_3$ PeNCs within borosilicate glasses (2023)	$31.25SiO_2$-$31.25B_2O_3$-20.22ZnO-$5.51CaF_2$-X[$4.42Cs_2CO_3$-$1.84PbBr_2$-5.51NaBr] $30.36SiO_2$- $30.36B_2O_3$-19.64ZnO-$5.36CaF_2$-Y[$6.34Cs_2CO_3$-$0.99PbBr_2$-$0.99PbI_2$-2.98NaBr-2.98NaI]	1200 °C for 8 min	CsPbBr3- 517 $CsPbBr_{1.5}I_{1.5}$- 640	23.3–26.7 34.8– 37.3	12–58 40–102	93.8 78.1	[57]
Applying heat treatment or focused femtosecond laser irradiation for crystallization of $CsPbBr_3$ PeNCs (2023)	$21SiO_2$–$52B_2O_3$–6ZnO–$5SrO_2$–6NaBr–$7Cs_2O$–3PbO	1000 °C for 20 min (annealing at 470 °C)	515	23	131.2	–	[50]

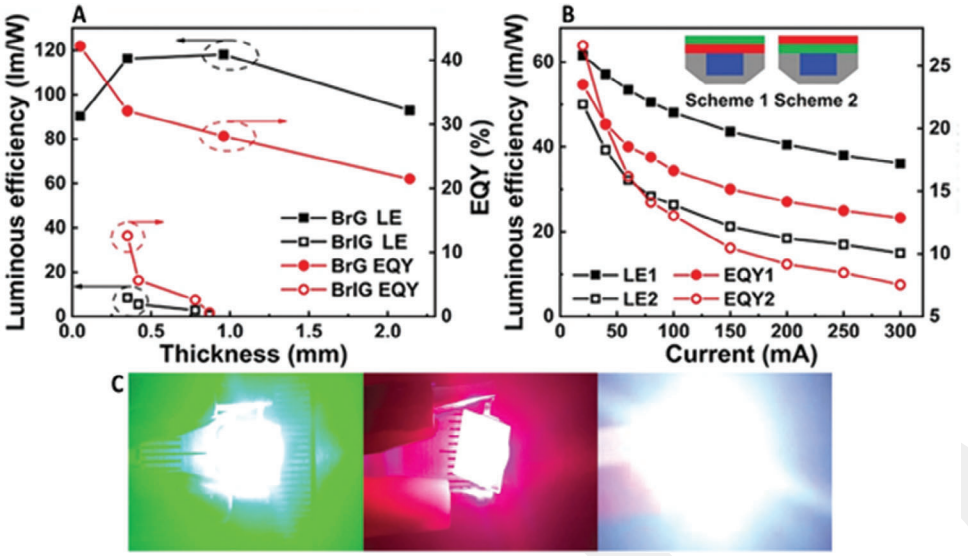

Figure 23. A) Thickness variation of LE and EQE of green-emitting (BrG) and red-emitting (BrIG) PeNCs@ glass-based LEDs. B) LE-current and EQE-current curves of two WLEDs (Scheme 1 and Scheme 2) based on those composites, and C) photographs of operating green, red, and white LEDs. Reproduced with permission.[20] Copyright 2019, Wiley-VCH.

and the maximum LE reaching 65 lm W^{-1}. The use of doped PeNCs in a glass matrix was also explored, where potassium-doped $CsPbBr_3$ NCs@glass composite yielded a PLQE of 62% at the molar ratio of $K^+/Cs^+ = 0.6/0.4$. Even though LED based on a combination of the green $K_{0.6}Cs_{0.4}PbBr_3$ NCs@glass and red $CsPbBr_{1.2}I_{1.8}$ NCs@glass deposited on blue InGaN chip showed better stability and higher color rendering index (CRI) compared to undoped PeNCs@glass composite as a green light source, their LE (30.4 lm W^{-1}) required further improvement.[175] Fabrication of flexible light-emitting devices has attracted a growing demand, especially in the case of initially rigid PeNCs@glass composites. Lee et al. fabricated a remote color converter, which included the phosphor in silicon pasted over a transparent glass substrate that has been mounted on a blue LED, using $CsPbBr_3$ NCs@glass powders as the green phosphor and KSF: Mn^{4+} as the red phosphor to improve the thermal stability during the device operation.[176] White LED based on such a combination of phosphors showed an enhanced color gamut of 130% NTSC color standard, whereas the commercial analog made of β-SiAlON: Eu^{2+} as the green phosphor only reached 100.4% of this value. The recyclability of the $CsPbBr_3$ NCs@ borosilicates glass was also studied to fulfill the requirements of environmental sustainability. Naji et al. used periodic melt quenching and heat-treatment processes to confirm its recyclable emission properties and fabricated a white LED to prove the structural and optical integrity of these composites.[177] WLED constructed from a blue LED chip, $CsPbBr_3$ NCs@glass composite, and a commercial red phosphor showed an aLE of 68.3 lm W^{-1} at a driving current of 20 mA.

Lin et al. reported the use of PeNCs@glass composite for backlight displays, reaching high PLQE for $CsPbBr_{1.5}I_{1.5}$ NCs@glass (≈80%) and almost 100% for $CsPbBr_3$ NCs@glass composites.[32] They were prepared following a physical dilution strategy of the dual encapsulation described in Section 4.3, where $CsPbX_3$ NCs@glass was precipitated in PDMS achieving near-unity PLQEs. The maximum luminance and EQE reported for those devices were high, namely 3 00 000, 25 000, 3 50 000 cd m^{-2}, and 5.1%, 3.3%, and 7.2% for green, red and white electroluminescence (EL), respectively, with such high luminance values proving their practicality in backlit liquid crystal displays (LCDs). **Figure** 24A,B demonstrate the appearance of $CsPbX_3$ NCs@glass@PDMS films used as an LCD backlight unit under visible light (orange emission) and 3.3 V applied bias (white emission); a schematic illustration of its implementation into an LCD device is provided in Figure 24C. In comparison to commercial LCD screens with Ce: YAG yellow phosphor (spectrum of its white light is shown in Figure 24D, the $CsPbX_3$ NCs@glass@PDMS (with a white spectrum provided in Figure 24E) allows for more vivid object colors, as illustrated by the photographs of the respective LCD screens in Figure 24F–I, respectively. Objects in varying colors such as green leaves and red fruits/vegetables in Figure 24F–I show better image quality and contrast in the case of PeNCs@glass-based displays as compared to commercial units based on Ce: YAG yellow phosphor, demonstrating the potential of these composites for future display technology with enhanced viewing experience. These composite films also endured harsh stability tests like twisting and stretching with no obvious change in PL intensities, and their spectra did not change after the backlight was turned on for 48 h. Using the same strategy, Lu et al. reported $CsPbBr_3$ NCs@glass@PDMS and $CsPbBr_{1.5}I_{1.5}$ NCs@glass@PDMS with a narrower PL emission of FWHM ≈16 and 33 nm, respectively, and used those composites to fabricate a display that covered 101% and 123% of NTSC 1953 standard with and without the color filters.[178] The idea of using multiphase composites of PeNCs@glass was further expanded by Wang et al. who prepared dual-phase PeNCs@glass@SEBS composites with excellent thermal/water/UV light stabilities and improved flexibility due to the encapsulation into a polymer. As an application in backlit display, the device covered 97.7% and 131% of Rec. 2020 standard and

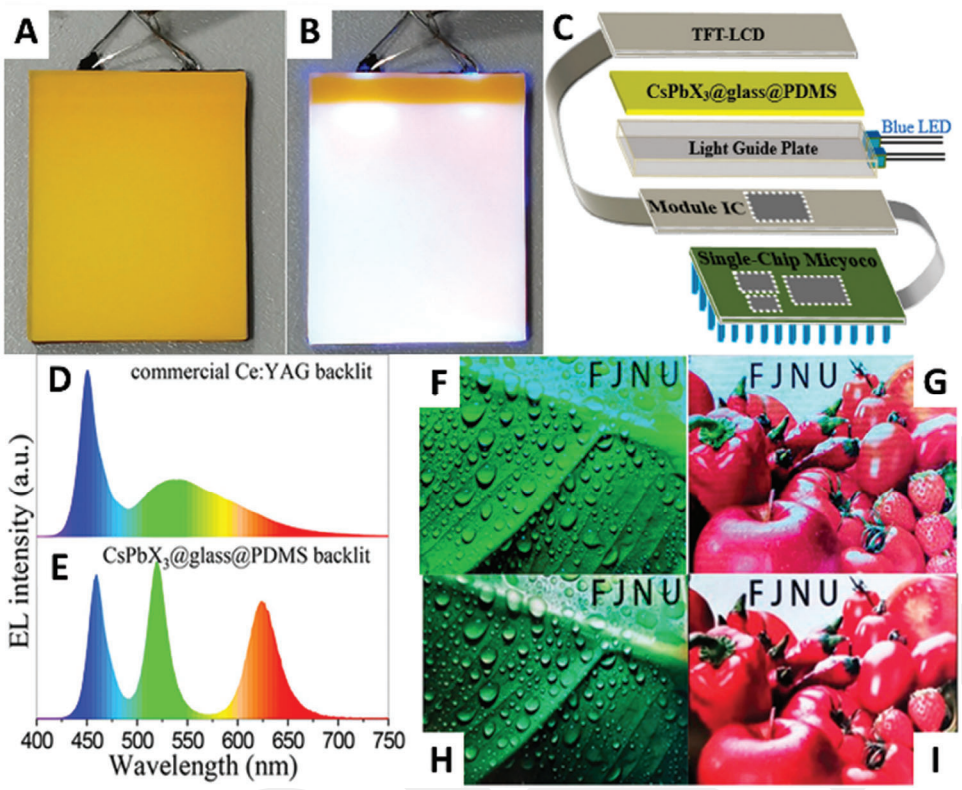

Figure 24. $CsPbX_3$ NCs@glass@PDMS film of the size of 4 cm × 6 cm used as a backlight unit for LCD: A) under visible light and B) under 3.3 V, and C) schematic illustration of its implementation within the LCD structure. Spectra of white backlight films using blue LEDs with D) commercial Ce: YAG yellow phosphor and E) $CsPbX_3$@glass@PDMS film. The color rendition of LCD screens with F,G) commercial backlight unit and H,I) $CsPbX_3$ NCs@glass@PDMS film backlight unit. Reproduced with permission.[32] Copyright 2021, ACS Publications.

NTSC space, respectively, which is even broader than LEDs relying on cadmium-based NCs (NTSC 104%).[146]

Tuning the size of the PeNCs to achieve the desired PL emission color has been explored by Chen et al. who produced green and red light-emitting $CsPbX_3$ NCs@glass for backlight application.[179] As the color purity of display materials is crucial, they demonstrated tunability of the emission of $CsPbBr_3$ NCs@glass and $CsPbBr_xI_{3-x}$ NCs@glass composites through control of various experimental variables like precursors' concentration and thermal treatment features, to obtain green and red light close to the ideal peak positions, which are 530 and 630 nm, respectively. Those green- and red-emitting composites were sandwiched between two layers of hydrophobic and transparent polyethylene terephthalate films providing a backlight display with resistance to thermal, moisture, and light stresses, which showed a consistent device performance for more than 60 h. The accelerated stress test was conducted on these devices by subjecting them to 60 °C and 90% relative humidity conditions. Excellent endurance in these tests was reported for both green- and red-emitting composites maintaining 92% and 95% of their initial PL intensity, respectively, after 48 h. By tailoring the Cl^- to Br^- and Br^- to I^- ratio, Yang et al. fabricated PeNCs@glass composites spanning broad spectral range from 499 to 627 nm, based on $CsPbBr_3$ NCs@glass (PL maximum at 517 nm, green light) and $CsPbBr_{1.5}I_{1.5}$ NCs@glass (PL maximum at 627 nm, red light) with 63% and 46% PLQE, respectively.[51] Even though the reported LE of the backlit white LEDs based on the combination of these green- and red-emitting composites deposited on a blue chip was rather low (6 lm W^{-1}), their superior stability toward heating/cooling cycles and moisture stood out in that study. Apart from the size alterations of PeNCs, the dimensional tunability of perovskites has also been explored by researchers, through the utilization of 0D Cs_4PbBr_6 perovskites to encompass $CsPbBr_3$ NCs to undergo mutual transformation between 3D and 0D structures in the final $CsPbBr_3/Cs_4PbBr_6$ NCs@glass composite.[35] White LED fabricated using this composite as a green light source showed a reasonably high LE of 29.9 lm W^{-1} with a wide color gamut of 126% NTSC value, outlining the potential of such composites in display devices.

LEDs fabricated from the globoid and cuboid-shaped $CsPbBr_3$ NCs@borosilicate glasses showed a very high luminance of 2.6×10^7 cd m^{-2} at a current density of 162 A cm^{-2}. This material was used as the green light source in the backlight display with a LE of 66.11 lm W^{-1} at a 20 mA driving current.[169] In another related study, Hao et al. introduced dysprosium (Dy^{3+}) ions to reduce the lead toxicity in the $CsPbBr_3$ NCs@glass which at the same time enhanced the stability and optical properties of this composite, and resulted in narrow PL FWHM of 18 nm. The white LED fabricated using this composite maintained 99.8% of the initial value of PL intensity during 48 h of continuous illumination with an average luminance of 1193 cd m^{-2}.[38]

Table 6. Summary on $CsPbX_3$ NCs@glass composites used for displays and LEDs.

Compositions	Strategy	Color of emission (device)	LE [lm W^{-1}]	Maximum luminance [cd m^{-2}]	EQE	Rec. 2020	NTSC 1953	Reference
$CsPbX_3$ NCs@glass@PDMS	Physical dilution (dual encapsulation)	Green and red	–	3 00 000 green 25 000 red 3 50 000 white	5.1% green 3.3% red 7.2% white	–	103%	[32]
$CsPbBr_3$ NCs@glass	PET supportive films	Green	–	–	–	94%	126.27%	[179]
$CsPbBr_3$ NCs@glass	In situ crystallization	Green	66	2.6×10^7	35%	94%	126%	[169]
$CsPb(Cl/Br)_3$ NCs@glass@SEBS	Dual encapsulation	Green	–	–	–	97%	131%	[146]
Dy^{3+}-$CsPbBr_3$ NCs@glass	Water quenching method	Green	–	–	–	96%	128%	[38]
$CsPbBr_3/Cs_4PbBr_6$ NCs@glass	Melt-quenching in situ growth	Green	29	–	–	–	126%	[35]
$CsPbX_3$ NCs@glass	In situ glass crystallization	Green and red	6	–	–	92%	123%	[51]
$CsPbBr_3$ NCs@glass	Boron-germanium glass	Green	–	–	–	–	125%	[180]
$CsPbBr_3$ NCs@glass	Nucleation agent addition – TiO_2	Green	22	–	–	93.15%	125.20%	[65]
$CsPbBr_3$ NCs@glass@PDMS and $CsPbBr_{1.5}I_{1.5}$ NCs@glass@PDMS	In situ nucleation/growth	Green and red	–	–	–	–	123%	[178]
$CsPb(Br/I)_3$ NCs@glass	ZnO induced self-crystallization	Red	19	–	–	94%	126%	[181]
$CsPbBr_3$ NCs@glass	Glass network modifiers	Green	67	–	–	–	124%	[149]
$CsPbCl_{1.5}Br_{1.5}$ NCs@SiO_2@glass, $CsPbBr_3$ NCs@SiO_2@glass and $CsPbBrI_2$ NCs@SiO_2@glass	Solution combustion	Blue, green, and red	–	–	–	–	134%	[134]
$CsPbBr_3$ NCs@glass and $CsPbBr_{1.5}I_{1.5}$ NCs@glass	In situ crystallization	Green and red	25.8	6 00 000 green 1 00 000 red 5 00 000 white	15.1% green 8.0% red 13.8% white	–	127%	[57]
$CsPbBr_3$ NCs@glass and $CsPbBr_{1.5}I_{1.5}$ NCs@glass	Sintering	Green and red	–	–	–	–	107%	[56]
$CsPbX_3$ NCs@glass	Self-crystallization melt-quenching	Green and red	–	–	–	–	–	[151]
$CsPbBr_{1.2}I_{1.8}$ NCs@glass and $CsPbBr_3$ NCs@glass	Water quenching method	Green and red	–	–	–	90%	120%	[182]
$CsPbBr_3$ NCs@glass and $CsPb(Br/I)_3$ NCs@glass	Melt-water quenching method	Green and red	–	–	–	93%	125%	[183]
$CsPbX_3$ NCs@glass	Alkaline earth metal oxides optimized crystallization	Blue, green, and red	6.8			–	112%	[184]

PET: Polyethylene terephthalate; SEBS: Styrene-ethylene-butylene-styrene; PDMS: Polydimethylsiloxane.

Pang et al. used boro-germanate glass instead of the silica-based matrix because of its high melting temperature which facilitated the crystallization of $CsPbBr_3$ PeNCs; white LEDs fabricated using this $CsPbBr_3$ NCs@glass composite spanned 125% of the NTSC color space.[180] Introducing nucleation agent TiO_2 into the glass matrix favored the crystallization of $CsPbBr_3$ NCs, and the resulting composite showed outstanding resistance to heat, retaining almost 100% of the initial PL intensity after 10 heating/cooling cycles.[65] Fabricated white LEDs showed LE of 22 lm W^{-1} with emission covering 93.15% of the Rec.2020 color space. Likewise, using ZnO as the nucleation agent which induced self-crystallization of the PeNCs, Wang et al. reported white LEDs with a LE of 19.33 lm W^{-1}, which exhibited high resistivity to bending stresses.[181] Strontium-doped $CsPbBr_3$ NCs@glass composites demonstrated excellent stability and high PLQE and were used to fabricate white LEDs with an LE of 60 lm W^{-1}.[149] A summary of the device characteristics of $CsPbX_3$ NCs@glass composite-based displays and LEDs is given in **Table 6**.

5.2. Anti-Counterfeiting/Security and Information Storage

Related to anti-counterfeiting/security applications of luminescent materials, Wang et al. employed homogenously mixed $CsPbX_3$ NCs ($X_3 = Cl_2Br$, $Cl_{1.8}Br_{1.2}$, Br_3, $Br_{2.5}I_{0.5}$, $Br_{1.8}I_{1.2}$, and

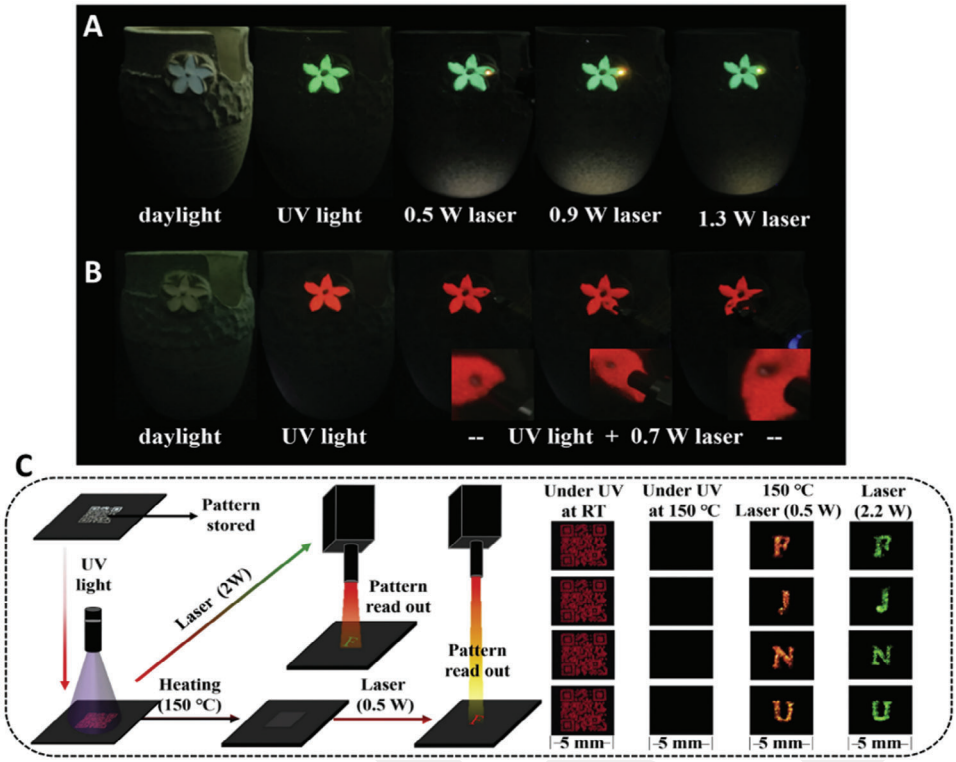

Figure 25. Porcelain glass decorated with flower patterns using composites of A) Er: $CsYb_2F_7$ NCs@glass and $CsPbBr_3$ NCs@glass and B) $CsYb_2F_7$ NCs@glass and $CsPbBr_{1.5}I_{1.5}$ NCs@glass. The patterns are illuminated by UV light and NIR laser with laser power increasing from left to right for (A) and moving in a clockwise direction for (B). C) Storage and read-out schemes of dual-layer pattern (letters and QR code) experiencing quenching of PL of $CsPbBr_{1.5}I_{1.5}$ NCs and the emergence of upconversion luminescence from Er/Eu: $CsYb_2F_7$ NCs during heating or irradiation with NIR laser. Reproduced under the term of CC BY-NC-ND 4.0.[42] Copyright 2022, Cell Press.

$Br_{1.5}I_{1.5}$ for blue, cyan, green, yellow, orange, and red emissions, respectively) and photothermal material (Ln^{3+}-doped $CsYb_2F_7$ NCs) with upconversion PL in glass matrix.[42] The combination of PL emission or quenching (at elevated temperatures) from the $CsPbX_3$ NCs and the upconversion emission from the Ln^{3+}-doped $CsYb_2F_7$ NCs was utilized for anti-counterfeiting and optical encoding. Illumination with a high-power near-infrared (NIR) laser generated significant heat (≈200 °C at 1 W) from the $CsYb_2F_7$ NCs owing to the laser-induced photothermal effect, which quenched the emission of $CsPbX_3$ NCs; whereas lanthanide-doped $CsYb_2F_7$ NCs@glass produced color-tunable upconversion emissions for different NIR-laser powers. Different lanthanide ions (Eu^{3+}, Er^{3+}, Ho^{3+}, Tm^{3+}) were introduced as dopants and co-dopants into $CsYb_2F_7$ NCs@glass. A flower pattern was created on a porcelain glass cup decorated with Er: $CsYb_2F_7$ NCs@glass and $CsPbBr_3$ NCs@glass; upon UV illumination green PL corresponding to $CsPbBr_3$ NCs was observed, while upon NIR laser irradiation a superimposing (over the green light) upconverted emission from Er^{3+} was detected (**Figure** 25A). The superimposing upconversion emission was tunable from red to green with an increase in NIR laser power. A similar pattern of the flower was also demonstrated with homogenously mixed $CsYb_2F_7$ NCs@glass and $CsPbBr_{1.5}I_{1.5}$ NCs@glass, which under UV illumination appeared red corresponding to $CsPbBr_{1.5}I_{1.5}$ NCs emission. Besides, when certain areas were illuminated simultaneously with a NIR laser, the emission was erased which was recoverable upon removal of the laser (Figure 25B). Moreover, the authors also realized dual layer patterns with Er^{3+} doped and Eu^{3+} co-doped $CsYb_2F_7$ NCs@glass and $CsPbBr_{1.5}I_{1.5}$ NCs@glass mixture. As shown in Figure 25C, letters F, J, N, and U were made using Er/Eu: $CsYb_2F_7$ NCs@glass which was concealed by a QR code pattern fabricated using $CsPbBr_{1.5}I_{1.5}$ NCs@glass. The QR code was visible under UV light whereas the letters were hidden, and only became visible under NIR laser illumination. Under high-power (2.2 W) laser irradiation and UV light, the QR code was invisible, and only the upconversion emission from the letters was visible, owing to the laser-induced photothermal effect. Optical coding was also demonstrated, where the PL colors of different $CsPbX_3$ NCs represented the digits 1, 2, 3, 4, 5, and 6, whose PL was quenched under laser illumination representing the dark state denoted as 0. Replacement of non-emitting $CsYb_2F_7$ NCs@glass with lanthanide-doped materials offering tunable upconversion colors expanded the optical-encoding states with an increase in complexity, making them difficult to duplicate.[42]

In Ref.[185], photon upconversion of $CsPbX_3$ NCs was achieved in glasses in their combination with Tm: KYb_2F_7 acting as the energy donor. Both downconversion and upconversion dual emission were utilized to create screen-printed luminescent patterns, using different excitation modes such as UV light and NIR laser. However, there is still a demand to achieve higher security, faster response, easier/stable operation,

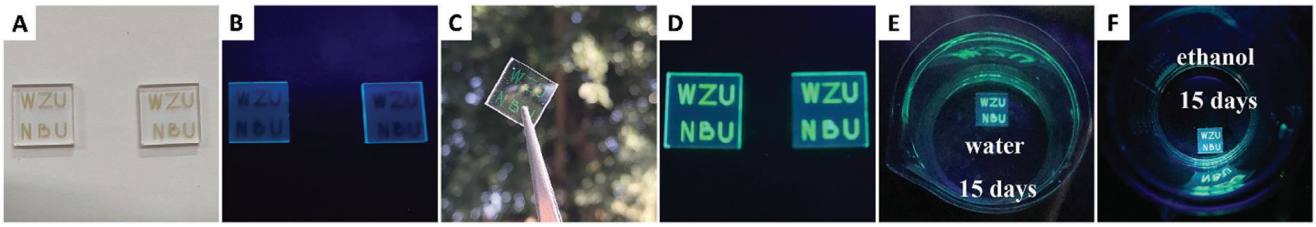

Figure 26. Photographs illustrating the femtosecond-laser-induced crystallization in $CsPbBr_3$ NCs@glass under A) daylight and B) UV light, as well as of samples subjected to further heat-treatment under C) daylight and D) UV light. Stable green emissions of these composites could be detected in (E) water and (F) ethanol for 15 days. Reproduced with permission.[44] Copyright 2022. Elsevier.

and improved selectivity for real-time and non-invasive detection. In this respect, luminescent polarized patterns are an excellent tool and PeNCs@glasses can enable this feature. By using a programmable femtosecond laser and annealing, Chen et al. generated linear patterns of $CsPbBr_3$ NCs in borogermanate glasses, which showed optical polarization properties.[163] Multilayer luminescent patterns of $CsPbBr_3$ NCs with anisotropic emission were constructed for 3D polarized optical anti-counterfeiting and encryption. 2D and 3D patterns of $CsPbBr_3$ NCs in the glass matrix made of horizontal and vertical lines showed different output optical images under different polarization angles.

Extending the use of PeNCs@glass composites into information storage technology, Jin et al.[44] demonstrated direct laser writing on colorless and transparent $CsPbBr_3$ NCs@glass composites produced by inhibiting their self-crystallization with varying ZnO content (**Figure 26**). A femtosecond laser was used to induce the crystallization of $CsPbBr_3$ NCs resulting in the appearance of green emission; the same kind of illumination was further used for the decomposition of $CsPbBr_3$ NCs, termed laser erasing. The crystallized green dots represented the logical binary number 1, while the decomposed regions denoted the binary state 0. Using a combination of femtosecond laser-induced crystallization (50 mW, 5 s) and heat-treatment at 460 °C, the possibility of rewritable information storage was demonstrated. As an example, Arabic numbers (15, 15, 15, 15) were written as binary numbers, followed by erasing certain data points by re-illumination with laser (20 mW, 50 μm s^{-1}) to change them to (13, 10, 6, 3), and finally restoring them to the initial numbers via annealing. Achieving high-speed and low-power consumption in optical storage devices with reversible characteristics are prerequisite to fabricating high-performance data storage devices. PeNCs@glass composites are capable of meeting these requirements because various patterns and binary data arrays can be written or erased in any depth of glass. Sun et al. demonstrated a reversible 3D optical storage technique utilizing laser-induced PL degradation and recovery by heat treatment of $CsPbBr_3$ NCs doped in borosilicate glass with a composition of $38SiO_2$-$34B_2O_3$-11ZnO-$6Cs_2O$-$2PbX_2$-9NaBr.[186] Laser irradiation was used to write data into the glass, which can then be read under 485 nm excitation as local dark PL images. By varying the laser power, repetition, and pulse rate, the PL degradation of the darkened regions could be modified. The written data was recovered by heat treatment and multiple "write-read-erase" cycles showed that the PL intensity of the laser-darkened regions recovered to the initial state after each stage. Huang et al. also established direct laser patterning of $CsPbBr_3$ NCs in a glass matrix using an 800 nm near-infrared femtosecond laser.[50] The femtosecond laser-induced crystallization of Cs, Pb, and Br elements to form 3D bright green $CsPbBr_3$ NCs, and also was able to decompose these NCs, which could be recovered by annealing. Such a reversible in situ crystallization and decomposition of $CsPbBr_3$ NCs can be extended to the patterning of PeNCs in glass and also to the application of these composites in optical data storage or information security. In general, this laser-assisted writing or designing provides some sort of hidden capability at which luminescent PeNCs show a luminescent-on-demand property.

5.3. Lasers

Several researchers have demonstrated amplified spontaneous emission from the PeNCs@glass composites, making use of their improved stability provided by the glass encapsulation. $CsPbBr_3/Cs_4PbBr_6$ PeNCs@glass composite exhibited low-threshold amplified spontaneous green emission at room temperature upon excitation with 800 nm femtosecond pulse laser, with FWHM narrowing down to almost 5 nm above the threshold (1.66 mJ cm^{-2}).[35] The composite was heat-treated at different temperatures and showed a decrease in threshold pump intensity with an increase in crystallization temperature from 520 to 580 °C, which was attributed to the enhanced crystallinity. Similarly, by varying heat-treatment temperatures, Zhang et al.[40] produced surface-passivated $CsPbBr_3$ PeNCs@glass composites exhibiting both amplified spontaneous emission and lasing under 800 nm femtosecond laser excitation. With the crystallinity of PeNCs improving upon an increase in heat-treatment temperature from 440 to 530 °C, the lasing threshold decreased from 0.752 to 0.138 mJ cm^{-2}. A recent study on PeNCs@glass showed that the halogen migration during excitation by laser still exists, and limits the ability of the composite to reach stable stimulated emission. Liu's group studied the effect of femtosecond laser irradiation on the structural and optical properties of $CsPbBr_3$ PeNCs@ borosilicate glasses (at different concentrations of NaBr).[187] Their findings showed that laser irradiation did not influence the structure and optical bandgap of PeNCs. Instead, it induced surface Br vacancies which functioned as surface defects and were responsible for carrier trapping and subsequent quenching of PL emission. The PL and transient absorption spectroscopies further showed that composites with higher concentrations of NaBr experienced a new carrier trapping route upon irradiation with a femtosecond laser. That means that

enhanced PLQE in the case of a higher concentration of NaBr would not guarantee the appearance of lasing, and further modifications may still be required to prevent the anion migration in PeNCs@glass composite.

5.4. Photodetectors and X-Ray Detectors

PeNCs with their high absorption coefficients in the UV and visible spectral range are also of interest for their use as an active layer in photodetectors. However, like in many other applications, it is the detrimental stability of perovskites that hindered the progress. Thus, as the PeNCs@glass composites offered better stability against extrinsic factors without detrimentally affecting the intrinsic optoelectronic properties of the PeNCs, there were some attempts to employ them in photodetectors. In one such demonstration, Ye et al.[33] coated the surface of a silicon photodiode with Tb^{3+}-doped $CsPbCl_2Br_1$ NCs@glass composite, which improved both the responsivity and EQE of the device in the range of 200–400 nm. The responsivity reached 0.005 A W^{-1}, five times that of the uncoated silicon photodetector in the UV range (200–400 nm), and EQE was 3.79% at 320 nm.

PeNCs@glass composites were also tested for use in X-ray detectors (scintillators). Wang et al.[188] employed $CsPb(Cl/Br)_3$ NCs@glass composites as scintillators generating radioluminescence in the range of violet to green by tuning the Cl/Br molar ratio. Though X-rays caused damage to PeNCs, the irradiated spots recovered their luminescence after thermal annealing at a temperature higher than the T_g by facilitating ionic migration, which regenerated $CsPbX_3$ NCs in the glass. This recoverability enabled the reuse of these scintillators for high-intensity X-ray detection. It was found that $CsPb(Cl/Br)_3$ NCs@glass crystallized at 520 and 470 °C demonstrated radioluminescence intensity of 1/18 and 1/570 as compared to that of commercial $Bi_4Ge_3O_{12}$ single crystal scintillator. Recoverability of X-ray-damaged PeNCs in scintillators was also demonstrated for $CsPbBr_3$:Lu^{3+} NCs@glass by applying heat treatment. The scintillator achieved a high-resolution X-ray imaging of 16.8 lp mm^{-1}, as well as a record-low detectable dose (50 nGy_{air} s^{-1}).[52]

5.5. Photocatalysis

Photocatalytic hydrogen generation through water splitting is an attractive technology to generate renewable, environmental-friendly and sustainable hydrogen fuel which can contribute to decarbonization of the energy sector. Over the years, many research groups have explored the possibilities of various semiconductors – including perovskites – as photoelectrodes for water splitting. Optimal materials for water splitting should possess a bandgap in the range of 1.7–2.2 eV, suitable band energy offsets to drive redox half-reactions of hydrogen/oxygen generation, a large absorption coefficient, efficient carrier mobility, and high stability in aqueous electrolytes. The severe stability issue of the metal halide perovskites in the aqueous medium could be solved to a certain degree by using chemically inert matrices such as PeNCs@glass composite, which set the possibility for their use as photocatalysts in water splitting. In one of the initial reports, using Zn^{2+}-doped $CsPbBr_3$ NCs@borosilicate glass powders for hydrogen generation, Ding et al.[189] demonstrated a hydrogen production rate of 127 μmol g^{-1}. The conduction band potential (E_{CB}) of the $CsPbBr_3$:$0.5Zn^{2+}$ NCs@glass composite was 0.043 eV which was lower than the hydrogen reduction potential ($EH_2/H^+ = 0$ V), favoring the hydrogen generation. $CsPbBr_3$:$0.5Zn^{2+}$ NCs@glass composite realized a higher photocurrent density (0.1343 μA cm^{-2}) as compared to the pristine $CsPbBr_3$ NCs@glass samples (0.1198 μA cm^{-2}).

In a study focused on the use of PeNCs@glass as a photocatalyst, Li et al.[45] used phase separation-induced $CsPbBr_3$ NCs@glass composites for tetracycline hydrochloride (TC-HCl) antibiotic residue degradation. In this case, the electrons and holes generated by photon absorption in the conduction and valence bands of the photocatalyst reacted with the organic pollutants to transform them into harmless substances. The $CsPbBr_3$ NCs@glass composite showed a 73% degradation efficiency for 20 mg L^{-1} of the TC-HCl concentration after 60 min of light illumination. After three cycles of the TC-HCl degradation, the composite retained 85% of the photocatalytic effect to its initial value, with 60% of the antibiotic decomposed. In addition, green emission from the $CsPbBr_3$ NCs@glass composite could be detected in the black precipitate in water, indicating their aqueous stability. The photodegradation mechanism of the TC-HCl with $CsPbBr_3$ NCs@glass was ascribed to the formation of highly reactive substances like hydroxyl radicals and superoxide radicals at the interface of the composite and the environment, which oxidized the organic molecules into inorganic compounds.

5.6. Optical Filters

Materials that exhibit wide absorption with a steep excitonic absorption edge, combined with narrow and symmetrical PL spectra and small Stokes shift between the band edge absorption and emission are considered perfect candidates for long-pass optical filters, which are able to pass long wavelengths while serving as a shield for shorter wavelengths. As a result, the long-pass filters attenuate the shorter wavelength regions in the targeted range of the electromagnetic spectrum while transmitting the longer wavelengths. This type of filter is used in Raman spectroscopy to separate the excitation wavelength from that of the Raman scattered light; they are also employed in other spectroscopic techniques like fluorescence spectroscopy to reduce the excitation light leakage and improve the fluorescence from the sample and in photometric instruments for the elimination of optical aberrations. Among the current three materials used for the long-wavelength pass filters in glass matrix – noble metal nanoparticles, high/low dielectric coatings, and semiconductor NCs in glass – the PeNCs@glass composites fall under the latter category. Zhang et al.[190] demonstrated how green emitting compositions of $CsPbBr_3$ NCs@glass could work as long-wavelength pass filters for the 494–525 nm spectral region, with superior cut-off depth. They crystallized the PeNCs at different heat-treatment temperatures; as a determining factor, the maximum transmittance (T_{max}) for the filters was 84%, 80%, 76%, and 64% for the samples treated at temperatures of 490, 510, 530, and 550 °C, respectively. The authors demonstrated that the transition wavelength, which is defined as the 50% of maximum transmittance, of these $CsPbBr_3$ NCs@glass filters varied with the change in the

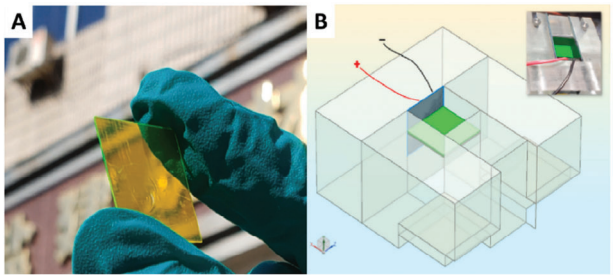

Figure 27. A) Photograph (taken under sunlight) of yellow $CsPbBr_3$ NCs@glass sheet with a size of $2.0 \times 2.0 \times 0.11$ cm^3. B) A schematic illustration of the LSC-solar cell setup; the inset shows its photograph under solar simulation illumination. Reproduced with permission.[55] Copyright 2022, Elsevier.

treatment temperature, constituting 494, 511, 518, and 525 nm for the order of temperatures mentioned above, respectively. The optical density demonstrated for these $CsPbBr_3$ NCs@glass filters was on the order of 2–5 in the cut-off band, and thus very close to the commercial requirement.

In another work demonstrating the potential of PeNCs@glass composite as filters, Wang et al.[43] made use of the broadband absorption of $CsPbBr_3$ NCs to demonstrate the shielding effect in the deep blue wavelength region. They used a V^{5+}-doped tellurite-based glass matrix, where $CsPbBr_3$ PeNCs crystallized at different treatment temperatures. In this case, the V^{5+} ions not only replaced the Pb^{2+} ionic sites and reduced the emission intensity of the PeNCs, but also improved the self-absorption characteristic of the composite beneficial for short-wavelength shielding. The undoped $CsPbBr_3$ NCs@glass composites with absorption cut-off at 471 and 507 nm (treated at 280 and 310 °C, respectively) could not cover entirely their corresponding emission peak. Upon increase in the V^{5+} dopant concentration and/or heat-treatment temperature, the samples exhibited 80% transmittance, and at the same time, the V^{5+}-doping extended the absorption cut-off edge and changed the bimodal emission to a single peak emission, indicating self-absorption of the blue emission part by the material itself.

5.7. Solar Concentrators

Luminescent solar concentrators (LSCs) are considered promising for smart windows and photovoltaic modules integrated into the windows/buildings. Zhang et al.[55] incorporated $CsPbBr_3$ NCs into a glass matrix to fabricate perovskite-based LSCs with remarkable stability, which were combined with a silicon photovoltaic system reaching power conversion efficiency of 0.57% alongside optical efficiency (defined as the ratio of photons emitted from the edges of $CsPbBr_3$ NCs@glass sheet to the photons striking on the LSC top surface) of 6.17%. **Figure 27**A provides a photograph of the LSC based on the $CsPbBr_3$ NCs@glass sheet with dimensions of $2.0 \times 2.0 \times 0.11$ cm^3, which appears intense-yellow under sunlight. The LSC-photovoltaic system was fabricated by mounting commercial silicon solar cells on one of the four edges of the 2×2 cm^2 $CsPbBr_3$ NCs@glass sheet, while black tapes covered all the remaining three edge surfaces to prevent effects from the light scattering (Figure 27B). By reducing the thickness of the LSC sheet from 1.1 to 0.24 mm, the geometric factor (G factor) varied from 4.5 to 20.8 showing a gradual decrease in optical efficiency from 6.17% (G factor ≈4.5) to 2.10% (G factor ≈20.8).[55]

5.8. Batteries

Lithium-ion batteries are considered to be one of the most efficient energy storage devices nowadays. However, they still face several limitations in terms of lithium storage capacity, interphase charge transfer, cycling stability, and safety features. Even though graphite is the most commercially successful lithium anode, the capacity of these materials still requires further improvement which has encouraged researchers to look for alternative materials. Glass-based open network anodes have been found to prevent the large volumetric expansion of electrodes during the lithiation/delithiation process.[191–193] Also, their flexibility, crystal content tunability, and easy processibility have caught the attention of researchers. Thus, PeNCs@glass ceramics have been tested as anodes for Li-ion batteries, as well. Cao et al.[39] employed SnF_2-doped 0D Cs_4PbBr_6 NCs@glass ceramic as a Li-ion battery anode, which demonstrated excellent cyclic stability with the specific capacity achieving 773 mAh g^{-1} at 0.5 A g^{-1} and maintaining 741 mAh g^{-1} after 350 cycles and 292 mAh g^{-1} at 10 A g^{-1}. As the presence of F^- ions reduced the glass viscosity and Sn ions replaced some Pb ion sites in the PeNCs, SnF_2 doping into Cs_4PbBr_6 NCs@glass ceramic improved the structural stability of the composite. In addition, with the $[GeO_\delta]$-$[BO_\gamma]$ networks acting as lithium storage sites, and Pb, Ge, and Sn alloying (Pb/Ge/Sn−Li) reactions occurring during lithium storage, these anodes showed excellent cyclic stability and performance. Low-dimensional perovskite Cs_4PbX_6 NCs@glass (X = Cl, Br, or I) ceramic anode for Li-ion batteries was also reported by Xie et al.[194] who studied interfacial transport using electrochemical impedance spectroscopy. The best discharging capability among the different halides was found for Cl^--based perovskite with a specific capacity at 510.5 mAh g^{-1} whereas the Br-based one retained the specific capacity at 429.6 mAh g^{-1} after 1000 cycles. A high ionic conductivity was demonstrated for the $Cs_4Pb(Cl/Br/I)_6$ NCs@glass, in the order of 10^{-5}–10^{-4} S cm^{-1}.[194]

6. Conclusion and Outlook

This review presented promising aspects and wide opportunities that PeNCs@glass composites hold to resolve the issue of stability or degradation of metal halide perovskites, thus broadening their application in various optoelectronic devices. Particularly, we introduced and classified the approaches used for the fabrication of PeNCs@glass composites with enhanced functionality, such as composition modification, structural modification, and dual encapsulation. We discussed the beneficial aspects of inorganic oxide glasses as a platform to trigger the nucleation and growth of luminescent PeNCs with improved stability against external conditions. Finally, the use of PeNCs@glass composites as active layers in LEDs, backlit displays, security, lasing, and sensing applications as well as electrodes in batteries was considered.

Different solvent-free approaches used for the fabrication of PeNCs@glass composites such as sol-gel and melt-quenching techniques are simple, facile, and scalable. Many authors focused on high-quality PeNCs@glass composite prepared via the melt-quenching process, where the desired precursors in powder form (usually metal oxides, or metal fluorides) are mixed in the required ratios, followed by heating up to the melting point and subsequent quenching to a lower temperature, and finally maintaining the temperature to minimize the lattice strain. Even though this route toward embedding PeNCs in various glass matrices addresses the crucial question of stability and solves it to a significant extent, there are still some shortcomings and physicochemical aspects that have to be further studied and optimized. The high melting temperature that is required during the fabrication processes of amorphous glasses prohibits the formation of hybrid organic-inorganic metal halide PeNCs within the glass networks, which excludes a large category of luminescent PeNCs, apart from all-inorganic (Cs as an A-site cation) counterparts considered in this review. We are aware of only one report on organic-inorganic PeNCs@glasses, which used pre-synthesized PeNCs to incorporate them into the glass matrix,[195] but this approach is different from in situ precipitation of PeNCs inside the glass network. Still, their emission intensity and stability were not comparable to all-inorganic PeNCs in glass. Therefore, any development toward mitigation of the role of melting temperature would extend accessibility to other types of luminescent PeNCs in glasses.

Also, most of the reports considered in this review were focused on lead-containing PeNCs as an active material. Thus, there is still a lot of room for exploring non-toxic lead-free PeNCs fabricated in glass matrices Figuring out new synthetic routes on less-toxic or non-toxic PeNCs in different glass matrices and understanding their physicochemical properties, which was addressed in part in Ref.[61], is a promising research direction. With the focus on the ultimate applications of PeNCs@glass composites in advanced technologies, one should also resolve the challenges related to the high rigidity of the final luminescent composites. Beyond this, developing approaches to functionalize the surface of PeNCs@glass composites may enable more advancements toward their broader use. From the chemistry perspective, there is a still lack of knowledge of the interaction and bonding nature between amorphous glass matrix and perovskite lattice, and its influence on the photophysical properties of the resulting composites. Also, in-depth characterization of electronic and optical features of the PeNCs@glass composite is necessary and should include the studies of charge carrier dynamics and radiative/non-radiative pathways and the effect of defect passivation and improved structural integrity of the PeNCs as a result of glass medium encapsulation. This may offer useful insights into electron-phonon interactions and polaron formation in PeNCs. Polarons are quasiparticles emerging from the interaction of electrons with atomic lattice, which were found to exist in transition metal glasses[115] and also in colloidal perovskite NCs.[196] To the best of our knowledge, there are no reports related to the interactions with polarons and their possible roles in the optical features of the PeNCs@glass composites. Overall, embedding PeNCs in structurally stable and chemically inert glass matrices will further help researchers broaden the applicability of these materials in future applications.

Acknowledgements

E.S. acknowledges the funding support from Ilam University. A.L.R. acknowledges financial support from the Croucher Foundation of Hong Kong.

Conflict of Interest

The authors declare no conflict of interest.

Keywords

amorphous oxide glasses, composite materials, light emission, perovskite nanocrystals, stability

Received: September 12, 2023
Revised: November 9, 2023
Published online: December 10, 2023

[1] Y. Wei, Z. Cheng, J. Lin, *Chem. Soc. Rev.* **2019**, *48*, 310.
[2] C. R. Kagan, D. B. Mitzi, C. D. Dimitrakopoulos, *Science* **1999**, *286*, 945.
[3] L. Protesescu, S. Yakunin, M. I. Bodnarchuk, F. Krieg, R. Caputo, C. H. Hendon, R. Xi Yang, A. Walsh, M. V. Kovalenko, *Nano Lett.* **2015**, *15*, 3692.
[4] F. Zhang, H. Zhong, C. Chen, X. G. Wu, X. Hu, H. Huang, J. Han, B. Zou, Y. Dong, *ACS Nano* **2015**, *9*, 4533.
[5] X. Wang, Z. Bao, Y.-C. Chang, R.-S. Liu, *ACS Energy Lett.* **2020**, *5*, 3374.
[6] M. C. Brennan, M. Kuno, S. Rouvimov, *Inorg. Chem.* **2019**, *58*, 1555.
[7] X. Zhang, W. Wang, B. Xu, S. Liu, H. Dai, D. Bian, S. Chen, K. Wang, X. W. Sun, *Nano Energy* **2017**, *37*, 40.
[8] J. Zeng, C. Meng, X. Li, Y. Wu, S. Liu, H. Zhou, H. Wang, H. Zeng, *Adv. Funct. Mater.* **2019**, *29*, 1904461.
[9] C. Zhang, S. Wang, X. Li, M. Yuan, L. Turyanska, X. Yang, *Adv. Funct. Mater.* **2020**, *30*, 1910582.
[10] C.-Y. Huang, C. Zou, C. Mao, K. L. Corp, Y.-C. Yao, Y.-J. Lee, C. W. Schlenker, A. K. Y. Jen, L. Y. Lin, *ACS Photonics* **2017**, *4*, 2281.
[11] E. Soheyli, S. Zargoush, A. F. Yazici, R. Sahraei, E. Mutlugun, *J. Phys. D. Appl. Phys.* **2021**, *54*, 505110.
[12] Y. Altintas, U. Quliyeva, K. Gungor, O. Erdem, Y. Kelestemur, E. Mutlugun, M. V. Kovalenko, H. V. Demir, *Small* **2019**, *15*, 1804854.
[13] P. Yu, S. Cao, Y. Shan, Y. Bi, Y. Hu, R. Zeng, B. Zou, Y. Wang, J. Zhao, *Light Sci. Appl.* **2022**, *11*, 162.
[14] H. Huang, M. I. Bodnarchuk, S. V. Kershaw, M. V. Kovalenko, A. L. Rogach, *ACS Energy Lett.* **2017**, *2*, 2071.
[15] R. E. Brandt, J. R. Poindexter, P. Gorai, R. C. Kurchin, R. L. Z. Hoye, L. Nienhaus, M. W. B. Wilson, J. A. Polizzotti, R. Sereika, R. Žaltauskas, L. C. Lee, J. L. MacManus-Driscoll, M. Bawendi, V. Stevanović, T. Buonassisi, *Chem. Mater.* **2017**, *29*, 4667.
[16] F. Shabani, P. L. H. Martinez, N. Shermet, H. Korkut, I. Sarpkaya, H. Dehghanpour Baruj, S. Delikanli, F. Isik, E. G. Durmusoglu, H. V. Demir, *Small* **2023**, *19*, 2205729.
[17] N. N. Jawhar, E. Soheyli, A. F. Yazici, E. Mutlugun, R. Sahraei, *J. Alloys Compd.* **2020**, *824*, 153906.
[18] E. Soheyli, A. Biçer, S. S. Ozel, K. Sahin Tiras, E. Mutlugun, *ACS Omega* **2023**, *8*, 39690.
[19] A. Dey, J. Ye, A. De, E. Debroye, S. K. Ha, E. Bladt, A. S. Kshirsagar, Z. Wang, J. Yin, Y. Wang, L. N. Quan, F. Yan, M. Gao, X. Li, J. Shamsi, T. Debnath, M. Cao, M. A. Scheel, S. Kumar, J. A. Steele, M. Gerhard, L. Chouhan, K. Xu, X. Wu, Y. Li, Y. Zhang, A. Dutta, C. Han, I. Vincon, A. L. Rogach, *ACS Nano* **2021**, *15*, 10775.

[20] Y. Ye, W. Zhang, Z. Zhao, J. Wang, C. Liu, Z. Deng, X. Zhao, J. Han, *Adv. Opt. Mater.* **2019**, *7*, 1801663.
[21] T.-H. Han, K. Y. Jang, Y. Dong, R. H. Friend, E. H. Sargent, T.-W. Lee, *Nat. Rev. Mater.* **2022**, *7*, 757.
[22] Y. Xu, X. Zhao, M. Xia, X. Zhang, *J. Mater. Chem. C* **2021**, *9*, 5452.
[23] Z. Zhang, L. Shen, Y. Zhao, Y. Zhang, H. Yang, W. Xiang, X. Liang, G. Chen, H. Yu, *Chem. Eng. J.* **2020**, *385*, 123415.
[24] K. Li, Y. Ye, W. Zhang, Y. Hu, Y. Yang, Y. Zhou, C. Liu, *J. Mater. Chem. C* **2021**, *9*, 11261.
[25] S. Wang, J. Lin, Y. He, J. Chen, C. Yang, F. Huang, D. Chen, *Chem. Eng. J.* **2020**, *394*, 124889.
[26] J. Xue, X. Wang, J. H. Jeong, X. Yan, *Chem. Eng. J.* **2020**, *383*, 123082.
[27] Q. Pan, D. Yang, G. Dong, J. Qiu, Z. Yang, *Prog. Mater. Sci.* **2022**, *130*, 100998.
[28] A. I. Ekimov, A. L. Efros, A. A. Onushchenko, *Solid State Commun.* **1985**, *56*, 921.
[29] M. Xia, J. Luo, C. Chen, H. Liu, J. Tang, *Adv. Opt. Mater.* **2019**, *7*, 1900851.
[30] J. Jiang, G. Shao, Z. Zhang, L. Ding, H. Zhang, J. Liu, Z. Chen, W. Xiang, X. Liang, *Chem. Commun.* **2018**, *54*, 12302.
[31] D. Chen, S. Yuan, X. Chen, J. Li, Q. Mao, X. Li, J. Zhong, *J. Mater. Chem. C* **2018**, *6*, 6832.
[32] J. Lin, Y. Lu, X. Li, F. Huang, C. Yang, M. Liu, N. Jiang, D. Chen, *ACS Energy Lett.* **2021**, *6*, 519.
[33] H. Ye, Q. Wang, Z. He, Y. Tong, W. Xia, H. Fan, W. Xiang, X. Liang, *ACS Appl. Nano Mater.* **2022**, *5*, 6447.
[34] Y. Lu, X. Liu, P. Li, Y. Duan, S. Xu, J. Zhang, *J. Phys. Chem. C* **2021**, *125*, 27497.
[35] Z. He, Q. Wang, X. Liang, K. Yang, W. Xiang, *Appl. Phys. Lett.* **2021**, *119*, 161902.
[36] B. Liu, G. Wang, Y. Lu, W. Wang, Z. Liu, J. Li, *ACS Appl. Nano Mater.* **2022**, *5*, 9503.
[37] J. Deng, H. Wang, J. Xun, J. Wang, X. Yang, W. Shen, M. Li, R. He, *Mater. Des.* **2020**, *185*, 108246.
[38] M. Hao, Q. Wang, J. Li, W. Xiang, H. Fan, X. Liang, *Mater. Today Chem.* **2022**, *26*, 101020.
[39] J. Cao, W. Xie, K. Liu, X. Meng, J. Zhang, J. Zhang, Z. Yao, M. Fan, *J. Phys. Chem. C* **2022**, *126*, 3359.
[40] H. Zhang, L. Yuan, Y. Chen, Y. Zhang, Y. Yu, X. Liang, W. Xiang, T. Wang, *Chem. Commun.* **2020**, *56*, 2853.
[41] X. Liu, E. Mei, Z. Liu, J. Du, X. Liang, W. Xiang, *ACS Photonics* **2021**, *8*, 887.
[42] S. Wang, J. Zhu, H. Huang, J. Lin, C. Yang, S. Liao, F. Huang, D. Chen, *Cell Reports Phys. Sci.* **2022**, *3*, 100794.
[43] Z. Wang, Y. Duan, P. Li, S. Xu, J. Zhang, *J. Lumin.* **2022**, *250*, 118918.
[44] M. Jin, W. Zhou, W. Ma, Q. Wang, X. Liang, P. Zhang, W. Xiang, *Chem. Eng. J.* **2022**, *427*, 129812.
[45] P. Li, Y. Lu, Y. Duan, S. Xu, J. Zhang, *J. Phys. Chem. C* **2021**, *125*, 2382.
[46] B. Ai, C. Liu, J. Wang, J. Xie, J. Han, X. Zhao, J. Heo, *J. Am. Ceram. Soc.* **2016**, *99*, 2875.
[47] X. Di, Z. Hu, J. Jiang, M. He, L. Zhou, W. Xiang, X. Liang, *Chem. Commun.* **2017**, *53*, 11068.
[48] S. Yuan, D. Chen, X. Li, J. Zhong, X. Xu, *ACS Appl. Mater. Interfaces* **2018**, *10*, 18918.
[49] D. Chen, Y. Liu, C. Yang, J. Zhong, S. Zhou, J. Chen, H. Huang, *Nanoscale* **2019**, *11*, 17216.
[50] X. Huang, Q. Guo, D. Yang, X. Xiao, X. Liu, Z. Xia, F. Fan, J. Qiu, G. Dong, *Nat. Photonics* **2020**, *14*, 82.
[51] C. Yang, B. Zhuang, J. Lin, S. Wang, M. Liu, N. Jiang, D. Chen, *Chem. Eng. J.* **2020**, *398*, 125616.
[52] H. Zhang, Z. Yang, M. Zhou, L. Zhao, T. Jiang, H. Yang, X. Yu, J. Qiu, Y. (M.). Yang, X. Xu, *Adv. Mater.* **2021**, *33*, 2102529.
[53] K. Sun, D. Tan, X. Fang, X. Xia, D. Lin, J. Song, Y. Lin, Z. Liu, M. Gu, Y. Yue, J. Qiu, *Science* **2022**, *375*, 307.
[54] Y. Duan, P. Li, L. Lei, F. Huang, Y. Tian, S. Xu, J. Zhang, *J. Phys. Chem. C* **2022**, *126*, 4220.
[55] Y. Zhang, W. Zhang, Y. Ye, K. Li, X. Gong, C. Liu, *Sol. Energy Mater. Sol. Cells* **2022**, *238*, 111619.
[56] S. Liao, Z. Yang, J. Lin, S. Wang, J. Zhu, S. Chen, F. Huang, Y. Zheng, D. Chen, *Adv. Funct. Mater.* **2023**, *33*, 2210558.
[57] S. Chen, J. Lin, S. Zheng, Y. Zheng, D. Chen, *Adv. Funct. Mater.* **2023**, *33*, 2213442.
[58] Y. Le, X. Huang, H. Zhang, Z. Zhou, D. Yang, B. Yin, X. Liu, Z. Xia, J. Qiu, Z. Yang, G. Dong, *Adv. Photonics* **2023**, *5*, 46002.
[59] Z. Zhang, X. Zhang, L. Li, J. Xu, H. Yin, X. Gong, R. Ding, Y. Zhang, C. Li, *ACS Appl. Electron. Mater.* **2021**, *3*, 4824.
[60] H. Chen, Z. Gao, P. Lv, L. Sun, C. Xu, *J. Non. Cryst. Solids* **2022**, *597*, 121867.
[61] K. Li, W. Zhang, L. Niu, Y. Ye, J. Ren, C. Liu, *Adv. Sci.* **2023**, *10*, 2204843.
[62] Y. Zhang, X. Zhang, C. Li, M. Chen, S. Huang, Z. Zhang, X. Gong, R. Ding, J. Xu, L. Li, *ACS Sustainable Chem. Eng.* **2023**, *0*, null.
[63] Y. H. Nam, K. Han, W. J. Chung, W. Bin Im, *ACS Appl. Nano Mater.* **2021**, *4*, 7072.
[64] Y. Zhao, C. Shen, L. Ding, J. Liu, W. Xiang, X. Liang, *Opt. Mater.* **2020**, *107*, 110046.
[65] Y. Tong, Q. Wang, X. Liu, E. Mei, X. Liang, W. Xiang, *Chem. Eng. J.* **2022**, *429*, 132391.
[66] X. Xiang, H. Lin, R. Li, Y. Cheng, Q. Huang, J. Xu, C. Wang, X. Chen, Y. Wang, *Nano Res.* **2019**, *12*, 1049.
[67] Z. Yang, H. Zhang, Z. Fang, J. Yi, P. Song, X. Yu, D. Zhou, J. Qiu, X. Xu, *Chem. Eng. J.* **2022**, *427*, 131379.
[68] R. Syah, A. Davarpanah, M. K. M. Nasution, Q. Wali, D. Ramdan, M. D. Albaqami, M. Ouladsmane, S. M. Noori, *Coatings* **2021**, *11*, 1173.
[69] D. Zhang, S. W. Eaton, Y. Yu, L. Dou, P. Yang, *J. Am. Chem. Soc.* **2015**, *137*, 9230.
[70] E. V. Kolobkova, M. S. Kuznetsova, N. V. Nikonorov, *J. Non. Cryst. Solids* **2021**, *563*, 120811.
[71] W. Wang, J. Li, P. Ni, B. Liu, Q. Chen, Y. Lu, H. Wu, B. Cao, Z. Liu, *ES Mater. Manuf.* **2019**, *4*, 66.
[72] L. Glasser, *Inorg. Chem.* **1995**, *34*, 4935.
[73] R. J. Sutton, G. E. Eperon, L. Miranda, E. S. Parrott, B. A. Kamino, J. B. Patel, M. T. Hörantner, M. B. Johnston, A. A. Haghighirad, D. T. Moore, H. J. Snaith, *Adv. Energy Mater.* **2016**, *6*, 1502458.
[74] A. K. Jena, A. Kulkarni, T. Miyasaka, *Chem. Rev.* **2019**, *119*, 3036.
[75] W. Yao, S. Fang, Y. Wang, Z. Hu, L. Huang, X. Liu, T. Jiang, J. Zhang, J. Wang, Y. Zhu, *Appl. Phys. Lett.* **2021**, *118*, 123502.
[76] L. Protesescu, S. Yakunin, O. Nazarenko, D. N. Dirin, M. V. Kovalenko, *ACS Appl. Nano Mater* **2018**, *1*, 1300.
[77] B. Zhao, S. Bai, V. Kim, R. Lamboll, R. Shivanna, F. Auras, J. M. Richter, L. Yang, L. Dai, M. Alsari, X.-J. She, L. Liang, J. Zhang, S. Lilliu, P. Gao, H. J. Snaith, J. Wang, N. C. Greenham, R. H. Friend, D. Di, *Nat. Photonics* **2018**, *12*, 783.
[78] J. De Roo, M. Ibáñez, P. Geiregat, G. Nedelcu, W. Walravens, J. Maes, J. C. Martins, I. Van Driessche, M. V. Kovalenko, Z. Hens, *ACS Nano* **2016**, *10*, 2071.
[79] E. M. Sanehira, A. R. Marshall, J. A. Christians, S. P. Harvey, P. N. Ciesielski, L. M. Wheeler, P. Schulz, L. Y. Lin, M. C. Beard, J. M. Luther, *Sci. Adv.* **2017**, *3*, eaao4204.
[80] L. M. Wheeler, E. M. Sanehira, A. R. Marshall, P. Schulz, M. Suri, N. C. Anderson, J. A. Christians, D. Nordlund, D. Sokaras, T. Kroll, S. P. Harvey, J. J. Berry, L. Y. Lin, J. M. Luther, *J. Am. Chem. Soc.* **2018**, *140*, 10504.
[81] A. Dutta, R. K. Behera, N. Pradhan, *ACS Energy Lett.* **2019**, *4*, 926.

[82] Z.-J. Li, E. Hofman, J. Li, A. H. Davis, C.-H. Tung, L.-Z. Wu, W. Zheng, *Adv. Funct. Mater.* **2018**, *28*, 1704288.
[83] S. Huang, Z. Li, L. Kong, N. Zhu, A. Shan, L. Li, *J. Am. Chem. Soc.* **2016**, *138*, 5749.
[84] H. Liu, Y. Tan, M. Cao, H. Hu, L. Wu, X. Yu, L. Wang, B. Sun, Q. Zhang, *ACS Nano* **2019**, *13*, 5366.
[85] Q. Zhong, M. Cao, Q. Zhang, *Nanoscale* **2021**, *13*, 19341.
[86] B. Tang, X. Zhao, L. J. Ruan, C. Qin, A. Shu, Y. Ma, *Nanoscale* **2021**, *13*, 10600.
[87] H.-C. Wang, S.-Y. Lin, A.-C. Tang, B. P. Singh, H.-C. Tong, C.-Y. Chen, Y.-C. Lee, T.-L. Tsai, R.-S. Liu, *Angew. Chem., Int. Ed.* **2016**, *55*, 7924.
[88] D. N. Dirin, L. Protesescu, D. Trummer, I. V. Kochetygov, S. Yakunin, F. Krumeich, N. P. Stadie, M. V. Kovalenko, *Nano Lett.* **2016**, *16*, 5866.
[89] V. Malgras, S. Tominaka, J. W. Ryan, J. Henzie, T. Takei, K. Ohara, Y. Yamauchi, *J. Am. Chem. Soc.* **2016**, *138*, 13874.
[90] Z. Chen, Z.-G. Gu, W.-Q. Fu, F. Wang, J. Zhang, *ACS Appl. Mater. Interfaces* **2016**, *8*, 28737.
[91] V. A. Hintermayr, C. Lampe, M. Löw, J. Roemer, W. Vanderlinden, M. Gramlich, A. X. Böhm, C. Sattler, B. Nickel, T. Lohmüller, A. S. Urban, *Nano Lett.* **2019**, *19*, 4928.
[92] X. Jin, K. Ma, J. Chakkamalayath, J. Morsby, H. Gao, *ACS Energy Lett.* **2022**, *7*, 610.
[93] A. Pan, J. Wang, M. J. Jurow, M. Jia, Y. Liu, Y. Wu, Y. Zhang, L. He, Y. Liu, *Chem. Mater.* **2018**, *30*, 2771.
[94] Z. Zhenfu, W. Zhihai, C. Jiong, J. Liang, H. Yafei, *J. Phys. Chem. C* **2018**, *122*, 16887.
[95] C. Guhrenz, A. Benad, C. Ziegler, D. Haubold, N. Gaponik, A. Eychmüller, *Chem. Mater.* **2016**, *28*, 9033.
[96] V. K. Ravi, S. Saikia, S. Yadav, V. V. Nawale, A. Nag, *ACS Energy Lett.* **2020**, *5*, 1794.
[97] Y. Hong, C. Yu, H. Je, J. Y. Park, T. Kim, H. Baik, G. M. Tomboc, Y. Kim, J. M. Ha, J. Joo, C. W. Kim, H. Y. Woo, S. Park, D. H. Choi, K. Lee, *Adv. Sci.* **2023**, *10*, 2302906.
[98] Y. Wei, K. Li, Z. Cheng, M. Liu, H. Xiao, P. Dang, S. Liang, Z. Wu, H. Lian, J. Lin, *Adv. Mater.* **2019**, *31*, 1807592.
[99] Z. Lu, Y. Li, Y. Xue, W. Zhou, S. Bayer, I. D. Williams, A. L. Rogach, S. Nagl, *ACS Appl. Nano Mater.* **2022**, *5*, 5025.
[100] S. Huang, B. Wang, Q. Zhang, Z. Li, A. Shan, L. Li, *Adv. Opt. Mater.* **2018**, *6*, 1701106.
[101] J. Pan, L. N. Quan, Y. Zhao, W. Peng, B. Murali, S. P. Sarmah, M. Yuan, L. Sinatra, N. M. Alyami, J. Liu, E. Yassitepe, Z. Yang, O. Voznyy, R. Comin, M. N. Hedhili, O. F. Mohammed, Z. H. Lu, D. H. Kim, E. H. Sargent, O. M. Bakr, *Adv. Mater.* **2016**, *28*, 8718.
[102] M. Imran, P. Ijaz, L. Goldoni, D. Maggioni, U. Petralanda, M. Prato, G. Almeida, I. Infante, L. Manna, *ACS Energy Lett.* **2019**, *4*, 819.
[103] M. Suri, A. Hazarika, B. W. Larson, Q. Zhao, M. Vallés-Pelarda, T. D. Siegler, M. K. Abney, A. J. Ferguson, B. A. Korgel, J. M. Luther, *ACS Energy Lett.* **2019**, *4*, 1954.
[104] F. Liu, C. Ding, Y. Zhang, T. S. Ripolles, T. Kamisaka, T. Toyoda, S. Hayase, T. Minemoto, K. Yoshino, S. Dai, M. Yanagida, H. Noguchi, Q. Shen, *J. Am. Chem. Soc.* **2017**, *139*, 16708.
[105] R. K. Behera, A. Dutta, D. Ghosh, S. Bera, S. Bhattacharyya, N. Pradhan, *J. Phys. Chem. Lett.* **2019**, *10*, 7916.
[106] S. Zou, Y. Liu, J. Li, C. Liu, R. Feng, F. Jiang, Y. Li, J. Song, H. Zeng, M. Hong, X. Chen, *J. Am. Chem. Soc.* **2017**, *139*, 11443.
[107] J. Ren, X. Zhou, Y. Wang, *Chem. Eng. J.* **2020**, *391*, 123622.
[108] X. Di, L. Shen, J. Jiang, M. He, Y. Cheng, L. Zhou, X. Liang, W. Xiang, *J. Alloys Compd.* **2017**, *729*, 526.
[109] Y. Xin, H. Zhao, J. Zhang, *ACS Appl. Mater. Interfaces* **2018**, *10*, 4971.
[110] C. Sun, X. Shen, Y. Zhang, Y. Wang, X. Chen, C. Ji, H. Shen, H. Shi, Y. Wang, W. W. Yu, *Nanotechnology* **2017**, *28*, 365601.
[111] E. von Schneidemesser, P. S. Monks, J. D. Allan, L. Bruhwiler, P. Forster, D. Fowler, A. Lauer, W. T. Morgan, P. Paasonen, M. Righi, K. Sindelarova, M. A. Sutton, *Chem. Rev.* **2015**, *115*, 3856.
[112] J. E. Stanworth, *J. Soc. Glas. Technol.* **1946**, *30*, 54.
[113] J. E. Stanworth, *Nature* **1952**, *169*, 581.
[114] M. Baazm, E. Soheyli, M. H. Hekmatshoar, A. Rostamzad, A. Karami Cheragh Abad, *Ceram. Int.* **2018**, *44*, 9414.
[115] E. Soheyli, M. H. H. Shoar, *Phys. Scr.* **2014**, *89*, 075801.
[116] A. Atila, Y. Ouldhnini, S. Ouaskit, A. Hasnaoui, *Phys. Rev. B* **2022**, *105*, 134101.
[117] M. Schuch, C. Trott, P. Maass, *RSC Adv.* **2011**, *1*, 1370.
[118] W. Nie, H. Tsai, *J. Mater. Chem. A* **2022**, *10*, 19518.
[119] Q. Zhang, B. Wang, W. Zheng, L. Kong, Q. Wan, C. Zhang, Z. Li, X. Cao, M. Liu, L. Li, *Nat. Commun.* **2020**, *11*, 31.
[120] W. H. Kim, J. Bae, K.-P. Kim, S. Woo, *Polymers* **2022**, *14*, 381.
[121] S. Liu, M. He, X. Di, P. Li, W. Xiang, X. Liang, *Ceram. Int.* **2018**, *44*, 4496.
[122] O. Kıbrıslı, E. Erol, M. Çelikbilek Ersundu, A. E. Ersundu, *Chem. Eng. J.* **2021**, *420*, 130542.
[123] Y. Jiao, J. Qian, Q. Zhao, Y. Dai, X. Yu, X. Zhao, *Opt. Mater. Express* **2022**, *12*, 2260.
[124] R. R. Petersen, J. König, M. M. Smedskjaer, Y. Yue, *J. Non. Cryst. Solids* **2014**, *400*, 1.
[125] B. W. Veal, D. J. Lam, A. P. Paulikas, W. Y. Ching, *J. Non. Cryst. Solids* **1982**, *49*, 309.
[126] A. Paul, M. S. Zaman, *J. Mater. Sci.* **1978**, *13*, 1499.
[127] A. M. B. Silva, C. M. Queiroz, S. Agathopoulos, R. N. Correia, M. H. V. Fernandes, J. M. Oliveira, *J. Mol. Struct.* **2011**, *986*, 16.
[128] K. Kirdsiri, J. Kaewkhao, N. Chanthima, P. Limsuwan, *Ann. Nucl. Energy* **2011**, *38*, 1438.
[129] R. Zheng, J. Ueda, K. Shinozaki, S. Tanabe, *Chem. Mater.* **2022**, *34*, 1599.
[130] Y. Fan, J. Li, Z. Lu, H. Zhang, W. Li, J. Zhuang, C. Hu, Y. Liu, B. Lei, X. Zhang, *J. Mater. Chem. C* **2022**, *10*, 8634.
[131] L.-Y. Cao, S.-C. Si, J.-B. Yu, C.-G. Ma, J.-B. Qiu, J. Wang, *Chem. Eng. J.* **2021**, *417*, 129177.
[132] Y. Zhou, C. Liu, Y. Ye, Y. Zhang, W. Zhang, Y. Hu, *J. Eur. Ceram. Soc.* **2022**, *42*, 7587.
[133] Z. Hu, Y. Jiang, F. Zhou, C. Chen, J. He, Z. Zhan, Z. Liu, J. Du, L. Zhang, Y. Leng, *Adv. Opt. Mater.* **2023**, *11*, 2202131.
[134] G. Li, Q. Pan, Z. Zhou, R. Gu, H. Zhang, X. Huang, G. Dong, X. Xiao, *Adv. Opt. Mater.* **2023**, *11*, 2203028.
[135] X. Xiang, H. Lin, J. Xu, Y. Cheng, C. Wang, L. Zhang, Y. Wang, *Chem. Eng. J.* **2019**, *378*, 122255.
[136] D. Wang, J. Qiu, D. Zhou, S. Hu, Y. Wen, K. Zhang, Q. Wang, Y. Yang, H. Wu, Z. Long, X. Li, J. Pi, E. Cao, *Chem. Eng. J.* **2021**, *421*, 127777.
[137] K. Zhang, D. Zhou, J. Qiu, Z. Long, R. Zhu, Q. Wang, J. Lai, H. Wu, C. Zhu, *J. Am. Ceram. Soc.* **2020**, *103*, 2463.
[138] Y. Chen, L. Shen, J. Liu, X. Liang, W. Xiang, *J. Am. Ceram. Soc.* **2021**, *104*, 2579.
[139] L. Ding, S. Liu, Z. Zhang, G. Shao, W. Xiang, X. Liang, *Ceram. Int.* **2019**, *45*, 22699.
[140] S. Liu, G. Shao, L. Ding, J. Liu, W. Xiang, X. Liang, *Chem. Eng. J.* **2019**, *361*, 937.
[141] Z.-J. Yong, S.-Q. Guo, J.-P. Ma, J.-Y. Zhang, Z.-Y. Li, Y.-M. Chen, B.-B. Zhang, Y. Zhou, J. Shu, J.-L. Gu, L.-R. Zheng, O. M. Bakr, H.-T. Sun, *J. Am. Chem. Soc.* **2018**, *140*, 9942.
[142] G. Pan, X. Bai, D. Yang, X. Chen, P. Jing, S. Qu, L. Zhang, D. Zhou, J. Zhu, W. Xu, B. Dong, H. Song, *Nano Lett.* **2017**, *17*, 8005.
[143] E. Erol, N. Vahedigharehchopogh, U. Ekim, N. Uza, M. Çelikbilek Ersundu, A. E. Ersundu, *J. Alloys Compd.* **2022**, *909*, 164650.
[144] S. Li, L. Nie, S. Ma, G. Yao, F. Zeng, X. Wang, C. Sun, G. Hu, Z. Su, *J. Eur. Ceram. Soc.* **2020**, *40*, 3270.
[145] C. Lu, Y. Duan, P. Li, Y. Lu, S. Xu, J. Zhang, *Ceram. Int.* **2022**, *48*, 13826.

[146] Q. Wang, Y. Tong, H. Ye, X. Liang, K. Yang, W. Xiang, *ACS Sustainable Chem. Eng.* **2021**, *9*, 11548.
[147] W. Lv, L. Li, M. Xu, J. Hong, X. Tang, L. Xu, Y. Wu, R. Zhu, R. Chen, W. Huang, *Adv. Mater.* **2019**, *31*, 1900682.
[148] D. Möncke, B. Topper, A. G. Clare, *Rev. Mineral Geochem.* **2022**, *87*, 1039.
[149] S. Si, J. Yu, S. Lou, B. Lan, J. Zhang, X. Zhang, M.-R. Li, L. Huang, J. Wang, *J. Eur. Ceram. Soc.* **2022**, *42*, 3586.
[150] S. Cheng, M. Yang, M. Hao, X. Liang, X. Fang, W. Xiang, *Mater. Today Chem.* **2023**, *31*, 101628.
[151] J. Li, D. Zhou, Y. Liu, Y. Chen, J. Chen, Y. Yang, Y. Gao, J. Qiu, *ACS Appl. Mater. Interfaces* **2023**, *15*, 22219.
[152] W. Van der Stam, J. J. Geuchies, T. Altantzis, K. H. W. Van Den Bos, J. D. Meeldijk, S. Van Aert, S. Bals, D. Vanmaekelbergh, C. De Mello Donega, *J. Am. Chem. Soc.* **2017**, *139*, 4087.
[153] C. Shen, Y. Zhao, L. Yuan, L. Ding, Y. Chen, H. Yang, S. Liu, J. Nie, W. Xiang, X. Liang, *Chem. Eng. J.* **2020**, *382*, 122868.
[154] R. Sahraei, E. Soheyli, Z. Faraji, M. Soleiman-Beigi, *Nanotechnology* **2017**, *28*, 475604.
[155] W. Liu, Q. Lin, H. Li, K. Wu, I. Robel, J. M. Pietryga, V. I. Klimov, *J. Am. Chem. Soc.* **2016**, *138*, 14954.
[156] Y. Zhou, C. Liu, Z. Zhao, W. Zhang, K. Li, Y. Ye, C. F. Zhu, X. G. Meng, *J. Alloys Compd.* **2020**, *827*, 154349.
[157] D. Guo, S. Xu, C. Wang, Z. Wang, H. Yin, H. Deng, Y. Jiang, Z. Zhang, X. Zhang, H. Shao, *J. Phys. Chem. C* **2021**, *125*, 989.
[158] F. K. Kharabaneh, E. Ghavidel, E. Soheyli, A. F. Yazici, N. N. Jawhar, E. Mutlugun, R. Sahraei, *Ceram. Int.* **2021**, *47*, 5523.
[159] M. He, L. Ding, S. Liu, G. Shao, Z. Zhang, X. Liang, W. Xiang, *J. Alloys Compd.* **2019**, *780*, 318.
[160] P. Li, Y. Duan, Y. Lu, A. Xiao, Z. Zeng, S. Xu, J. Zhang, *Nanoscale* **2020**, *12*, 6630.
[161] Y. Cheng, C. Shen, L. Shen, W. Xiang, X. Liang, *ACS Appl. Mater. Interfaces* **2018**, *10*, 21434.
[162] Q. He, Y. Zhang, Y. Yu, Y. Chen, M. Jin, E. Mei, X. Liang, L. Zhai, W. Xiang, *Chem. Eng. J.* **2021**, *411*, 128530.
[163] Q. Chen, X. Huang, D. Yang, Y. Le, Q. Pan, M. Li, H. Zhang, J. Kang, X. Xiao, J. Qiu, Z. Yang, G. Dong, *Adv. Opt. Mater.* **2023**, *11*, 2300090.
[164] P. Li, W. Xie, W. Mao, Y. Tian, F. Huang, S. Xu, J. Zhang, *J. Alloys Compd.* **2020**, *817*, 153338.
[165] X. Pang, S. Si, L. Xie, X. Zhang, H. Huang, S. Liu, W. Xiao, S. Wang, T. Xuan, J. Zhuang, C. Hu, Y. Liu, B. Lei, H. Zhang, *J. Mater. Chem. C* **2020**, *8*, 17374.
[166] F. Qi, X. Shao, Y. Ma, Y. Sun, J. Zhu, P. Yin, G. Zhao, *Opt. Mater.* **2022**, *124*, 111981.
[167] Y. Ye, W. Zhang, Y. Zhang, K. Li, J. Han, C. Liu, *Chem. Eng. J.* **2022**, *445*, 136867.
[168] J. Lin, S. Wang, G. Chen, R. Chen, S. Chen, N. Jiang, F. Huang, Y. Zheng, Y. Zheng, D. Chen, *J. Mater. Chem. C* **2022**, *10*, 7263.
[169] J. Li, Y. Fan, T. Xuan, H. Zhang, W. Li, C. Hu, J. Zhuang, R.-S. Liu, B. Lei, Y. Liu, X. Zhang, *ACS Appl. Mater. Interfaces* **2022**, *14*, 30029.
[170] P. Li, W. Xie, W. Mao, Y. Tian, F. Huang, S. Xu, J. Zhang, *J. Mater. Chem. C* **2020**, *8*, 473.
[171] Y. Liu, X. Luo, S. Yang, D. Wang, H. Wu, Q. Wang, T. Han, C. Wang, D. Zhou, J. Qiu, *J. Am. Ceram. Soc.* **2022**, *105*, 4699.
[172] G. Zheng, B. Yang, R. Hu, Y. Li, J. Zou, *J. Mater. Sci. Mater. Electron.* **2023**, *34*, 711.
[173] M. Lin, X. Zhang, L. Guo, Y. Zhang, R. Song, S. Xu, H. Zhu, C. Cheng, Y. Cao, Y. Wang, B. Chen, *Opt. Mater.* **2021**, *122*, 111654.
[174] L. Niu, H. Shi, Y. Ye, C. Liu, B. Jia, Y. Chu, L. Liu, J. Ren, J. Zhang, *J. Non. Cryst. Solids* **2022**, *581*, 121429.
[175] G. Shao, S. Liu, L. Ding, Z. Zhang, W. Xiang, X. Liang, *Chem. Eng. J.* **2019**, *375*, 122031.
[176] J. Lee, H. Lee, U. Kim, W. J. Chung, W. Bin Im, *J. Mater. Chem. C* **2023**, *11*, 898.
[177] N. Vahedigharehchopogh, E. Erol, O. Kıbrıslı, A. Genç, M. Çelikbilek Ersundu, A. E. Ersundu, *J. Mater. Chem. C* **2022**, *10*, 16088.
[178] Y. Lu, Y. Xu, S. Chen, J. Lin, J. Zhu, S. Wang, Y. Zheng, F. Huang, D. Chen, *J. Lumin.* **2022**, *248*, 118952.
[179] Z. Chen, Q. Wang, Y. Tong, X. Liu, J. Zhao, B. Peng, R. Zeng, S. Pan, B. Zou, W. Xiang, *J. Phys. Chem. Lett.* **2022**, *13*, 4701.
[180] X. Pang, H. Zhang, L. Xie, T. Xuan, Y. Sun, S. Si, B. Jiang, W. Chen, J. Zhuang, C. Hu, Y. Liu, B. Lei, X. Zhang, *J. Mater. Chem. C* **2019**, *7*, 13139.
[181] Q. Wang, Y. Tong, M. Yang, H. Ye, X. Liang, X. Wang, W. Xiang, *J. Mater. Sci. Technol.* **2022**, *121*, 140.
[182] X. Liu, Y. Tong, Q. Wang, X. Liang, Z. Zhang, H. Fan, W. Xiang, *Mater. Today Nano* **2023**, *21*, 100288.
[183] H. Ye, L. Huang, X. Liu, M. Yang, W. Chen, Y. Chen, W. Xiang, S. Pan, X. Liang, *Ceram. Int.* **2023**, *49*, 9010.
[184] B. Yang, S. Mei, Y. Zhu, D. Yang, H. He, R. Hu, Y. Li, J. Zou, R. Guo, *Ceram. Int.* **2023**, *49*, 6720.
[185] J. Lin, C. Yang, P. Huang, S. Wang, M. Liu, N. Jiang, D. Chen, *Chem. Eng. J.* **2020**, *395*, 125214.
[186] S. Sun, Z. Cheng, J. Song, C. Yan, T. Man, G. Dong, B. Qian, J. Qiu, *Adv. Mater. Technol.* **2022**, *7*, 2200470.
[187] W. Zhang, Y. Ye, Y. Hu, K. Li, C. Liu, *Chem. Eng. J.* **2023**, *454*, 140142.
[188] C. Wang, H. Lin, Z. Zhang, Z. Qiu, H. Yang, Y. Cheng, J. Xu, X. Xiang, L. Zhang, Y. Wang, *J. Eur. Ceram. Soc.* **2020**, *40*, 2234.
[189] L. Ding, C. Shen, Y. Zhao, Y. Chen, L. Yuan, H. Yang, X. Liang, W. Xiang, L. Li, *Mol. Catal.* **2020**, *483*, 110764.
[190] X. Zhang, M. Lin, L. Guo, Y. Zhang, C. Cheng, J. Sun, Y. Cheng, Y. Cao, S. Xu, X. Li, J. Zhang, B. Chen, *Opt. Laser Technol.* **2021**, *138*, 106857.
[191] Y. Idota, T. Kubota, A. Matsufuji, Y. Maekawa, T. Miyasaka, *Science* **1997**, *276*, 1395.
[192] Y. Zhang, *Int. J. Appl. Glas. Sci.* **2020**, *11*, 577.
[193] S. H. Choi, S. J. Lee, H. J. Kim, S. Bin Park, J. W. Choi, *J. Mater. Chem. A* **2018**, *6*, 6860.
[194] W. Xie, J. Cao, P. Li, M. Fan, S. Xu, J. Du, J. Zhang, *Mater. Des.* **2022**, *220*, 110860.
[195] K. Shinozaki, N. Kawano, *Sci. Rep.* **2020**, *10*, 1237.
[196] H. Zhang, E. Debroye, B. Vina-Bausa, D. Valli, S. Fu, W. Zheng, L. Di Virgilio, L. Gao, J. M. Frost, A. Walsh, J. Hofkens, H. I. Wang, M. Bonn, *ACS Energy Lett.* **2023**, *8*, 420.

Ehsan Soheyli received his M.Sc. in Solid-State Physics in 2012 working on electrical and optical properties of metal oxide glasses. He graduated with a Ph.D. in the same field from Arak University (Iran), working on luminescent colloidal quantum dots. Since 2017, he has collaborated with the Faculty of Science at Ilam University (Iran) and the Department of Electrical-Electronics Engineering at Abdullah Gul University (Turkey) as a postdoc research fellow, where he engaged in the synthesis and development of various luminescent quantum dots for optoelectronic applications.

Andrey L. Rogach received his Ph.D. in Physical Chemistry from the Belarusian State University in Minsk in 1995 and completed his habilitation in Experimental Physics at the Ludwig-Maximilians-University in Munich (Germany) in 2009. Since 2011, he has been a Chair Professor and the founding Director of the Centre for Functional Photonics at City University of Hong Kong. His research focuses on the synthesis, assembly, and optical spectroscopy of a broad range of colloidal semiconductors, and metal nanocrystals, their hybrid structures, and their use in optoelectronics and energy-related applications.